A Population Model of the Thalamus and its Wave Interactions with the Cortex

A thesis submitted

for the degree of

Master of Science

in Physics

by

Eli Justin Müller

The University of Waikato
Te Whare Wānanga o Waikato

February 2014

The University of Waikato

To my mother and father,

for the sacrifices, patience, compassion, wisdom and belief,

to my brothers

for the bumps, bruises and banter

and to my friends

for the laughs, long nights and support.

Acknowledgements

I would like to acknowledge Professor Moira Steyn-Ross and Assoc. Professor Alistair Steyn-Ross and thank them for their guidance during my time at Waikato University. The remarkable level of patience they have shown and the wisdom they have imparted, not only academically, but with life in general is greatly appreciated. I would like to thank Fisher and Paykel Healthcare for the scholarship funds they supplied me, Professor Jamie Sleigh, for his helpful guidance, Dr Michael Cree and Dr Marcus Wilson, for their resilience marking my assignments and my post-graduate colleagues for putting up with my idiosyncrasies. Mum and Dad, thanks for letting me make mistakes and for the belief that I would find my way and thanks to my brothers, for all the times we got to be idiots. Finally thanks to Arjun, Jazz, Jack, Dan, Nick, Mawsey, Crazy, Bomb, Jaim, Finn, Cam, Wilko, Jimmy, Lyndon, Cade, Liam, Junior, Raimundo, Luis and my old friend Jordan Crockett.

Abstract

In this thesis we construct a population model of the thalamus based on the mean-field cortex developed by Steyn-Ross *et al.* [20] and Liley *et al.* [10]. We allow interactions between the thalamus and cortex via damped wave equations and show spindle-like oscillations ($10 - 15$ Hz) propagating from the thalamic reticular population into the cortical populations.

We first consider a mean-field model of a cortex that is isolated from time-dependent sub-cortical inputs. The model is a continuum theory based on the electrical activity of a neural mass called the macrocolumn, containing groups of excitatory and inhibitory neurons. We demonstrate induction of '*unconsciousness*' in the macrocoulmn under propofol-like general anaesthetic, and show there is a hysteretic separation between points of '*loss of consciousness*' and '*recovery of consciousness*'.

The thalamus, a sub-cortical structure important to the relay of sensory input into the cortex, is described using a revised set of equations based on the mean-field cortical model. We define two neuron types within the thalamus: the *specific* group, assumed to be excitatory, and the *reticular* group, assumed to be inhibitory. A new bimodal mapping function is developed to relate mean membrane potentials to mean firing rates within the thalamic macrocolumn. This bimodal function is generated by combining two sigmoidal functions, and is a representation of the observed increase in the firing rates of reticular neurons at *hyperpolarized* membrane potentials. In contrast, the mapping function for specific population is modelled by a standard sigmoid. We investigate the isolated dynamics of the mean-field thalamus, using parameters from Robinson *et al* [18], and find spindle-like oscillations emerge following a transition from unstable equilibrium states to stable states consistent with the linear stability analysis.

A coupling of the isolated cortical and thalamic systems is accomplished using four damped wave equations. We investigate the stationary states of the thalamo-cortical model and find the

spindle-like oscillations present in the thalamus propagate into the cortical populations.

Contents

List of Figures

List of Tables

Chapter 1

Introduction

1.1 Introduction

> *"I do not know how I may appear to the world, but to myself I seem to have been only like a boy, playing on the sea-shore, and diverting myself, in now and then finding a smoother pebble or prettier shell than ordinary, whilst the great ocean of truth lay all undiscovered before me."* – Isaac Newton[1]

Newton might have suggested that to understand and accurately predict the behaviour of a large population, all one would require is the exact set of initial conditions and correct equations governing each individual within the population. While this approach may indeed have value for a small group, the complexity that comes with understanding the dynamics of a large population, such as the molecules in a cube of atmosphere, makes it less attractive. Mean-field population models place less emphasis on individuals and use averages of subpopulations to describe patterns of behaviour observed globally.

Modelling of the brain using a mean-field approach is favourable because it simplifies the complexities that come with modelling billions of neurons interconnected potentially thousands of times. The variables of a mean-field model of the brain are also easily relatable to electroencephalographic (EEG) recordings taken from the scalp, which are themselves averages, and are a common and vital tool used in neuroscience.

[1] Source: `http://www.physics.wustl.edu/~alford/newton.html`

1.2 Context

Sleep and anaesthesia are states of the brain associated with distinct features on EEG recordings [4]. An understanding of the mechanisms driving these features is an active area of research. The slow-wave sleep state, which is part of non-REM (non-rapid eye movement) sleep, is characterized by low frequency oscillations ($0.1 - 1$ Hz). The interaction between spindle ($10 - 15$ Hz) and delta ($0.1 - 4$ Hz) activity is thought to play an important role in the generation of slow-wave oscillations.

The thalamus, a sub-cortical structure located mid-brain, is known to generate $10-15$ Hz spindle oscillations [6]. The Waikato University mean-field model does not presently include a thalamic component to generate these spindle frequencies [24].

1.3 Novel Material

> *"The Book of Nature is written in mathematical characters, without whose help it is impossible to comprehend a single word, without which one wanders in vain through a dark labyrinth."* – Galileo Galalei[2]

In this thesis we propose a new mean-field model of the thalamus based on the cortical models of Steyn-Ross *et al* 1999 [20] and Liley *et al* 2001 [10]. Our model of the thalamus excludes *long-range* excitatory connections, assuming interaction terms within thalamus to be localized.

The reticular neurons within the thalamus have been shown to possess ionic current flows for hyperpolarized membrane potentials, Zhu [28]. These currents can be mapped to high firing rates within the reticular population that do not appear to drop off with further reduction of membrane potentials. We propose the use of a bimodal function, constructed from the sum of a sigmoid and its mirror image, to model these hyperpolarized currents. A method for inverting this function computationally is also given.

[2]Source: `http://www.personal.psu.edu/faculty//s/a/sac130/links/quotes.html`

1.4 Thesis Overview

> *"As our circle of knowledge expands, so does the circumference of darkness surrounding it."* – Albert Einstein[3]

In Chapter 2 we give a brief background of neurophysiology. We highlight the general structure of the cortex and the mechanisms that drive it, describing the physiological architecture we intend to model in later chapters. In Chapter 3 we review the history of mean-field models of the brain. We compare the models of Beurle, Wilson and Cowan, Nunez, Robinson *et al.*, Liley *et al.* and Steyn-Ross *et al.*, noting common elements between the models and the differences that distinguish them.

In Chapter 4 we give an overview of the Waikato mean-field cortical model based on Steyn-Ross *et al* 1999 [20] and Liley *et al* 2001 [10]. We provide the defining set of equations for the cortical model and the basis behind them. Following the work of Wilson and Cowan, [26] [27], we assume homogeneity within a cortex, isolated from subcortical structures, and investigate the equilibrium states of the model. We further investigate the effect changes in an anaesthetic scaling parameter have on the distribution of the cortical equilibrium states and perform a Jacobian stability analysis to determine the likelihood of the model occupying them in simulation.

In Chapter 5 a novel description of the thalamus based on the mean-field cortical model is given. We consider a spatially localized thalamus, ignoring *long-range* excitation terms, and isolate it from the cortical activity. We also introduce a new bimodal mapping function relating mean firing rates to mean membrane potentials for the reticular neuron population. The parameters used for this model are based on the work of Robinson *et al.* [18]. We investigate the equilibrium states of the model and their stabilities, relating it to the cortical model in chapter 4.

In Chapter 6 we propose a mean-field thalamo-cortical system. A *long-range* coupling of the isolated cortical and thalamic models is proposed by defining damped wave equations connecting excitatory neurons to the thalamus and specific neurons to the cortex. A method for computing the steady states of the thalamo-cortical model is outlined and we perform a Jacobian stability analysis.

[3]Source: `http://http://www.notable-quotes.com/e/einstein_albert.html`

In Chapter 7 we give a brief summary of the results of this thesis and suggest features to incorporate in future mean-field models of the thalamus.

A poster of the work in chapter 5 was presented at the New Zealand Institute of Physics conference,

Müller, E.J., Steyn-Ross, M.L., Steyn-Ross, D.A., Sleigh, J.W.: Modelling the Mean-field Dynamics of an Isolated Thalamus, NZIoP, Nelson, New Zealand (2013).

Chapter 2

Neurophysiology

2.1 Structure of the Brain: Neurons

The human brain consists of groups of neurons. A neuron is a biological cell with a compact cell body called the soma and two branching structures. The dendrites are channels for electrical and chemical signals from other neurons to be relayed to the soma. The axon is the output of a neuron allowing for a signal to be transmitted to other neurons. The neuron membrane as a whole is an insulator with ion channels that can be open or closed. When a neuron is in its resting state with no synaptic input, an ion pump uses energy to transport Na^+ and K^+ ions across the membrane against their electrochemical gradients. The pump moves sodium ions out of the neuron faster than it moves potassium ions in resulting in a net negative charge of the cell (-70mV) relative to the cortical fluid.

2.2 Connections

A connection between neurons is termed a synapse, with the pre-synaptic neuron's axon connecting to a dendrite of the post-synaptic neuron. A synaptic connection can occur through a direct electrical connection synapse known as a gap junction. Here, ions flow from neuron to neuron via a direct channel at the axon-dendrite interface. Another type of synaptic connection is the chemical synapse, where an inter-neuronal signal is passed via an indirect connection mediated by a neuro-transmitter. A pre-synaptic neuron will send out a burst of current along its axon, detectable as an"action potential" generated when its membrane potential rises above a threshold voltage (-60 mV), when this reaches the synaptic cleft (chemical synapse), neurotransmitters are released and diffuse across the gap. The neurotransmitters bind to the receptors

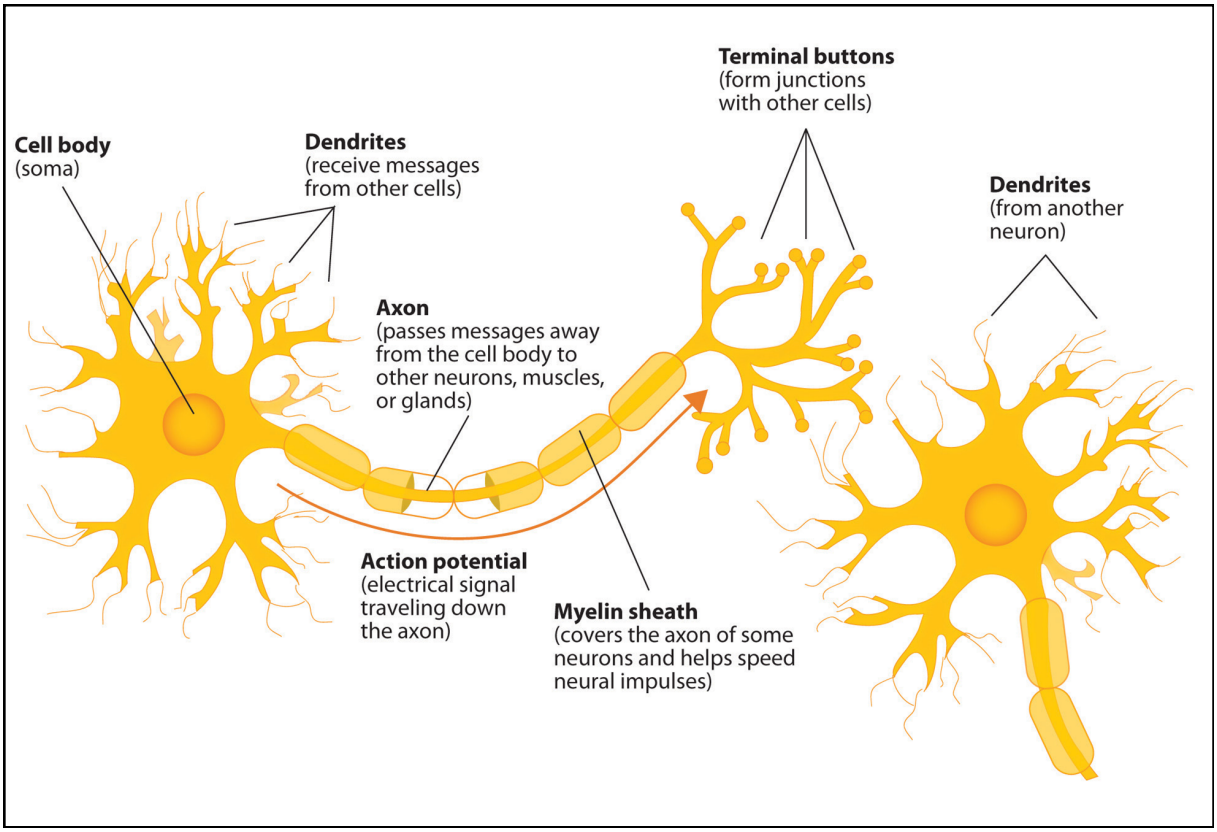

Figure 2.1: The general structure of a *white matter* neuron, consisting of a soma, a branching structure of dendrites and an axon. This is a white matter neuron as the axon has a fatty sheath of myelin insulating it. For a grey matter neuron this layer is not present. An *action potential* will propagate down the axon into the branches at the end and potentially communicate with any post-synaptic neurons through a synapse.[Source: http://2012books.lardbucket.org/books/beginning-psychology/s07-brains-bodies-and-behavior.html]

of the post-synaptic neuron, activating specific gated ion channels and allow selected ionic flow across the membrane.

2.3 The Cerebral Cortex

Distinguishing between groupings of neurons in the brain is done by characterizing them based on their observed roles in brain function. The majority of the outer layer of the brain is called the cerebral cortex. In humans this region is relatively large when compared to the cortex of other mammals. It is constructed of *grey matter* known to play an important role in memory, attention, perceptual awareness, thought, language and consciousness. Within the cortex there exists two neuron types. (i) *Excitatory* neurons, which when firing, will tend to increase the membrane potential of post-synaptic neurons they communicate with, driving them towards their threshold potential and making them more likely to fire; this is called **depolarization**. (ii) *Inhibitory* neurons, when firing, will tend to decrease post-synaptic neuron membrane potentials

driving them away from their threshold potentials and subsequently lessening their tendency to fire; this is called **hyperpolarization**.

2.4 The Thalamus

As well as the cortex, the brain contains many subcortical structures. In this thesis we consider one structure specifically, called the *thalamus*. The thalamus is a small grouping of neurons forming a symmetrically paired structure located between the cerebral cortex and the mid-brain. Almost all sensory information coming from the periphery must first pass through the thalamus before reaching the cortex. A traditional view of the thalamus was that it is just a simple relay, however more recently evidence suggests that the thalamus plays a much more dynamic role in information transmission and processing. It is also thought to be important in sleep and alertness [9]. Two neuron types within the thalamus are considered. The *specific* neurons (sometimes referred to as relay neurons) are analogous to the *excitatory* neurons of the cortex and will also tend to drive towards threshold, or depolarize, post-synaptic neurons. The *reticular* neurons will tend to inhibit, or hyperpolarize, post-synaptic neurons, driving them away from their threshold membrane potentials.

2.5 The Macrocolumn

In Chapters 4 and 5 an outline of the mean-field models used to represent the isolated cortex and the isolated thalamus is presented. For these models, we consider a neural mass containing both excitatory and inhibitory populations, called the *macrocolumn*. As neurons are known to act cooperatively within small volumes, that is there exists a certain amount of local redundancy, it is not unreasonable to group them together in this way. The neurons occupy a cylindrical volume of diameter $\sim$1 mm and depth $\sim$3 mm. Each contains between 40,000 and 100,000 neurons. Figure 2.2 shows the macrocolumn for the cortex detailing the connections entering and leaving the column as well as internal connections.

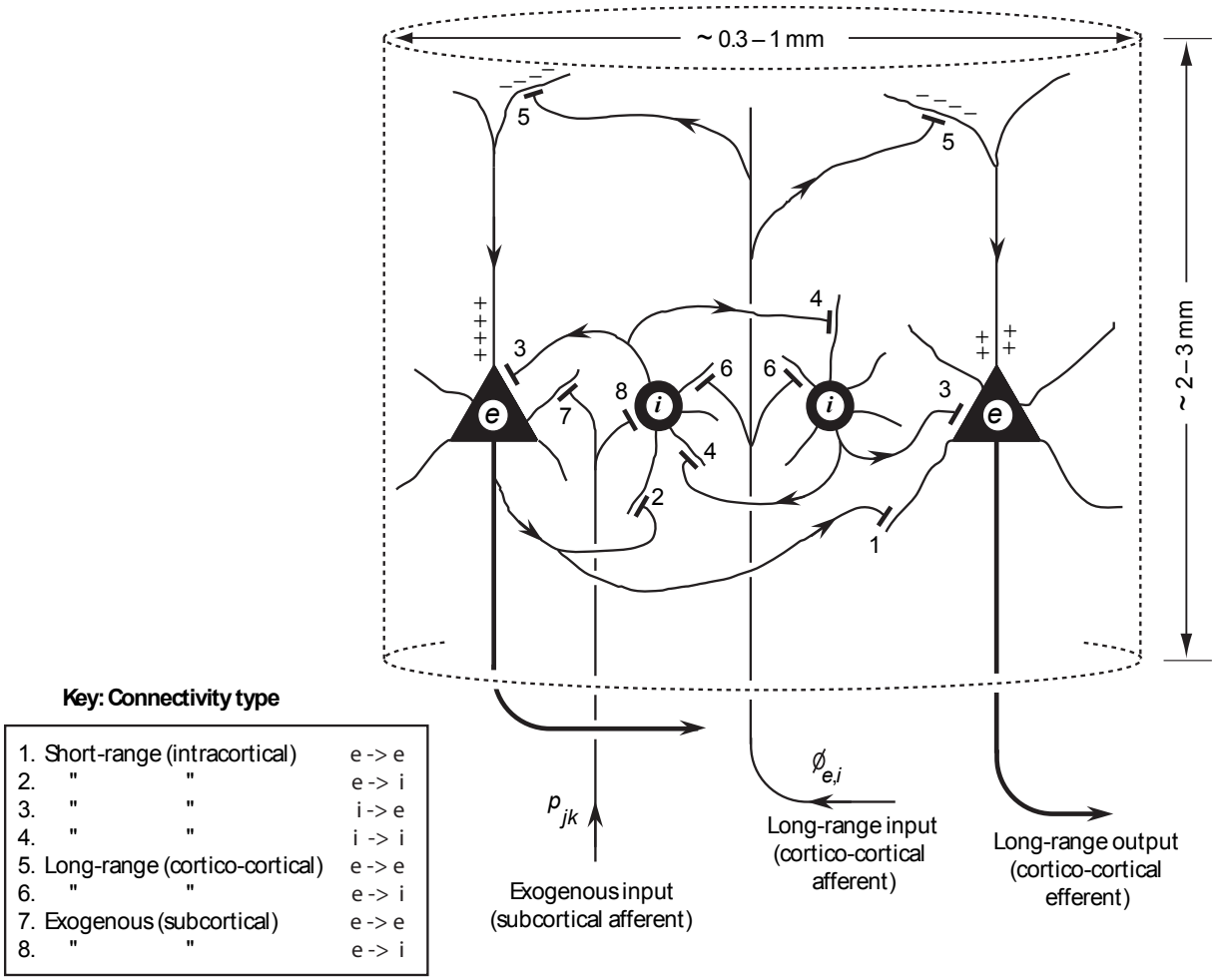

Figure 2.2: The macrocolumn, a neural mass consisting of excitatory and inhibitory neurons. [Source: Steyn-Ross (1999) [20]]

Chapter 3

Literature Review

3.1 Introduction

Here we present a history of mean-field modelling of the cortex over the past half a century, covering the work of Beurle, Wilson and Cowan, Nunez, Robinson *et al.*, Liley *et al.* and Steyn-Ross *et al.*

3.2 Beurle, 1956

In 1956 Beurle presented one of the earliest mean-field models of the cortex [2]. Rather than concerning himself with the spike behaviour of any single neuron he looked at the properties of interconnected excitatory neurons randomly distributed with a fixed volume density ρ.

Beurle introduced a threshold membrane potential for the neurons that must be reached before they can become active. He supposed that a pre-synaptic neuron would only have an excitatory effect on connected post-synaptic neurons for a period, s, modelling it for simplicity as a square wave, $\chi(t)$. He argued that there was an associated recovery time, r, for a recently active neuron and that any excitation arriving during this period had no effect, terming the neuron "used". This meant that a neuron's membrane potential was dependent on its history and that only a proportion, R, of neurons in a population were "sensitive".

If a post-synaptic neuron has not been recently active, i.e. *is* "sensitive" to activity, Beurle assumed that it would respond to all synaptic inputs independently. The neuron membrane potential would then be the sum of the resting potential and the arriving post-synaptic potentials (PSPs).

His model focused on the proportion of neurons becoming active per unit time as a function of Cartesian coordinates: $F(x, y, z, t)$. Assuming invariance in the y, z planes the mean rate-of-arrival of spike activity at neurons in the x plane from all other cells is given as the convolution,

$$P(x,t) = \int_{-\infty}^{\infty} F(X,t)\xi(x-X)dX,$$

where $\xi(x)$ is the mean number of connections to a neuron at position x. He proposed that $\xi(x) = b\ \mathrm{e}^{-|x|/a_0}$ for connections from all the neurons in an infinite plane of unit thickness to a neuron at a distance x. Similarly the mean integrated excitation, $\overline{N}(x,t)$, for cells in the x plane is given by the convolution,

$$\overline{N}(x,t) = \int_{-\infty}^{0}\int_{-\infty}^{\infty} F(X,t)\xi(x-X)\chi(t-T)dXdT.$$

Beurle noted that for a homogeneous mass of cells in which there had been no recent activity his model neurons would remain static in a 'sensitive state'. With an absence of inhibition in his model, control of the system is maintain by the inclusion of the recovery time for 'used' neurons. Beurle also showed that his model predicted waves of activity which propagated radially from the point of origin of a stimuli, because the proportion of sensitive cells behind the wave front is less then in the region it is yet to pass. This asymmetry means the region in front of the wave is more able to support activity and allows the wave to propagate through it.

Another important feature of Beurle's paper is his investigation of external input sources. He showed that supplying a sub-threshold excitatory input stimulus through his population model resulted in an effective reduction in the attenuation of any wave propagating. He also found that raising this stimulus to an above-threshold level acts the opposite way: desensitizing areas that increase the attenuation for any propagating waves. Beurle also mentioned that the external source must be constant and continuous. If it were intermittent, the effect it would have on any wave attenuation would be dependent on the timing of activation in relation to the passage of the wave. Beurle was able to show that basic forms of behaviour of living organisms can be simulated by a mass of simple units with a minimum degree of organization, setting the tone

for future work in the field of computational neuroscience.

3.3 Wilson and Cowan, 1972, 73

In their 1972 [26] and 1973 [27] papers, Wilson and Cowan, extended with the work of Beurle by proposing a mean-field model of the cortex. They argued that *"If a fluid is observed at the molecular level, what is seen is Brownian motion, whereas the same fluid, viewed macroscopically, may be undergoing very orderly streamlined flow"*, and this is an apt analogy for the cortex. The paper references Mountcastle [14] and others as showing that neurons within a small volume have a near identical response to external stimuli providing evidence for a high degree of local redundancy. Their deterministic model for the dynamics of neural populations may be interpreted as a treatment of the mean values of the underlying statistical processes.

They defined a population model where the cells comprising the population were assumed to be spatially close and randomly connected. The connections were further assumed dense enough that any two cells of the population are either connected directly or via inter neurons.

A crucial assumption made in the Wilson and Cowan papers is that: *"all nervous processes of any complexity are dependent upon the interaction of excitatory and inhibitory cells"*. This is an important statement and details the progression in the area of mean-field cortical modelling between the time of the Beurle and Wilson-and-Cowan papers. Wilson-and-Cowan based this assumption on the work of many others and specifically the conclusion of Ashby *et al.* 1962 [1] that the dynamical stability of the brain was paradoxical, and it was Griffith's introduction of inhibition (1963) [7] that resolved this paradox.

Their model's mathematical structure is concerned with four main variables and variations from their corresponding resting states:

$E(x,t)$ = proportion of excitatory cells at position x firing per unit time;
$I(x,t)$ = proportion of inhibitory cells at position x firing per unit time;
$\overline{N_e}(x,t)$ = mean integrated excitation (membrane potential) within excitatory neurons;
$\overline{N_i}(x,t)$ = mean integrated excitation (membrane potential) within inhibitory neurons.

Similar to Beurle, Wilson and Cowan include *refractoriness* in their model, where a neuron has a desensitized period after firing. During this *refractory* period the neuron cannot be driven to firing regardless of any stimulating synaptic inputs.

Table 3.1: Beurle Symbol Definitions

ρ_j	=	density of j-type neurons (where $j = e, i$)
v_j	=	propagation velocity of j-type action potentials
r_j	=	refractory period of j-type neurons
$\beta_{jk}(x - X)$	=	probability that a j-type neuron at X is connected to a k-type neuron at x
$P(x, t)$	=	sub-cortical input to excitatory neurons at x
$Q(x, t)$	=	sub-cortical input to inhibitory neurons at x
$\pm\alpha(t)$	=	post synaptic membrane potential (change in membrane potential caused by an action potential, +ve excitatory/-ve inhibitory)

They derive equations for neuronal activity by noting that neurons within their model will only become active if their post-synaptic potentials exceed threshold and if they are at the same time sensitive, i.e. non-refractory.

Note they consider the connection functions β_{jk} to be exponentially decreasing for increasing x, i.e. $\beta_{jk} = b_{jk}\mathrm{e}^{-|x|/\sigma_{jk}}$, due to the assumed isotropy and homogeneity of the cortical tissue.

Expressions for the proportion of neurons receiving above-threshold excitation are derived by computing an expression for the mean integrated excitation generated in neurons at x by afferent activity. The mean rate of arrival of impulses at excitatory neurons located at x caused by excitatory activity at the instant $t - \frac{|x-X|}{v_e}$ within a segment of length dX at x is defined to be,

$$\rho_e E\left(X, t - \frac{|x - X|}{v_e}\right)\beta_{ee}(x - X)\, dX, \tag{3.1}$$

The contribution of inhibitory activity to excitatory neurons located at x is similarly given as,

$$\rho_e I\left(X, t - \frac{|x - X|}{v_i}\right)\beta_{ie}(x - X)\, dX. \tag{3.2}$$

Wilson and Cowan then computed the convolutions of Eqs. (3.1–3.2), noting that they assume linear time-invariance of temporal summation in neurons; the difference gives the mean value of integrated excitation for excitatory neurons at x,

$$\overline{N_e}(x,t) = \int_{\infty}^{t} \Bigg[\int_{\infty}^{\infty} \rho_e E\Big(X, t - \frac{|x-X|}{v_e}\Big) \beta_{ee}(x-X)\, dX - \int_{\infty}^{\infty} \rho_i I\Big(X, t - \frac{|x-X|}{v_i}\Big) \beta_{ie}(x-X)\, dX \pm P(x,T) \Bigg] \alpha(t-T)\, dT \tag{3.3}$$

$$\overline{N_i}(x,t) = \int_{\infty}^{t} \Bigg[\int_{\infty}^{\infty} \rho_e E\Big(X, t - \frac{|x-X|}{v_e}\Big) \beta_{ee}(x-X)\, dX - \int_{\infty}^{\infty} \rho_e I\Big(X, t - \frac{|x-X|}{v_i}\Big) \beta_{ie}(x-X)\, dX \pm P(x,T) \Bigg] \alpha(t-T)\, dT \tag{3.4}$$

They defined $S_e(\overline{N_e})$ to be the expected proportion of excitatory neurons that receive at least threshold excitation per unit time. Letting $G(\theta_e)$ be the distribution function of excitatory neuronal thresholds in the tissue, they defined,

$$S_e(\overline{N_e}) = \int_{0}^{\overline{N_e}} G(\theta_e)\, d\theta_e. \tag{3.5}$$

S_e is a monotonically increasing function of $\overline{N_e}$ bounded by the asymptotes 0 and 1 and if $G(\theta_e)$ is unimodal they note that S_e will have only one point of inflection, i.e. it would be sigmoidal in shape. They refer to value of $\overline{N_e}$ at the point of inflection as the aggregate threshold for the excitatory neurons.

The number of excitatory neurons that are sensitive at a given time t (comprised of all neurons which have not been active in the interval $(t - r_e)$ to t) is given as,

$$R_e(t) = \Bigg[1 - \int_{t-r_e}^{t} E(x,T)\, dT \Bigg] \rho_e \delta x, \tag{3.6}$$

and the corresponding sensitive inhibitory neurons,

$$R_i(t) = \left[1 - \int_{t-r_i}^{t} I(x,T)\, dT\right] \rho_i \delta x. \tag{3.7}$$

Wilson and Cowan assume that the expected number of excitatory neurons receiving at least threshold excitation during a interval δt at t is statistically independent of the proportion which are sensitive. This leads them to define the expected number activated during an interval δt at $(t+\tau)$ to be,

$$E(x, t+\tau)\rho_e \delta x \delta t = R_e S_e(\overline{N_e})\delta t \tag{3.8}$$

and similarly,

$$I(x, t+\tau)\rho_i \delta x \delta t = R_i S_i(\overline{N_i})\delta t \tag{3.9}$$

In their 1972 paper [26], Wilson and Cowan considered a spatially invariant system of equations, deriving forms of Eqs. (3.8 – 3.9),

$$E(t+\tau) = \left[1 - \int_{t-r}^{t} E(t')dt'\right] S_e\left[\int_{-\infty}^{t} \alpha(t-t')[c_1 E(t') - c_2 I(t') + P(t')]dt'\right], \tag{3.10}$$

$$I(t+\tau') = \left[1 - \int_{t-r}^{t} I(t')dt'\right] S_i\left[\int_{-\infty}^{t} \alpha(t-t')[c_3 E(t') - c_4 I(t') + Q(t')]dt'\right]. \tag{3.11}$$

In order to simplify the equations which are mathematically complex they applied a temporal coarse-graining. They replace temporally-dependent variables by moving time averages i.e. $\overline{f}(t) = \frac{1}{s}\int_{t-s}^{t} f(t')dt'$. The effect of this is to average out rapid temporal variations taking place on a time scale less than s. If $\alpha(t)$ is close to unity for $0 \leq t \leq r$ and falls to zero quickly for $t > r$ then they argue it is reasonable to replace both integrals by the coarse-grained variables,

$$\int_{t-r}^{t} E(t')dt' \rightarrow r\overline{E}(t), \tag{3.12}$$

$$\int_{t-r}^{t} \alpha(t-t')E(t')dt' \rightarrow k\overline{E}(t), \tag{3.13}$$

They further replace $E(t+\tau)$ and $I(t+\tau)$ in Eq (3.10 – 3.11) by Taylor expansions in the coarse-grained variable about $\tau = 0$, leading to,

$$\tau\frac{d\overline{E}}{dt} = -\overline{E} + (1 - r\overline{E})S_e[kc_1\overline{E} - c_2k\overline{I} + kP(t)] \tag{3.14}$$

$$\tau'\frac{d\overline{I}}{dt} = -\overline{I} + (1 - r\overline{I})S_i[k'c_3\overline{E} - c_4k'\overline{I} + k'Q(t)] \tag{3.15}$$

Wilson and Cowan locate the steady states of their 1972 paper's cortical model by setting the time derivatives of the equations to zero, i.e. $\frac{d\overline{E}}{dt} = \frac{d\overline{I}}{dt} = 0$. Noting that solutions to these simultaneous equations cannot be determined analytically due to the required sigmoid inversions they undertake a numerical approach. Deriving expressions for the proportion of excitatory and inhibitory neurons firing per unit time as a function of each other, $E(I)$ for $\frac{d\overline{E}}{dt} = 0$ and $I(E)$ for $\frac{d\overline{I}}{dt} = 0$, the intersection of these two isoclines are the equilibrium (steady state) solutions of the system. They also comment on the necessity for the c_2 and c_3 parameters to be non-vanishing in order for the isoclines to be non-trivial, implying that negative feedback between the subpopulations is an essential component of the model.

This method is used in later Chapters (4, 5 and 6) to solve the steady states of similar neuron population models. Wilson and Cowan noted that certain selections of parameters allowed for changes in the shape of the isoclines leading always to either one, three or five equilibrium states. They also make mention of hysteresis effects present under certain parameter settings in which multiple stable states are present.

3.4 Nunez, 1995

In his book *Neocortical Dynamics and Human EEG Rhythyms* [15], Nunez outlines a model of the cortex based on global theory, considering a neural mass of a similar order to that of the macrocolumn, Fig. 2.5, defined in Chapter 2. On this scale he neglects local delays but includes delays due to finite velocity of action potential propagation along cortico-cortical fibres. He assumes intra-cortical interactions are both excitatory and inhibitory and long-range cortico-cortical are exclusively excitatory. Nunez relates the synaptic activity of a neural mass to action potentials at other locations by,

$$h_E(\mathbf{r},t) = u(\mathbf{r},t) + \int_0^\infty dv \int_s R_E(\mathbf{r},\mathbf{r}_1,v) g\left[\mathbf{r}_1, t - \frac{|\mathbf{r}-\mathbf{r}_1|}{v}\right] d^2 r_1, \tag{3.16}$$

$$h_I(\mathbf{r},t) = u_0 + \int_s R_I(\mathbf{r},\mathbf{r}_1) g(\mathbf{r}_1,t) d^2 r_1. \tag{3.17}$$

Eqs. (3.16)–(3.17) express the idea that action potentials firing at position $\mathbf{r}_1$, $g(\mathbf{r}_1,t)$, cause activity at position $\mathbf{r}$ at a later time which is dependent on separation and action potential velocity, $|\mathbf{r}_1 - \mathbf{r}|/v$.

$g(\mathbf{r},t)$ is a function of both $h_E(\mathbf{r},t)$ and $h_I(\mathbf{r},t)$ and in general this function is non-linear. Nunez simplifies this by considering small perturbations of $g(\mathbf{r},t)$ from its stable equilibrium state, g_0. This leads to the linear expression,

$$\delta g = Q_E H_E(\mathbf{r},t) - Q_I H_I(\mathbf{r},t) \tag{3.18}$$

Table 3.2: Nunez Symbol Definitions

$h_{E,I}(\mathbf{r},t)$	=	number of active excitatory/inhibitory synapses per unit volume at time t position $\mathbf{r}$.
$u(\mathbf{r},t)$	=	number of active sub-cortical excitatory synapses per unit volume at time t position $\mathbf{r}$.
u_0	=	number of active sub-cortical inhibitory synapses per unit volume, assumed to be constant.
$g(\mathbf{r},t)$	=	number of action potentials firing per unit volume at time t position $\mathbf{r}$.
$R_E(\mathbf{r},\mathbf{r}_1,v)$	=	number of excitatory fibres connecting positions, $\mathbf{r},\mathbf{r}_1$, with propagation velocity v.
$R_I(\mathbf{r},\mathbf{r}_1)$	=	number of inhibitory fibres connections positions, $\mathbf{r},\mathbf{r}_1$, assuming at short range $v\to\infty$.

where H_j is a perturbation of h_j from its equilibrium value, i.e. $H_E = \delta h_E$, $H_I = \delta h_I$. The control parameters, Q_E, Q_I are,

$$Q_E = \left(\frac{\partial g}{\partial h_E}\right)_{g=g_0}, \quad Q_I = \left(\frac{\partial g}{\partial h_I}\right)_{g=g_0} \tag{3.19}$$

Nunez then redefines Eq (3.16)–(3.17) in terms of this linearization about the fixed state g_0,

$$H_E(\mathbf{r},t) = U(\mathbf{r},t) = \int_0^\infty dv \int_s R_E(\mathbf{r},\mathbf{r}_1,v)\left[Q_E H_E\left(\mathbf{r}_1, t-\frac{|\mathbf{r}-\mathbf{r}_1|}{v}\right) - Q_I H_I\left(\mathbf{r}_1, t-\frac{|\mathbf{r}-\mathbf{r}_1|}{v}\right)\right] d^2 r_1, \tag{3.20}$$

$$H_I(\mathbf{r},t) = \int_s R_I(\mathbf{r},\mathbf{r}_1)\left[Q_E H_E(\mathbf{r}_1,t) - Q_I H_I(\mathbf{r}_1,t)\right] d^2 r_1. \tag{3.21}$$

where $U(\mathbf{r},t)$ is a perturbation from a stable equilibrium state of $u(\mathbf{r},t)$, i.e. $U(\mathbf{r},t) = \delta u(\mathbf{r},t)$.

Nunez considers a further simplified case of an infinite one-dimensional system and solves Eqs. (3.20)–(3.21). His model now describes an anisotropic neocortical circumference where cortico-cortical connections are linear and are modelled by the density function,

$$R_E(x,x_1,v) = \frac{1}{2}\sum_{n=1}^{N} \rho_n \lambda_n f_n(v) \mathrm{e}^{-\lambda_n |x-x_1|} \tag{3.22}$$

considering N different fibre systems. With each fibre system, n, the connection density decreases with characteristic distance λ_n^{-1}, the distribution of propagation velocities is described by f_n, and ρ_n is the number of synapses per neuron associated with the excitatory fibre system.

The corresponding inhibitory connection density function is given as,

$$R_I(x, x_1) = \frac{1}{2}\rho_I \lambda_I \mathrm{e}^{-\lambda_I |x - x_1|}. \tag{3.23}$$

Nunez relates the Fourier transforms the cortical input function, $U(k,\omega)$ and the excitatory synaptic firing density function, $H_E(k,\omega)$ by,

$$H_E(k,\omega) = \frac{U(k,\omega)}{D_G(k,\omega)} \tag{3.24}$$

where $D_G(k,\omega)$ is the dispersion relation function. The roots of $D_G(k,\omega)$ allow for ω to be expressed as a function k, where k is the wave number associated with a spatial disturbance. The real part of ω relates to the waves temporal frequency, i.e. $\mathrm{Real}(\omega) = 2\pi f$ and the wave speed $v = \mathrm{Real}(\omega)/k$. The imaginary part of ω describes the degree of damping present in the wave.

Nunez' cortical model investigates both travelling waves and standing waves, proposing the latter as a possible mechanism for alpha-rhythm frequencies present in EEG signals, ≈ 10 Hz.

3.5 Robinson, Rennie and Wright, 1997, 98

In Robinson, Rennie and Wright's 1997 and 1998 papers, [16], [17], they model the cortex as interactions between *excitatory* and *inhibitory* neuron populations, *e, i* respectively. By making a continuum approximation they consider local mean values of parameters averaged over many neurons. Their model focuses on the changes in mean membrane potential, V_j, and mean firing rate, Q_j, within a population.

In their model, due to the assumption of the unimodal distribution of threshold potentials the mean firing rate within the population is given as a sigmoid function,

$$Q_j = \frac{1}{1 + e^{-C(V_j - V_0)}} \tag{3.25}$$

where C is a positive constant controlling the width of the threshold distribution and V_0 is the mean value of the threshold potential.

Assuming that each synaptic input sums independently, Robinson *et al.* define the mean membrane potential, V_j as the convolution of a post-synaptic potential with the rate of arriving action-potentials,

$$V_{e,i}(\mathbf{r}, t) = g \int_{-\infty}^{t} w(t - t') Q_{ae,ai}(\mathbf{r}, t') dt' \tag{3.26}$$

where $Q_{aj}(\mathbf{r}, t)dt'$ represents the action potentials arriving at a j-type neuron located at $\mathbf{r}$ during the interval $t \to t + dt'$, and $gw(t)$ is the post-synaptic potential.

Robinson *et al.* define $w(t)$ as the impulse response function of the post-synaptic membrane with a characteristic width ≈ 10 ms and $\int_0^\infty w(t)dt = 1$. They go on to suggest a suitable choice for the response function,

$$w(t) = \begin{cases} \frac{\alpha\beta}{\beta - \alpha}[e^{-\alpha t} - e^{-\beta t}], & \beta \neq \alpha \\ \alpha^2 t e^{-\alpha t}, & \alpha = \beta \end{cases} \tag{3.27}$$

Their choice for the response function simplifies Eq. (3.26) for $\beta \neq \alpha$ enabling it to be split into two ordinary differential equations by introducing auxiliary potentials $U_{e,i}$ and $W_{e,i}$ where

$$U_{e,i}(\mathbf{r},t) = \int_{-\infty}^{t} e^{-\alpha(t-t')} Q_{ae,ai}(\mathbf{r},t')dt' \tag{3.28}$$

$$W_{e,i}(\mathbf{r},t) = \int_{-\infty}^{t} e^{-\beta(t-t')} Q_{ae,ai}(\mathbf{r},t')dt' \tag{3.29}$$

substituting Eqs. (3.28–3.29) into Eq. (3.26) gives,

$$V_{e,i}(\mathbf{r},t) = g\frac{\alpha\beta}{\beta-\alpha}\left[U_{e,i}(\mathbf{r},t) - W_{e,i}\right]. \tag{3.30}$$

Considering the second case from Eq. (3.27) where $\alpha = \beta$, Robinson *et al.* apply Fourier theory to produce an equation working directly with $V_{e,i}$ (or simply differentiating twice with respect to time),

$$\left(\frac{d^2}{dt^2} + 2\alpha\frac{d}{dt} + \alpha^2\right) V_{e,i}(\mathbf{r},t) = g\alpha^2 Q_{e,i}(\mathbf{r},t). \tag{3.31}$$

An important feature of the Robinson *et al.* model is the description of outgoing pulses of activity from each neuron by a wave equation. Assuming the isotropic distribution of axons exponentially decreasing as a function of radial distance and a pulse velocity v, their model description of these waves is,

$$\left(\frac{\partial^2}{\partial t^2} + 2\gamma_{e,i}\frac{\partial}{\partial t} + \gamma_{e,i}^2 - v^2\nabla^2\right) = \gamma_{e,i} Q_{e,i} \tag{3.32}$$

Robinson *et al.* define the incident action-potentials $Q_{ae,ai}$ at a given location to be comprised

of contributions from the wave potentials $\phi_{e,i}$ and sub-cortical inputs ϕ_s. The equations for this are,

$$Q_{ae} = a_{se}\phi_s + a_{ee}\phi_e - a_{ie}\phi_i \tag{3.33}$$

$$Q_{ai} = a_{si}\phi_s + a_{ei}\phi_e - a_{ii}\phi_i \tag{3.34}$$

where the a_{mn} are the fractional synaptic densities associated with the excitatory, inhibitory and sub-cortical inputs.

Note the formalism used here reads left to right, i.e. a $\rightarrow$ b, this is the opposite to that used by Robinson *et al.*

3.6 Liley, Cadusch, Wright, 1998, 99, 2001

In the Liley, Cadusch and Wright 1998, 99 papers, [11], [12] and later in the Liley, Cadusch and Dafilis 2001 paper [10], a spatially-averaged model of the cortex is presented. Their model focuses on a macroscopic description of electro-cortical activity that is easily relatable to electroencephalographic (EEG) data.

Their model consists of two functionally distinct homogeneous excitatory and inhibitory neuronal sub-populations, i.e. $j, j' \in \{e, i\}$. They consider interactions between these two populations as either cortico-cortical (long-range) or intra-cortical (short-range). The cortico-cortical connections are exclusively excitatory neurons terminating on both excitatory *and* inhibitory neurons. The density of the cortico-cortical connections drops off exponentially from the target neuron. The intra-cortical connections (local) include all possible combinations between neuron types, i.e. $e \rightarrow e$, $e \rightarrow i$, $i \rightarrow e$ and $i \rightarrow i$

Liley *et al.* define mean membrane potentials, h_j, and mean firing rates, S_j, for a j-type neuron, restricting any significant change over characteristic scales of intra-cortical connectivity (spatial

coarse graining). Using *RC* circuit theory Liley *et al.* define equations for the time derivatives of the membrane potentials,

$$\tau_j \frac{\partial h_j}{\partial t} = h_j^{\text{rest}} - h_j + \sum_{j'} \Psi_{j'j}(h_j) I_{j'j} \tag{3.35}$$

where τ_j is the mean membrane time constant and $I_{j'j}$ corresponds to the mean synaptic membrane potential source of a j-type neuron.

$$\left(\frac{\partial}{\partial t} + \gamma_{ej}\right)^2 I_{ej}(x,t) = e\Gamma_{ej}\gamma_{ej}[N_{ej}^{\beta} S_e(h_e) + \phi_j(x,t) + p_{ej}(x,t)] \tag{3.36}$$

$$\left(\frac{\partial}{\partial t} + \gamma_{ij}\right)^2 I_{ij}(x,t) = e\Gamma_{ij}\gamma_{ij}[N_{ij}^{\beta} S_i(h_i) + p_{ij}(x,t)] \tag{3.37}$$

$\Psi_{j'j}$ are reversal potential functions incorporating the notion that the average magnitude of post synaptic current flow in response to synaptic activity is dependent on the present mean soma membrane potential. This idea is covered in detail in Chapter 4. Liley *et al.* model this feature by,

$$\Psi_{j'j} = \frac{(h_{j'j}^{\text{eq}} - h_j)}{|h_{j'j}^{\text{eq}} - h_j^{\text{rest}}|} \tag{3.38}$$

where $h_{j'j}^{\text{eq}}$ is the reversal (Nernst or equilibrium) potential associated with the interaction of j'-type with j-type neuron populations and h_j^{rest} is the membrane potential of a j-type neuron removed from external inputs.

Liley *et al.* also define a function for mapping the mean population firing rate to the mean membrane potential. They follow Wilson and Cowan [26] assuming that the fraction of neurons above threshold will be equal to the definite integral of a normal distribution.

$$S_j(h_j) = \frac{S_j^{\max}}{1 + \exp(-\sqrt{2}(h_j - \overline{\mu_j})/\sigma_j)} \tag{3.39}$$

3.7 Summary

Beurle (1956) [2]

- Earliest mean-field model of the cortex
- Considered membrane thresholds for neuron firing and connectivity functions that exponentially deacy with radial distance
- Independent summation of inputs at the synapse
- Assumed a refractory period during which a neuron is insensitive to synaptic activity
- Excludes inhibitory neurons.

Griffith (1963) [7]

- Incorporates inhibitory terms in the neural mass which leads to the prediction of stable equilibrium states.

Wilson and Cowan (1972,73) [26] [27]

- Model focuses on mean membrane potential and the proportion of active neurons.
- Used temporal coarse graining to simplify their equations, showing no loss of significant dynamics
- Inhibition is assume to be localized, exponentially decreasing with radial distance item
- Predicts stable steady states of their cortical model.

Nunez (1995) [15]

- Investigated simplified versions of his equations by linearizing about steady states.
- Considered boundary conditions generating standing waves of long wavelength for certain wave numbers.
- Multiple cortico-cortical connections considered with varying propagation velocities and connectivity functions.

- Neglects local delays but includes cortico-cortical axonal delays
- Predicts both travelling and standing wave activity.

Robinson *et al.* (1997, 98) [16] [17]

- Model based on the work of Wilson and Cowan, Liley *et al*, Freeman
- Developed a novel post synaptic potential function
- Wave equation describing outward pulses of activity
- Predicts three root region containing one unstable state, a stable low-firing state and a stable high-firing or 'seizing' state.

Liley *et al.* (1998, 99, 2001) [11] [12] [10]

- Considered the response of a post-synaptic neuron to synaptic activity to be dependent on present membrane potentials, i.e. reversal potentials
- Used spatial coarse graining
- Inhibitory interactions considering exclusively internal to the macrocolumn
- Excitatory interactions are both internal and inter-macrocolumn.

Steyn-Ross *et al.* (1999),(2004) [20] [22]

- Detailed definition of the macrocolumn
- Focuses on soma potential
- Model effect of anesthesia as a change in the inhibitory rate constant, corresponding to the temporal lengthening of the inhibitory post-synaptic potentials
- Introduce stochastic terms describing non-specific noise entering the macrocolumn from subcortical structures, ignore noise in the long range cortico-cortical equations
- Maximum population firing rates on the order of 1000 s^{-1}, lowered to 60 s^{-1} in 2004 paper
- Prediction of three distinct regions of steady states; low firing, high firing, and a region containing three steady states, two of which are stable.

Chapter 4

An Isolated Cortex

4.1 A Mean-field Cortex

We consider a model of the cortex that focuses on the average values of membrane potential and neuron firing rate, V_k and Q_k where k is an index representing excitatory ($k = e$) or inhibitory ($k = i$) neuron groups, respectively, within a small population of neurons called the *macrocolumn* (Fig. 2.5). In this chapter we isolate the cortex from any time-dependent stimulating structures and investigate its equilibrium states and global dynamics during numerical simulation.

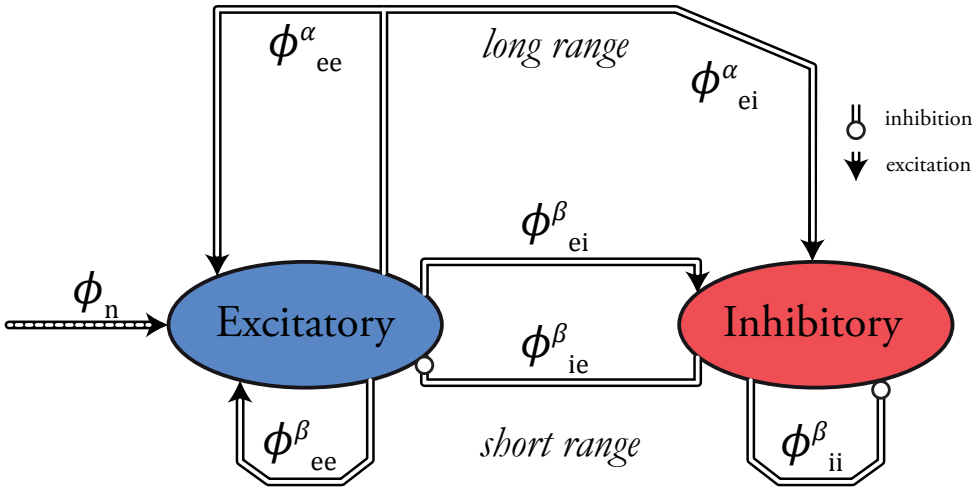

Figure 4.1: Relational diagram of interacting flux terms for the isolated cortical model. Subscripts describe the neuron groups interacting, reading left to right, i.e. a $\rightarrow$ b. Superscripts describe the range of an interaction, i.e. α - long range and β - short range.

4.2 The Cortical Model

The mathematical structure of this mean-field model of the cortex is based on the work of Steyn-Ross *et al* 1999 [20] and Liley *et al* 2001 [10].

The model focuses of two neuron types: the *excitatory* population and the *inhibitory* population. The soma voltage of these neuron populations will, in the absence of any synaptic inputs, tend towards their *resting voltage* $V_k^{\text{rest}} \approx -64$ mV. This potential is achieved by the actions of the cell's ionic pumps maintaining Na^+ and K^+ concentration differentials across the cells membrane.

Any spike activity received at the dendritic tree will be integrated at the soma forcing a time-dependent perturbation from the cell's rest potential V_k^{rest},

$$V_k(t) = V_k^{\text{rest}} + \int_{-\infty}^{t} L_k(t-t')[E_k(t') + I_k(t')]dt', \qquad k = e, i \tag{4.1}$$

where the $L_k(t)$ is the impulse response of the soma:

$$L_k(t) = \begin{cases} \frac{1}{\tau_k} e^{-t/\tau_k}, & t \geq 0 \\ 0, & t < 0 \end{cases} \tag{4.2}$$

see Fig 4.2.

The $E_k(t)$ and $I_k(t)$ terms in Eq. (4.1) are the respective time-varying voltage inputs to the soma arising from both excitatory and inhibitory neural activity. Each can be expressed as the product of a synaptic strength ρ [mV·s], a reversal potential function [dimensionless] and an input flux rate Φ [spikes/s],

$$E_k(t) = \rho_e \psi_{ek} \Phi_{ek}(t), \quad (\rho_e > 0) \tag{4.3}$$

$$I_k(t) = \rho_i \psi_{ik} \Phi_{ik}(t), \quad (\rho_i < 0) \tag{4.4}$$

4.2.1 Reversal Potentials

For a single-ion system in a biological membrane the *reversal potential* (also known as the Nernst potential) is numerically identical to the equilibrium potential. They both describe the point of zero net ion flow through the membrane. At a chemical synapse the post-synaptic neuron's reversal potential is the value of the membrane potential which causes zero net ion flow; flow direction is reversed either side of this point. At this potential, the arrival of neurotransmitters to the receptor ion channel would not result in any net ion flow through the channel.

As there are multiple ionic channel types for a neuron, the reversal potential and the equilibrium potential are no longer synonymous. A membrane potential for which the summation of the ionic currents is zero corresponds to a reversal potential as the current direction is reversed either side of this point. But this is not a true equilibrium potential however, as not all the ions and in some cases none are in equilibrium and therefore have net fluxes across the membrane. [Reference]

The effect of incoming spike activity on a post-synaptic neuron membrane potential depends on the membrane potential, V, in particular, on how far the potential is from its reversal value, $(V^{\text{rev}} - V)$. A large difference means spike events will be more effective at transferring charge

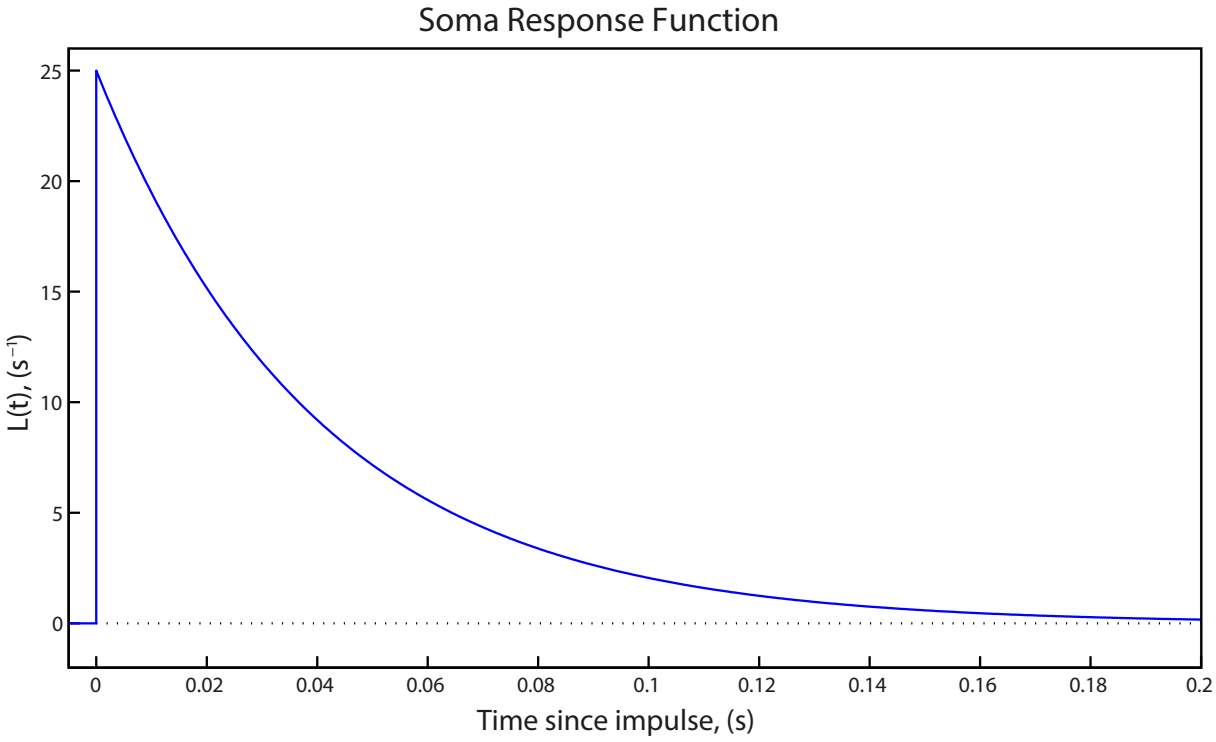

Figure 4.2: The response of a neuron to the arrival of a spike at its soma, $L(t) = \frac{1}{\tau} e^{-t/\tau}$ for $\tau = 40$ ms. The impulse response has unit area: $\int_0^\infty L(t)dt = 1$.

across the membrane and causing a voltage perturbation response in the post-synaptic neuron. This sensitivity is driven to zero as V approaches V^{rev} as illustrated in Fig. 4.3.

For the cortex, the reversal potential functions are written in the following normalized form [10],

$$\psi_{jk} = \frac{V_j^{\text{rev}} - V_k(t)}{V_j^{\text{rev}} - V_k^{\text{rest}}}, \qquad j,k = e,i \tag{4.5}$$

where $V_e^{\text{rev}} = 0$ mV for the excitatory receptors, and $V_i^{\text{rev}} = -70$ mV for inhibitory receptors; see Fig 4.3.

An incoming spike (action potential) causes a release of neurotransmitters into the synaptic cleft separating pre- and post-synaptic neurons. This allows charge transfer via membrane ion channels and a brief change in the voltage of the post-synaptic neuron. This momentary change in membrane potential defines the *dendrite impulse response function* and is represented by an *alpha*-function,

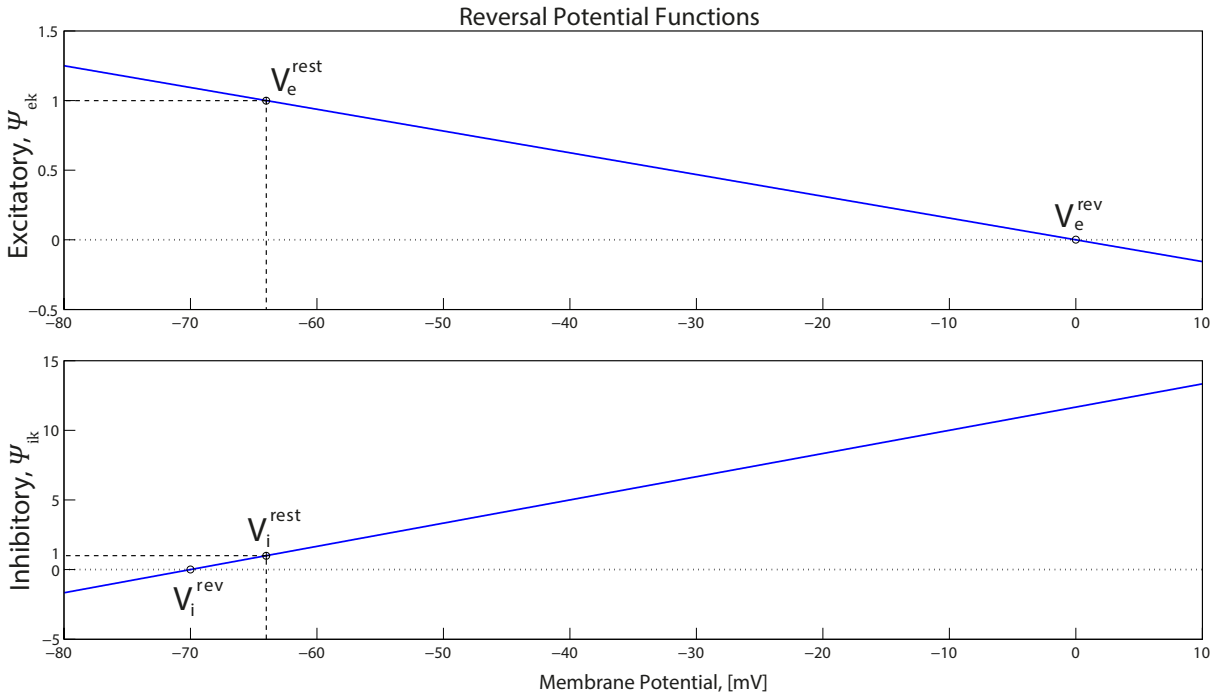

Figure 4.3: The reversal potential functions of Eq. (4.5) scale input fluxes entering a neuron based on the neuron's proximity to its resting and reversal potentials

$$H_{jk}(t) = \begin{cases} t\gamma_{jk}^2 e^{-t\gamma_{jk}}, & t \geq 0 \\ 0, & t < 0 \end{cases} \tag{4.6}$$

where γ_{jk} is the rate constant in s^{-1} whose inverse gives the rise time to peak; see Fig. 4.4.

The total excitatory and inhibitory input flux, Φ_{jk}, to a neuron k is written as a temporal convolution of the dendrite impulse response function $H(t)$ with the per-synapse spike-rate ϕ_{jk}. The spike rates are then scaled by the number of one-way $j \to k$ synaptic connections N_{jk},

$$\Phi_{ek}(t) = \int_{-\infty}^{t} H_{ek}(t-t') \left[N_{ek}^{\alpha} \phi_{ek}^{\alpha}(t') + N_{ek}^{\beta} \phi_{ek}^{\beta}(t') + \phi_{ek}^{\mathrm{sc}} \right] dt', \qquad k = e, i \tag{4.7}$$

$$\Phi_{ik}(t) = \int_{-\infty}^{t} H_{ik}(t-t') \left[N_{ik}^{\beta} \phi_{ik}^{\beta}(t') + \phi_{ik}^{\mathrm{sc}} \right] dt' \tag{4.8}$$

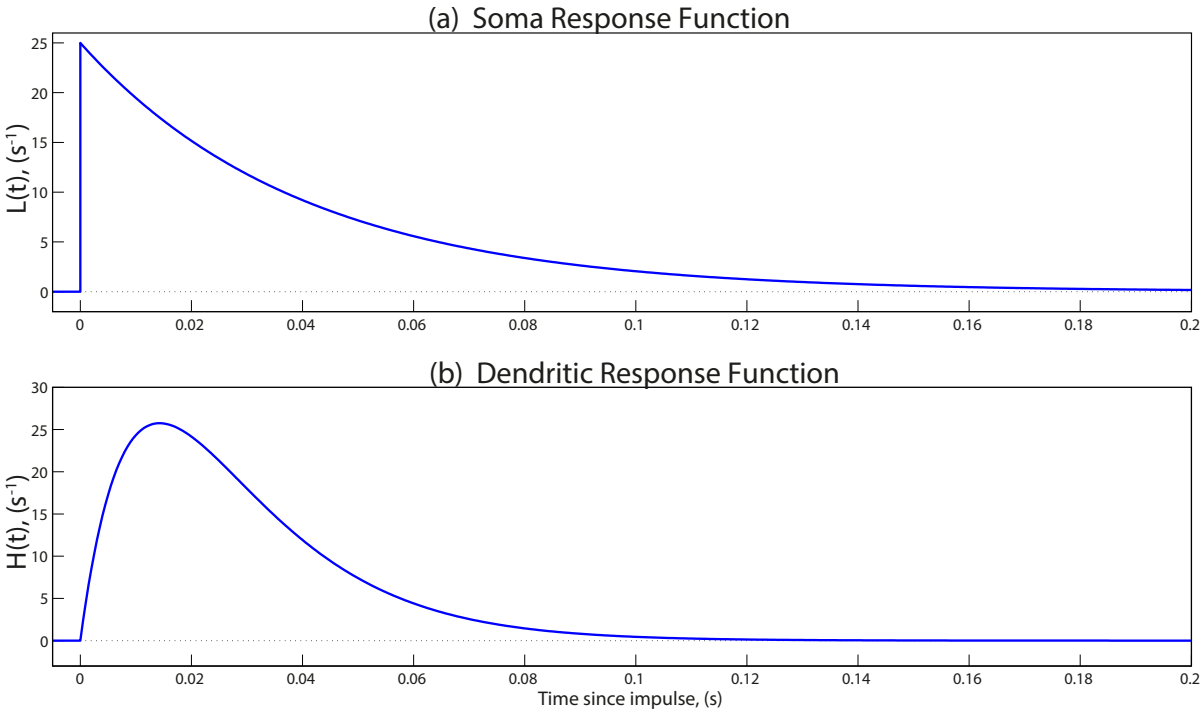

Figure 4.4: Comparison between impulse response of (a) soma and (b) dendrite of post-synaptic neuron. Here $\gamma = 70\ \mathrm{s}^{-1}$ and $\tau = 40$ ms

where the subscripting is read left to right, thus N_{ab} means the number of connections from a to b.

The superscripts in Eq. (4.7) identify flux contributions from *local* (β, within the macrocolumn), *distant* (α, excitatory input from other columns) and *subcortical* (sc, stimulation from subcortical structures). It is important to note that there is no long-range inhibitory flux term, ϕ^{α}_{ik} in Eq. (4.8) because inhibitory neurons have short axons [3].

Following Robinson's 1997 paper [16], we assume an isotropic distribution of axons in a continuum approximation with a characteristic axonal propagation velocity v. The outward propagation of a pulse generated by a source Q_e is modelled as a two-dimensional damped wave equation,

$$\left[\left(\frac{\partial}{\partial t} + v\Lambda_{ek}\right)^2 - v^2\nabla^2\right]\phi^{\alpha}_{ek}(\mathbf{r},t) = v^2\Lambda^2_{ek}Q_e(\mathbf{r},t) \tag{4.9}$$

where ϕ^{α}_{ek} are the long range excitatory flux terms and $\mathbf{r}$ represents position in 2-D space. Λ_{ek} are the inverse-length scales for long-range axonal connections, and ∇^2 is the Laplacian operator, $\nabla^2 = \partial^2/\partial x^2 + \partial^2/\partial y^2$.

The subcortical terms, ϕ^{sc}_{jk} represent fluxes entering the cortex from subcortical structures. In Ch. 6 we will use these terms to carry input from the thalamus to the cortex as well as incoming noise, however for the isolated cortical model we set these fluxes to a constant. Consideration was given to removing these terms from the flux equations altogether but we intend to use this model of the cortex for comparison with a cortico-thalamic system in which these terms will be non-zero and time-dependent so their exclusion could significantly alter the dynamics. For the isolated cortex they act as a 'DC-like' offset describing a static input entering the macrocolumn from unspecified subcortical structures ($\phi^{\mathrm{sc}}_{ek} = 40\ \mathrm{s}^{-1}$, $\phi^{\mathrm{sc}}_{ik} = 30\ \mathrm{s}^{-1}$).

Four second-order differential equations for the rate-change of the Φ_{jk} input flux terms are produced by twice differentiating the four dendrite convolution equations (4.7–4.8). The excitatory and inhibitory population inputs are,

$$\left(\frac{d}{dt}+\gamma_{ee}\right)^2\Phi_{ee}=\gamma_{ee}^2\left[N_{ee}^{\alpha}\phi_{ee}^{\alpha}(t)+N_{ee}^{\beta}\phi_{ee}^{\beta}(t)+\phi_{ee}^{\mathrm{sc}}\right] \tag{4.10}$$

$$\left(\frac{d}{dt}+\gamma_{ie}\right)^2\Phi_{ie}=\gamma_{ie}^2\left[N_{ie}^{\beta}\phi_{ie}^{\beta}(t)\right] \tag{4.11}$$

$$\left(\frac{d}{dt}+\gamma_{ei}\right)^2\Phi_{ei}=\gamma_{ei}^2\left[N_{ee}^{\alpha}\phi_{ei}^{\alpha}(t)+N_{ei}^{\beta}\phi_{ei}^{\beta}(t)+\phi_{ei}^{\mathrm{sc}}\right] \tag{4.12}$$

$$\left(\frac{d}{dt}+\gamma_{ii}\right)^2\Phi_{ii}=\gamma_{ii}^2\left[N_{ii}^{\beta}\phi_{ii}^{\beta}(t)\right] \tag{4.13}$$

By taking the time derivatives of the $k=e,i$ convolutions from equation (4.1) a pair of first-order differential equations for the macrocolumn-averaged excitatory and inhibitory membrane potentials, V_e and V_i, is obtained,

$$\tau_e\frac{dV_e(t)}{dt}=V_e^{\mathrm{rest}}-V_e(t)+\rho_e\psi_{ee}\Phi_{ee}(t)+\rho_i\psi_{ie}\Phi_{ie}(t) \tag{4.14}$$

$$\tau_i\frac{dV_i(t)}{dt}=V_i^{\mathrm{rest}}-V_i(t)+\rho_e\psi_{ei}\Phi_{ei}(t)+\rho_i\psi_{ii}\Phi_{ii}(t) \tag{4.15}$$

where ρ_e,ρ_i are the synaptic strengths with $\rho_e>0$ (excitation) and $\rho_i<0$ (inhibition). These strengths are represented as the product of a synaptic gain and a dimensionless scaling parameter, λ_k, defined in Sec. 4.2.2.

It is important to note that we have ignored spatial terms here for simplicity and also a coarse-graining limit of the short-range fluxes has been applied, i.e., $\phi_{eb}^{\beta}(t)\to Q_e(t)$ and $\phi_{ib}^{\beta}(t)\to Q_i(t)$.

Table 4.1: Cortical Model Parameters

Symbol	Description	Value	Unit
$\tau_{e,i}$	neuron time-constant	$0.040, 0.040$	s
$V_{e,i}^{\text{rev}}$	reversal potential at dendrite	$0, -70$	mV
$V_{e,i}^{\text{rest}}$	neuron resting potential	$-64, -64$	mV
$\rho_{e,i}^{0}$	non-scaled synaptic gain	1×10^{-3}, -1.05×10^{-3}	mVs
$\gamma_{ek,ik}^{0}$	non-scaled rate-constant	170, 50	s^{-1}
N_{ee}^{α}, N_{ee}^{β}	number of long/short range connections e $\to$ e	2000, 800	–
N_{ei}^{α}, N_{ei}^{β}	number of long/short range connections e $\to$ i	2000, 800	–
N_{ie}^{β}	number of short range connections i $\to$ e	600	–
N_{ii}^{β}	number of short range connections i $\to$ i	600	–
ϕ_{ee}^{sc}, ϕ_{ei}^{sc}	sub–cortical constant stimulus	$30, 40$	s^{-1}
$Q_{e,i}^{\max}$	maximum firing rates	30, 60	s^{-1}
$\theta_{e,i}$	sigmoid threshold voltage	$-58.5, -58.5$	mV
$\sigma_{e,i}$	standard deviation from threshold	$3, 5$	mV
c	sigmoid scaling constant	$\pi/\sqrt{3}$	–

4.2.2 Anaesthetic Effect

Inductive anaesthetics, such as isoflurane and propofol, are known to strongly increase the effect of inhibitory neurons. Clinical levels of propofol have been shown to have little effect on excitatory synapses and instead has a primary effect of lengthening the inhibitory response decay time without changing its peak amplitude [8].

We incorporate this feature into our model, based on Steyn-Ross *et al.* [20], by scaling the inhibitory rate constants in the dendrite response functions, Eq. (4.6). We introduce a dimensionless scale-factor, λ_k, to scale both the rate constants, γ_{jk} and the synaptic gains, ρ_k,

$$\gamma_{ek} = \gamma_{ek}^{0}/\lambda_e, \qquad \gamma_{ik} = \gamma_{ik}^{0}/\lambda_i \tag{4.16}$$

where $\gamma_{ek}^{0} = 170\ \text{s}^{-1}$ and $\gamma_{ik}^{0} = 50\ \text{s}^{-1}$, and

$$\rho_e = \lambda_e \rho_e^{0}, \qquad \rho_i = \lambda_i \rho_i^{0} \tag{4.17}$$

where $\rho_e^0 = 1 \times 10^{-3}$ mV·s, $\rho_i^0 = -1.05 \times 10^{-3}$ mV·s. In this thesis we will assume no anaesthetic effect on excitatory synapses and set $\lambda_e = 1$.

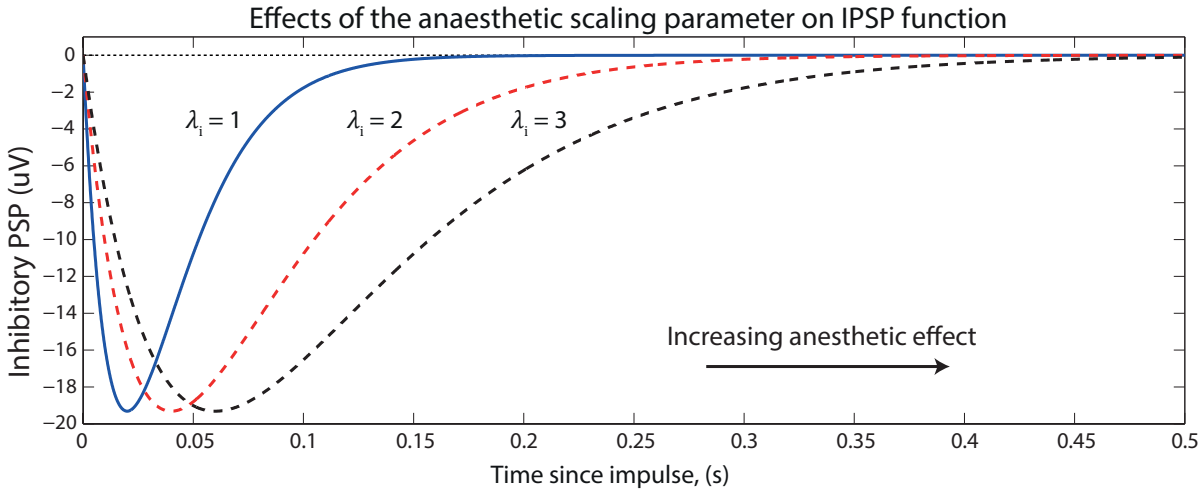

Figure 4.5: Effect of increasing the anaesthetic scaling parameter, λ_i, on the inhibitory post-synaptic potential function. The function is the product of the inhibitory synaptic gain and the dendrite response function Eq. (4.6), i.e. $\rho_i H_{ik}(t)$

The cortical model described consists of 8 differential equations which can be represented by 14 first-order coupled equations detailed in Sec 4.3.2.

4.2.3 Sigmoidal Mapping

It is well known that the firing rate of a neuron at the axon is an increasing function of the membrane potential at the soma [10]. It can, however, be extremely difficult to deduce a relationship directly mapping membrane potential to firing rate due to the nonlinearity of the relationships (multiple time-varying threshold/trigger points). Real though this obstacle is for networks of 10–100 neurons, when considering populations on the scale of a neural mass such is the macrocolumn containing, say, $\sim 10^4$ neurons, many of these difficulties can be overcome, as slowly-varying time averages can be replaced by spatial averages. An association between a *mean* firing rate of the macrocolumn can be mapped to spatial *mean* of membrane potentials within the column. Wilson and Cowan noted this in their 1972 paper [26] and set about deriving this mean mapping function. The functions proposed here follow the Robinson [16] form,

$$Q_e(t) = \frac{Q_e^{\max}}{1 + e^{-c(V_e(t) - \theta_e)/\sigma_e}} \tag{4.18}$$

$$Q_i(t) = \frac{Q_i^{\max}}{1 + e^{-c(V_i(t) - \theta_i)/\sigma_i}} \tag{4.19}$$

and their inverted forms,

$$V_e(t) = -\frac{\sigma_e}{c} \ln \left[\frac{Q_e^{\max}}{Q_e(t)} - 1 \right] + \theta_e \tag{4.20}$$

$$V_i(t) = -\frac{\sigma_i}{c} \ln \left[\frac{Q_i^{\max}}{Q_i(t)} - 1 \right] + \theta_i \tag{4.21}$$

4.3 Analysis

The equilibrium or stationary states of a system are points where the system will remain *static* in the absence of external stimulus. Locating these reference *static* states is essential for understanding the system's *dynamical* behaviour and the prediction of its behaviour at some later

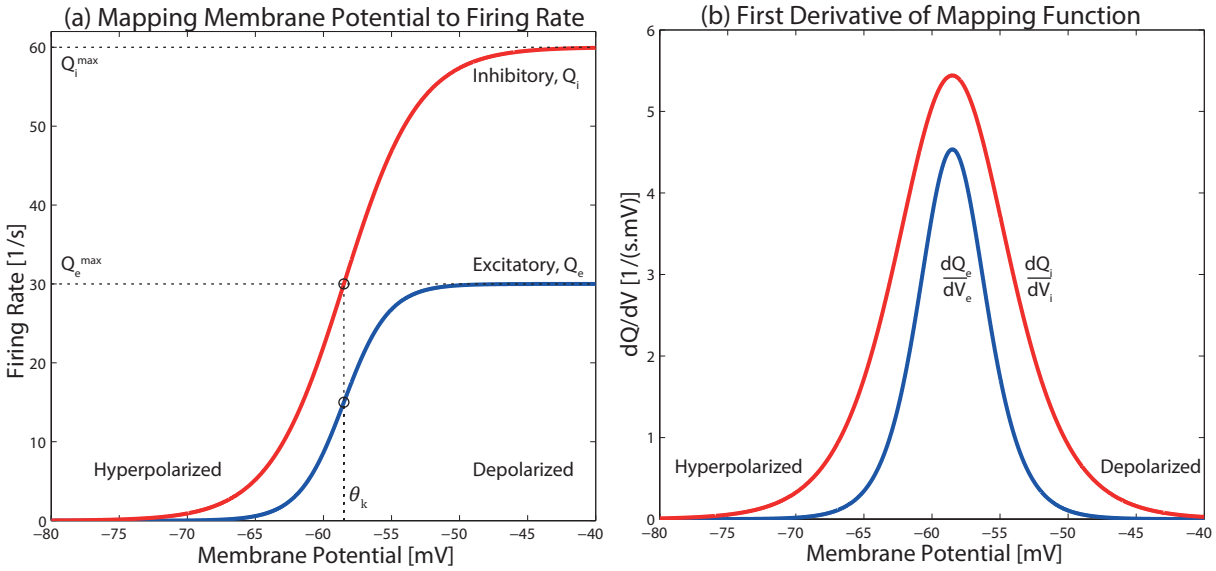

Figure 4.6: (a) The sigmoidal mapping from membrane potential to firing rate and (b) the first derivatives of these functions. θ_k is the threshold voltage for half the maximum firing rate, $Q_k^{\max}$ and is also the point maximum sensitivity to voltage change shown by the peak in (b).

time $t+dt$. Equilibrium states are said to be either *stable* or *unstable* depending on the system's response to a small perturbation away from equilibrium.

The equilibrium solutions of a rigid-arm simple pendulum, for example, are positions of the pendulum where it is neither moving nor accelerating, so is in a static time-independent state. The right image of Figure 4.7 shows the two equilibrium states: The *bottom* state is stable and will be approached by perturbations either side of it while the *top* state is unstable as small perturbations will cause the pendulum to 'fall away' to the stable state.

4.3.1 Stationary States for Cortical Model

With the cortical equations now outlined we investigate the model's stationary states. We can locate these time-independent equilibrium solutions by setting the time derivatives of the model equations to zero and solving. Performing this operation analytically is not possible, however, due to the nonlinearity of the mapping functions, so we use an iterative numerical approach.

By substituting the input flux equations (4.10 – 4.13) into membrane potential equations (4.14

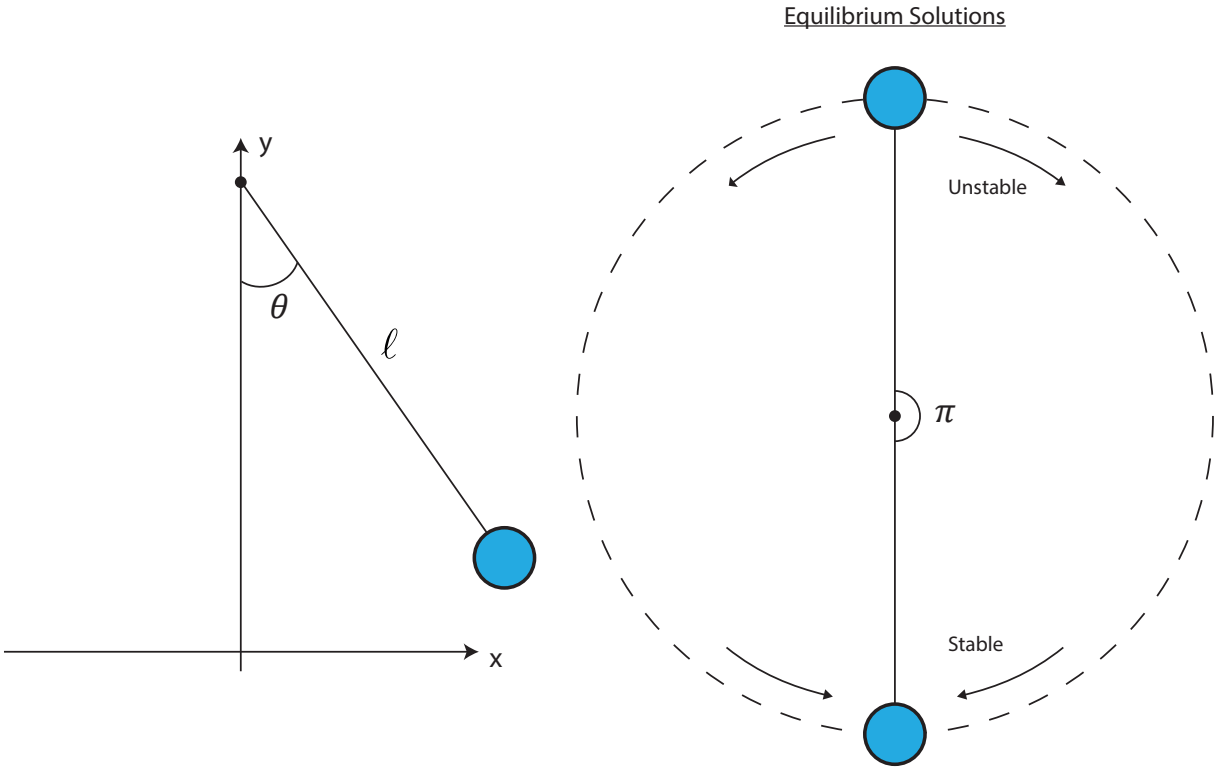

Figure 4.7: *left:* Two-dimensional rigid-arm simple pendulum. *right:* Locations of the pendulum where time-derivatives of the angular displacement function, $\theta(t)$, are zero. The top state is unstable as a small perturbation to either side will cause the pendulum arm to fall away. The bottom state is stable as the pendulum arm will approach the state when placed near it.

– 4.15) we are able to produce an expression for the mean-firing rates within the macrocolumn. The firing rate of one neuron type can now be described in terms of the membrane potential of the opposing population. [For notational simplicity (and unless otherwise stated) we will assume that all firing rates and membrane potentials in Sections 4.3.1 – 4.3.2 are at equilibrium, i.e. $Q_e = Q_e^{\text{eq}}$]

This rearrangement generates the following pair of coupled nonlinear equations for the equilibrium firing rates,

$$Q_e = f(V_i, Q_i) = \left(\frac{1}{N_{ei}}\right)\left(\frac{V_i - V_i^{\text{rest}} - \rho_i\psi_{ii}\left[N_{ii}Q_i + \phi_{ii}^{\text{sc}}\right]}{\rho_e\psi_{ei}} - \phi_{ei}^{\text{sc}}\right) \tag{4.22}$$

$$Q_i = g(V_e, Q_e) = \left(\frac{1}{N_{ie}}\right)\left(\frac{V_e^{\text{eq}} - V_e^{\text{rest}} - \rho_e\psi_{ee}\left[N_{ee}Q_e + \phi_{ee}^{\text{sc}}\right]}{\rho_i\psi_{ie}} - \phi_{ie}^{\text{sc}}\right) \tag{4.23}$$

By selecting a range of feasible excitatory firing rates, $Q_e = [0...Q_e^{\max}]$ inputting these into Eq. (4.22), and then carrying the output into Eq. (4.23) another excitatory firing rate can be produced, Q_e'. Plotting $\Delta Q_e = Q_e - Qe'$ vs Q_e in Fig. 4.8 shows x-axis intercepts which are points where the equations are consistent and correspond to Q_e equilibrium values.

This method does not give numerically exact values of these intercepts because a coarse grain for input firing rates was chosen to save computational time. Instead we utilize the `fzero()` function in MATLAB which accepts two points straddling the root, and the function that produced the bracketing pair. `fzero()` uses successive iterations to bisect the bracketing interval eventually returning an estimate for the root that is accurate to at least 15 significant figures. This is an efficient way of locating the equilibrium points as it is much less computationally expensive than choosing a very finely-spaced search region.

Figure 4.9 shows the characteristic 'S-bend' associated with a hysteresis effect. The three root region of the macrocolumn only occurs in a very narrow window of the anaesthetic parameter, suggesting the cortical model is extremely sensitive to its effects. The two lower firing roots are

lost for $\lambda_i \leq 0.91$ with only a high-firing solution remaining. This makes sense as by reducing the inhibitory anaesthetic parameter we are decreasing the effectiveness of the inhibitory neurons which in turn are responsible for maintaining a low firing rate in the excitatory neuron populations. Similarly, increasing λ_i causes the two upper roots to be lost and only low firing-rate solution is present consistent with an anaesthetic boost of the effectiveness of the inhibitory neurons.

4.3.2 Stability

To understand the stability properties of a given steady state, we compute the set of eigenvalues associated with it. The dominant eigenvalue (i.e., that which has the largest real component) provides information about models behaviour in the vicinity of or at the steady state.

We express the two long-range excitatory flux equations, Eq. (4.9), as four first-order differential equations by introducing two auxiliary variables κ_{ee}, κ_{ei} where,

$$\frac{\partial \phi^{\alpha}_{ee}}{\partial t} = \kappa_{ee}, \qquad \frac{\partial \phi^{\alpha}_{ei}}{\partial t} = \kappa_{ei}. \tag{4.24}$$

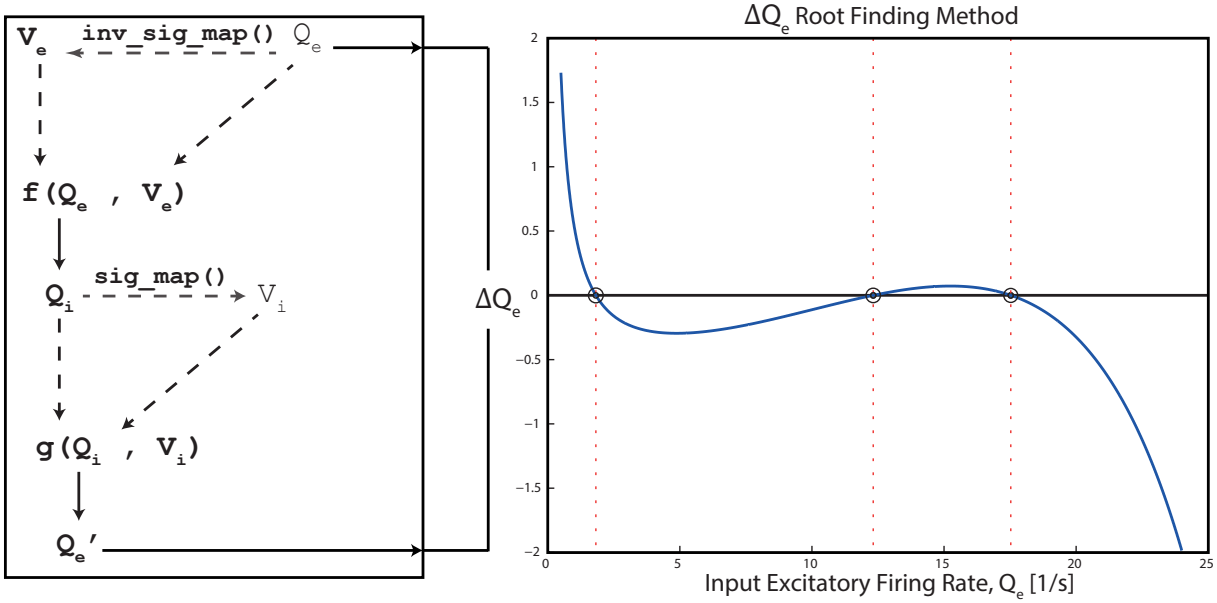

Figure 4.8: Algorithm for identifying the equilibrium values of Q_e. The left figure describes the information flow through the code that produces the plot on the right. The right figure shows the discrepancy function $\Delta Q_e = Q_e - Q'_e$ and the three points that correspond to $\Delta Q_e = 0$, locating three equilibrium value.

Substituting equations (4.24) into equation (4.9) and ignoring spatial terms gives the following,

$$\frac{\partial \kappa_{ee}}{\partial t} = (v\Lambda_{ee})^2 \left[Q_e - \phi^{\alpha}_{ee}\right] - 2v\Lambda_{ee}\kappa_{ee} \tag{4.25}$$

$$\frac{\partial \kappa_{ei}}{\partial t} = (v\Lambda_{ei})^2 \left[Q_e - \phi^{\alpha}_{ei}\right] - 2v\Lambda_{ei}\kappa_{ei}. \tag{4.26}$$

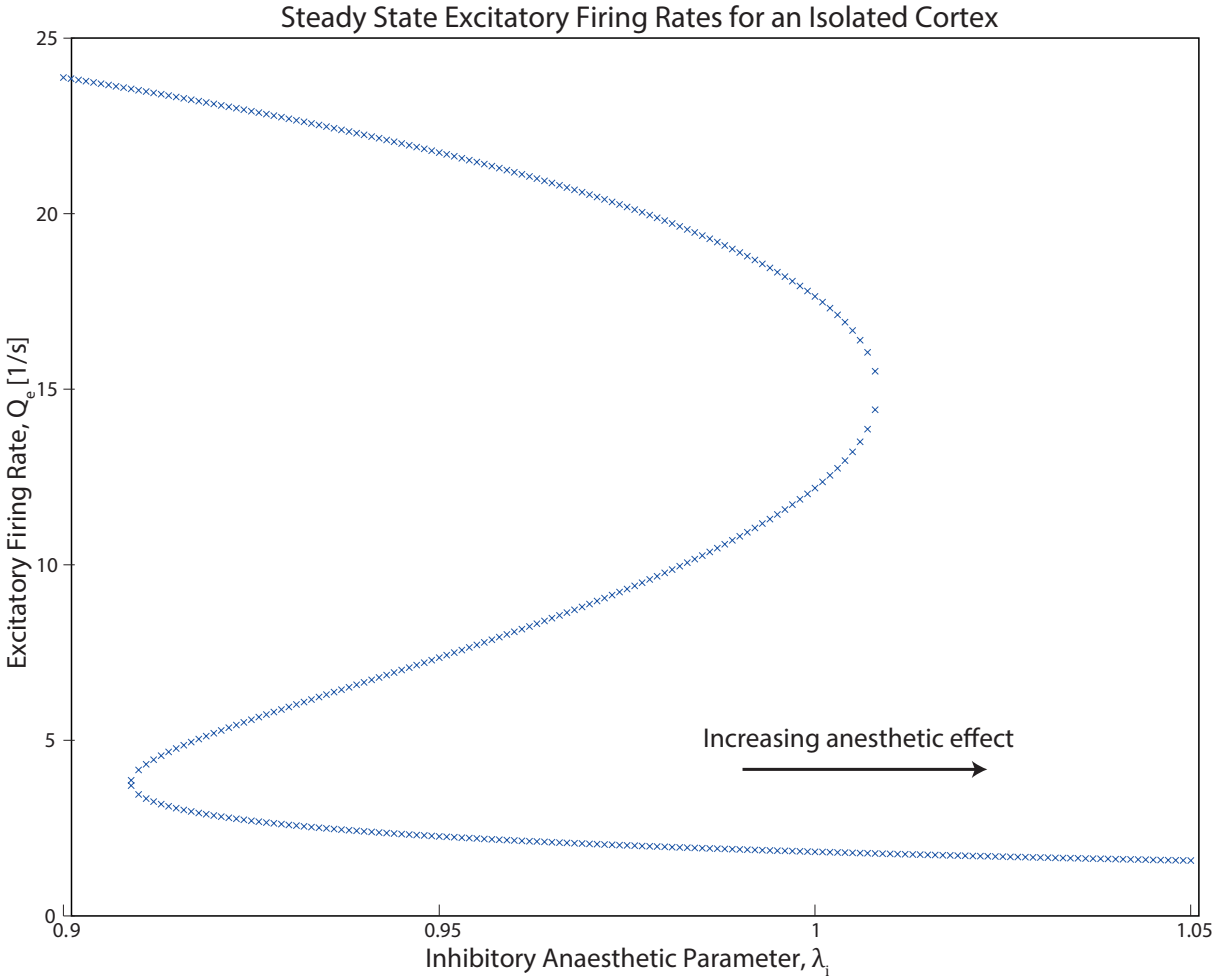

Figure 4.9: Distribution of equilibrium excitatory firing rates as a function of inhibitory anaesthetic parameter.

In a similar manner, we introduce auxiliary variables Π_{ee}, Π_{ie}, Π_{ei} and Π_{ii} for the input flux equations,

$$\frac{d\Phi_{ee}}{dt} = \Pi_{ee}, \qquad \frac{d\Phi_{ie}}{dt} = \Pi_{ie} \tag{4.27}$$

$$\frac{d\Phi_{ei}}{dt} = \Pi_{ei} \qquad \frac{d\Phi_{ii}}{dt} = \Pi_{ii} \tag{4.28}$$

giving,

$$\frac{d\Pi_{ee}}{dt} = \gamma_{ee}^2 \left[N_{ee}^{\alpha} \phi_{ee}^{\alpha} + N_{ee}^{\beta} Q_e + \phi_{ee}^{\mathrm{sc}} - \Phi_{ee} \right] \tag{4.29}$$

$$\frac{d\Pi_{ie}}{dt} = \gamma_{ie}^2 \left[N_{ie}^{\beta} Q_e + \phi_{ie}^{\mathrm{sc}} - \Phi_{ie} \right] \tag{4.30}$$

$$\frac{d\Pi_{ei}}{dt} = \gamma_{ei}^2 \left[N_{ei}^{\alpha} \phi_{ei}^{\alpha} + N_{ei}^{\beta} Q_e + \phi_{ei}^{\mathrm{sc}} - \Phi_{ei} \right] \tag{4.31}$$

$$\frac{d\Pi_{ii}}{dt} = \gamma_{ii}^2 \left[N_{ii}^{\beta} Q_e + \ phi_{ii}^{\mathrm{sc}} - \Phi_{ii} \right] \tag{4.32}$$

Thus, in the homogeneous limit, the cortical equations (4.9–4.13) are equivalent to 12 first-order differential equations (4.24–4.32). The set of eigenvalues corresponding to the steady states from Figure 4.9 can be determined by forming 14×14 Jacobian matrix of partial derivatives evaluated at each steady state, and solving the characteristic equation. The non-zero elements

of this matrix are given in Appendix A. In MATLAB , the `eig()` function enables this to be done efficiently: it takes an $n \times n$ matrix as input and returns the n eigenvalues owned by the matrix. For a given steady state of the homogeneous cortex there will be 14 eigenvalues.

If the dominant eigenvalue has a positive real component then the state is predicted to be unstable; conversely, if the real component is negative the state is predicted to be stable. The imaginary component of the eigenvalue (divided by 2π) describes the frequency of any oscillatory behaviour about the state; transitions to a stable steady state with a complex eigenvalue will manifest as damped oscillations about that steady state. An unstable state is not permanently occupiable, since even the smallest perturbation will grow with time causing the system to move elsewhere; they can, however, be useful in understanding system behaviour in the vicinity of the state.

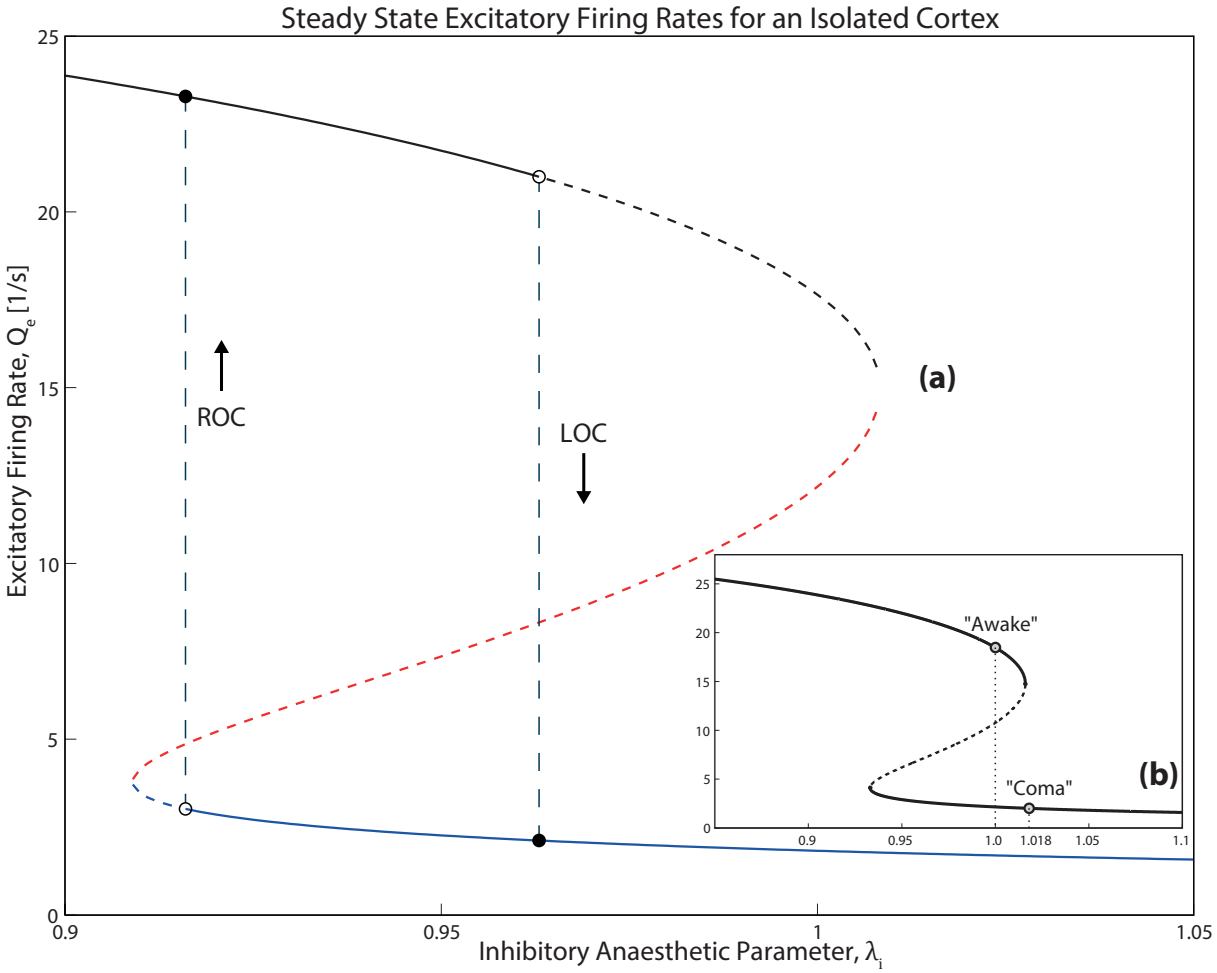

Figure 4.10: (a) Distribution and stability of equilibrium excitatory firing rates as a function of inhibitory anaesthetic parameter. Points of transition are shown where a branch of equilibrium states has become unstable, LOC - *loss of consciousness* ROC - *return of consciousness*. (b) Equilibrium curve from Steyn-Ross 2013 [21] where the upper and lower branches become unstable at the turning points.

Figure 4.10 shows the distribution of stationary-state excitatory firing rates and their stability; solid line indicates stable equilibrium, dashed line indicates unstable equilibrium.

The hysteresis S-bend is a defining feature of the cortical model and reveals the separation of the anaesthetic level required to drive the neuronal population into its low-firing "*unconscious*" (LOC) state versus the reduced level at which it returns to a high-firing "*conscious*" state (ROC). The same feature is observed clinically by anesthesiologists; however, they remain uncertain as to whether this is a unique property of cortical states or simply an artifact caused by measurement delay and indirect observations.

The location of LOC and ROC, i.e., points where the top and bottom branches transition to stable states, is a major difference from the previous Steyn-Ross [21] steady state stabilities where these points were synonymous with the two turning points of the S-bend. This is due to differences in the connection constants used to detail the flux contributions arising within the macrocolumn.

4.4 Simulation

To simulate the cortical equations we elected to use an Euler update method for the time-evolution of state parameters as this simplifies the implementation and tuning of noise entering the system. The state of the cortex is defined as a 14-element column vector

$$\text{state} = [V_e \;\; V_i \;\; \Pi_{ee} \;\; \Pi_{ie} \;\; \Pi_{ei} \;\; \Pi_{ii} \;\; \Phi_{ee} \;\; \Phi_{ie} \;\; \Phi_{ei} \;\; \Phi_{ii} \;\; \phi^{\alpha}_{ee} \;\; \kappa_{ee} \;\; \phi^{\alpha}_{ei} \;\; \kappa_{ei}]^{\mathrm{T}} . \tag{4.33}$$

Selecting the two initial membrane potentials, V_e^0, V_i^0, using parameters in Tab 4.2.1 and setting the time derivatives of the models equations to zero, we are then able to completely define an initial state of the system. We then Euler-update the state to time-step into the future,

$$\text{state}(i+1) = \text{state}(i) + \frac{d\,\text{state}(i)}{dt} * dt + \text{noise} * \sqrt{dt} \tag{4.34}$$

By selecting the total number of desired points to be simulated and the time step dt we are able to control the MATLAB loop implementing the Euler update method, Eq. (4.34), and subsequently the total amount of time simulated. We experimented with different values of dt in order to find a compromise between accuracy (small dt) and reasonable computational speeds (large dt) settling on a value where no significant change in the dynamics was observed with further reductions, $dt = 10^{-5}$ s.

The first simulations we ran had initial points set to the predicted steady states with no noise. As the simulation MATLAB code was written independently of the steady-state finding code, the simulation provided a good cross-check for consistency in the implementation of the mathematics. If the steady states are correct then, with no external noise, the state derivatives should be zero and the system will remain static.

We initialized the system to the state described by the middle branch of Fig. 4.10 setting $\lambda_i =$

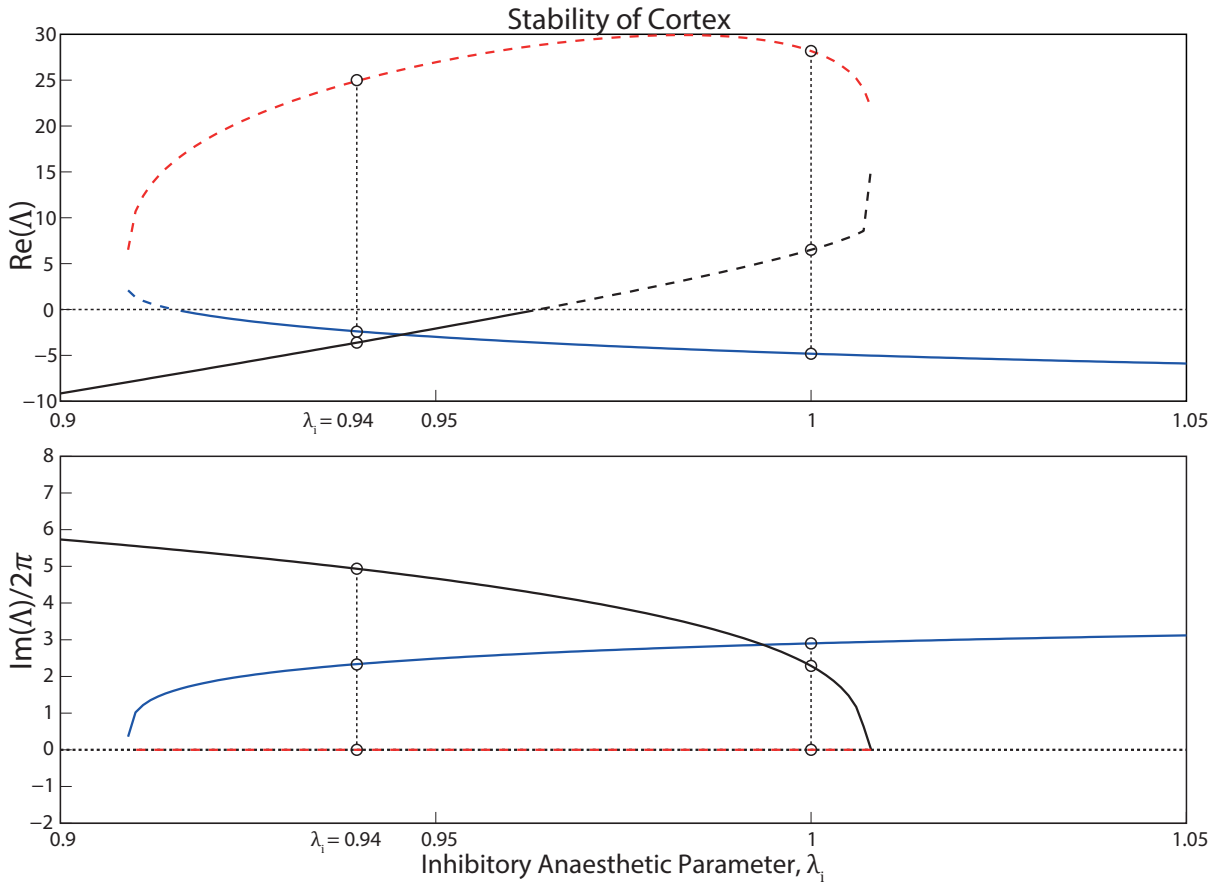

Figure 4.11: Real and Imaginary components of the dominant eigenvalues, Λ, for each of the steady states in Figure 4.10. The transition of the real component from negative to positive indicates the emergence of unstable dynamics. Here the instability of the upper and lower branches of Fig 4.10 are observed as x-axis intercepts. The imaginary component of the eigenvalue divided by 2π describes the frequency of any oscillatory dynamics near the steady state.

1 and applying noise. As predicted by the stability analysis this state is unstable and in both runs the cortical model transitioned to another steady state.

During the first experiment, Fig 4.12, the system approached the high firing steady state solution which is predicted to be unstable, it then 'fell-down' to the bottom steady state and settled with damp oscillations of ≈ 3 Hz which is correctly predicted on Fig 4.11.

The experiment in Fig 4.13 shows a brief, high firing rate, increase which then drops down to low firing state. The predicted stability for the low firing steady state is that it is unstable. The simulation then shows the system 'jump' back up to the high firing state, which is predicted to be stable and display damped oscillator dynamics of frequency ≈ 5 Hz.

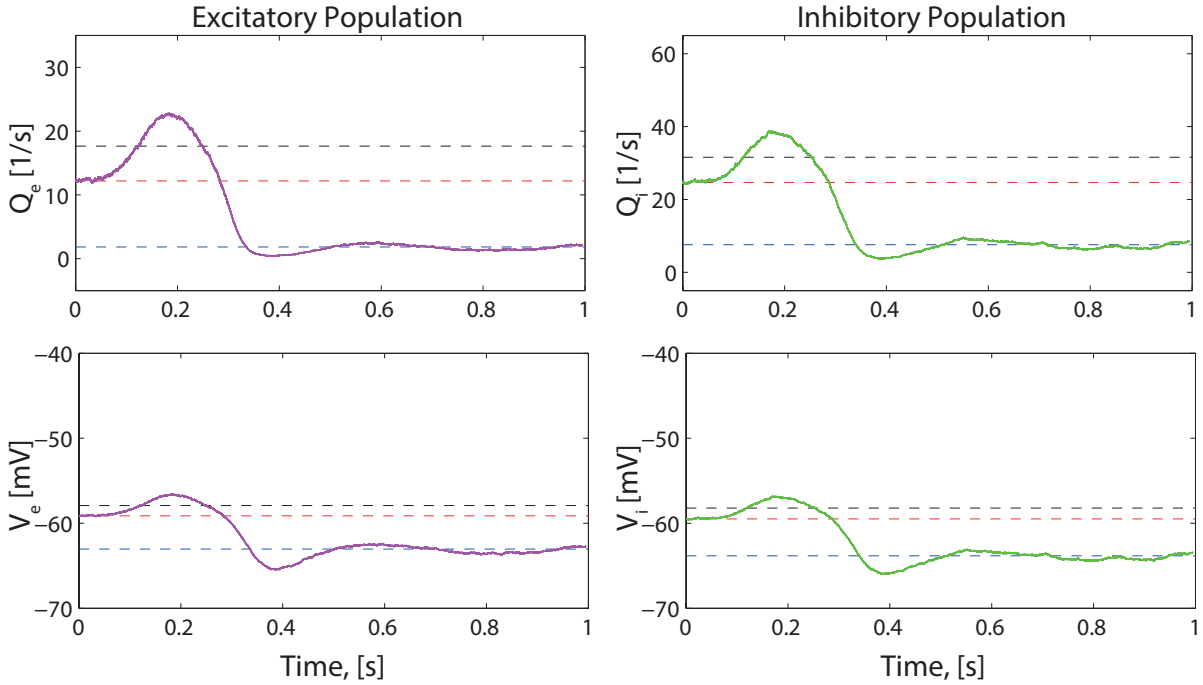

Figure 4.12: $\lambda_i = 1$. Initial state is the unstable middle branch of Fig. 4.10. Dashed lines show the upper, middle and lower branch steady states.

4.5 Conclusion

We present the mean-field cortical model outlined by Steyn-Ross *et al* 1999 [20] and Liley *et al* 2001 [10] demonstrating some of its characteristic features. A hysteresis effect is present in the steady state analysis of the model and lends weight to the argument that the hysteresis effect observed in anaesthetic application may in fact be a unique property of cortical states. With a mathematical structure describing an average neuron of the cortex, the framework has been laid

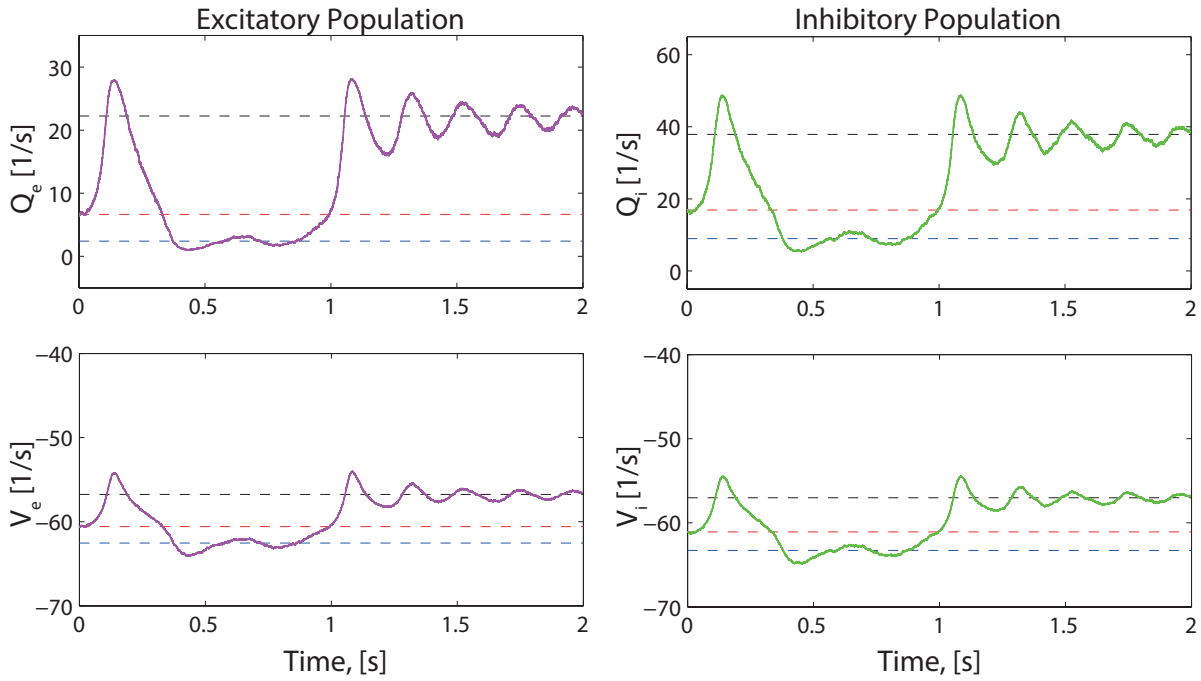

Figure 4.13: $\lambda_i = 0.94$. Initial state is the unstable middle branch of Fig. 4.10.

out for the addition of other subcortical structures and implementing a coupled thalamo-cortical system.

Chapter 5

An Isolated Thalamus

5.1 A Mean-field Thalamus

The thalamus plays a major role in the relay of information into the cerebral cortex. Sometimes termed the 'gateway' to the cortex, almost everything we perceive about the outside world is facilitated by messages passing through it. Here we propose a mean-field model of the thalamus. We investigate the behaviour of this model when isolated from all cortical and sub-cortical structures to better understand any dynamics it may contribute to the thalamo-cortical model proposed in Ch. 6.

5.2 The Thalamic Model

The general structure of this mathematical description of the thalamus provided by Prof. Moira Steyn-Ross is based on the cortical model outlined in Ch.4. However there are several key differences that distinguish this thalamic model from the cortical mean-field model; these differences are detailed below.

We have partitioned the thalamus into two distinct regions; the specific neuron population (sometimes referred to as the relay neurons) which we treat as purely excitatory to simplify the model, and the reticular neuron population which we similarly treat as having a purely inhibitory effect on post-synaptic neurons. Each of the two populations has a governing set of equations that can be distinguished by their subscript, s for *specific* neurons and r for *reticular* neurons.

As for the cortical model any spike activity received at the dendritic tree will be integrated at the soma forcing a time-dependent perturbation from the cells rest potential, $V_k^{\text{rest}} \approx -64$ mV,

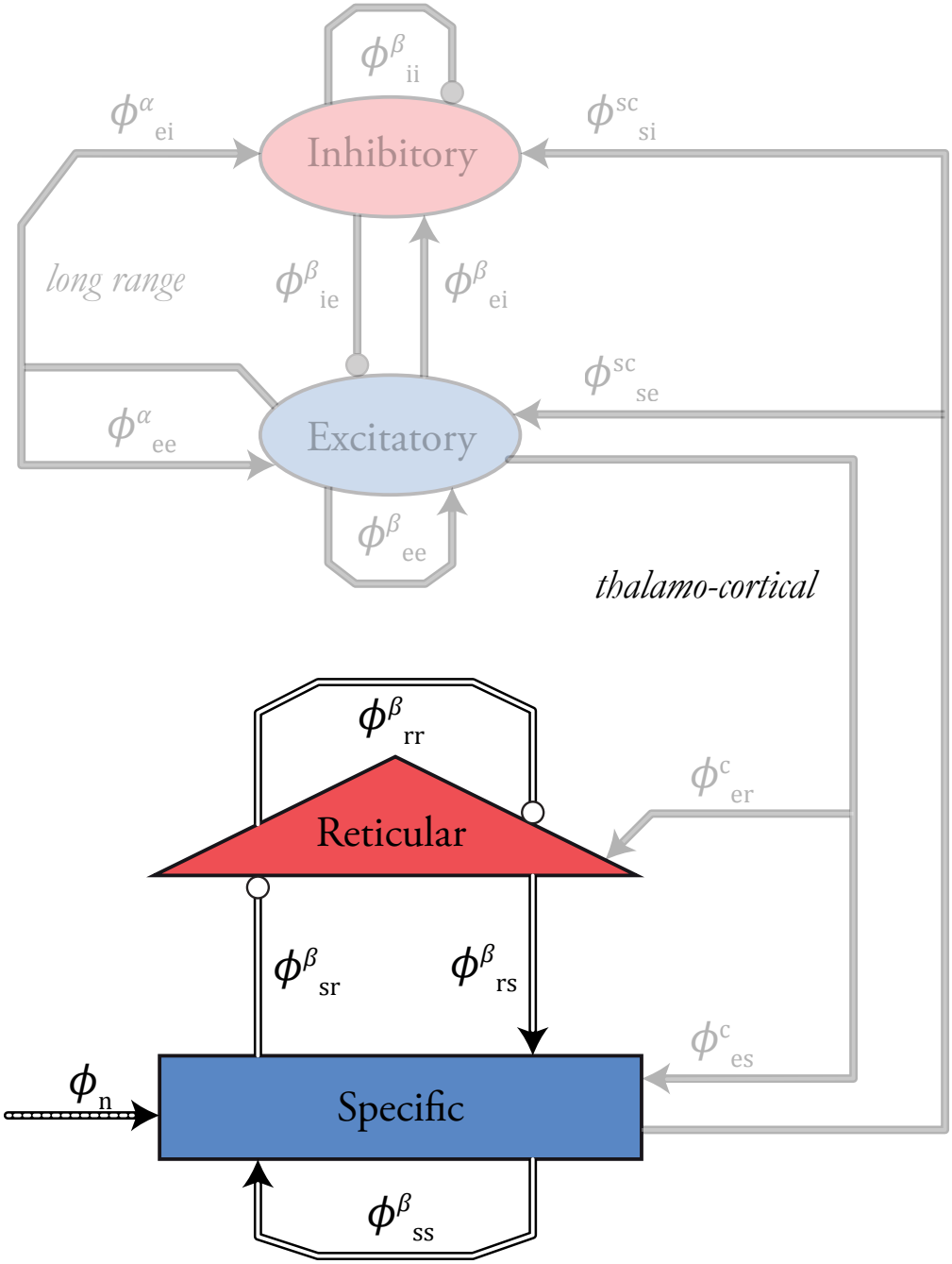

Figure 5.1: Relational diagram of interacting flux terms for the isolated thalamic model. Subscripts describe the neuron groups interacting, reading left to right, i.e. a $\rightarrow$ b. All connections in the isolated thalamic model are considered local, i.e. β - short range. Includes proposed cortical coupling for Chapter 6.

$$V_k = V_k^{\text{rest}} + \int_{-\infty}^{t} L_k(t-t') \left[E_k(t') + I_k(t')\right] dt, \qquad k = s, r \tag{5.1}$$

where the $L_k(t)$ is the exponential impulse response of the soma:

$$L_k(t) = \begin{cases} \frac{1}{\tau_k} e^{-t/\tau_k}, & t \geq 0 \\ 0, & t < 0 \end{cases} \tag{5.2}$$

The equations for the time-varying excitatory and inhibitory voltage input to the soma in Eq. (5.1) are,

$$E_k(t) = \rho_s \psi_{sk} \Phi_{ek}(t), \quad (\rho_s > 0) \tag{5.3}$$

$$I_k(t) = \rho_r \psi_{rk} \Phi_{ik}(t), \quad (\rho_r < 0) \tag{5.4}$$

The reversal potential functions in Eqs (5.3) and (5.4) are again the dimensionless weighting functions that scale the effectiveness of the input flux Φ_{jk},

$$\psi_{jk} = \frac{V_j^{\text{rev}} - V_k(t)}{V_j^{\text{rev}} - V_k^{\text{rest}}} \qquad j, k = s, r \tag{5.5}$$

where $V_s^{\text{rev}} = 0$ mV for the excitatory receptors and $V_r^{\text{rev}} = -70$ mV for inhibitory receptors.

The total excitatory and inhibitory input flux entering a thalamic neuron $k = s, r$ can be written as a temporal convolution of the dendrite impulse response functions, $H_{jk}(t)$, (given in Ch.4, Eq. (4.6)),

Table 5.1: Thalamic Fluxes

Symbol	Description
$\Phi_{es}(t)$	Excitation term entering the specific population
$\Phi_{is}(t)$	Inhibition term entering the specific population
$\Phi_{er}(t)$	Excitation term entering the reticular population
$\Phi_{es}(t)$	Inhibition term entering the reticular population

$$\Phi_{es}(t) = \int_{-\infty}^{t} H_{es}(t-t') \left[N_{ss}\phi_{ss}^{\beta}(t') + \nu_{ns}\phi_n \right] dt' \tag{5.6}$$

$$\Phi_{is}(t) = \int_{-\infty}^{t} H_{is}(t-t') N_{rs}\phi_{rs}^{\beta}(t') dt' \tag{5.7}$$

$$\Phi_{er}(t) = \int_{-\infty}^{t} H_{er}(t-t') N_{sr}\phi_{sr}^{\beta}(t') dt' \tag{5.8}$$

$$\Phi_{ir}(t) = \int_{-\infty}^{t} H_{ir}(t-t') N_{rr}\phi_{rr}^{\beta}(t') dt' \tag{5.9}$$

where the $\nu_{ns}\phi_n$ is a constant external stimulus term coming from sub-thalamic structures. [Note that there are no long-range connections for the thalamic flux equations as there were for the cortex.]

Table 5.1 describes the flux subscript convention used. In the case of the isolated thalamus, this convention seems unnecessary since only specific and reticular neuron types are present and Φ_{ss} could have been used instead of Φ_{es}. In Ch. 6, however, an excitatory input into the average specific neuron is defined as the combination of terms from both the thalamus and the cortex, i.e. input from the specific population *and* the excitatory population plus a term from unspecified sub-thalamic structures. The subscript e then is used more generally to mean *excitatory* input entering a target neuron rather then input exclusively from an excitatory neuron in the cortex. The same subscript convention is used for the response functions and the corresponding rate constants.

Differentiating the four dendrite convolutions (5.6–5.9) twice produces four second-order differential equations for excitatory and inhibitory input into the specific and reticular neurons populations,

$$\left(\frac{d}{dt}+\gamma_{es}\right)^2\Phi_{es}=\gamma_{es}^2[N_{ss}Q_s(t)+\nu_{sn}\phi_n] \tag{5.10}$$

$$\left(\frac{d}{dt}+\gamma_{is}\right)^2\Phi_{is}=\gamma_{is}^2N_{rs}Q_r(t) \tag{5.11}$$

$$\left(\frac{d}{dt}+\gamma_{er}\right)^2\Phi_{er}=\gamma_{er}^2N_{sr}Q_s(t) \tag{5.12}$$

$$\left(\frac{d}{dt}+\gamma_{ir}\right)^2\Phi_{ir}=\gamma_{ir}^2N_{rr}Q_r(t). \tag{5.13}$$

where the inhibitory rate constant is scaled, $\gamma_{ik}=\gamma_{ik}^0/\lambda_i$, and we have used a coarse-graining limit for the short range fluxes i.e., $\phi_{sk}^\beta(t)=Q_s(t)$ and $\phi_{rk}^\beta(t)=Q_r(t)$.

Taking the time derivatives of the $k=s,r$ convolutions from equation (5.1) we obtain a pair of first-order equations for the average specific and reticular soma voltages, $V_s(t), V_r(t)$,

$$\tau_s\frac{dV_s(t)}{dt}=V_s^{\text{rest}}-V_s(t)+\rho_s\psi_{ss}\Phi_{es}(t)+\rho_r\psi_{rs}\Phi_{is}(t) \tag{5.14}$$

$$\tau_r\frac{dV_r(t)}{dt}=V_r^{\text{rest}}-V_r(t)+\rho_s\psi_{sr}\Phi_{er}(t)+\rho_r\psi_{rr}\Phi_{ir}(t) \tag{5.15}$$

where ρ_s,ρ_r are the synaptic strengths. They are identical to the cortical model's synaptic strengths with $\rho_s>0$ (excitation) and $\rho_r<0$ (inhibition), and $\rho_r=\lambda_r\rho_r^0$.

Table 5.2: Thalamic Model Parameters

Symbol	Description	Value	Unit
$\tau_{s,r}$	neuron time-constant	$0.040, 0.040$	s
$V_{s,r}^{\text{rev}}$	reversal potential at dendrite	$0, -70$	mV
$V_{s,r}^{\text{rest}}$	neuron resting potential	$-64, -64$	mV
$\rho_{s,r}^{0}$	non-scaled synaptic gain	1×10^{-3}, -1.05×10^{-3}	mVs
$\gamma_{js,jr}^{0}$	non-scaled rate-constant	170, 50	s^{-1}
N_{ss}, N_{rs}	number of local connections to specific neurons	800, 550	–
N_{sr}, N_{rr}	number of local connections to reticular neurons	700, 700	–
$\nu_{sn}\phi_n$	sub–thalamic constant stimulus	2.4	s^{-1}
$Q_{s,r}^{\max}$	maximum firing rates	30, 60	s^{-1}
θ_s	specific sigmoid threshold voltage	-58.5	mV
$\theta_{r,(1,2)}$	reticular component sigmoid threshold voltage	$-53.5, -62.5$	mV
σ_s	specific standard deviation from threshold	3	mV
$\sigma_{r,(1,2)}$	reticular standard deviation from threshold	1.5, 1.5	mV
c	sigmoid scaling constant	$\pi/\sqrt{3}$	–

5.2.1 Sigmoidal Mapping

For cortical neurons, the mapping from membrane potential to firing rate can be modelled by a sigmoid function. This is because these neurons exhibit high firing rates for depolarized (less negative) membrane potentials and low firing rates for a hyperpolarizing (more negative) membrane potentials.

The neurons of the thalamus, however, are known to have extremely rich electrophysical properties. Soltesz *et al* [19], Williams *et al* [25], McCormick *et al* [13], Coulter *et al* [5] and Toth *et al* [23] have investigated some of the unique features of the specific neuron population which, in addition to the dynamics of the cortical neurons, exhibit a brief increase in population firing rates for hyperpolarizing membrane potentials, with further reductions of the potentials returning the population to a low firing state.

It has been shown by Zhu [28] that ionic currents are present in the reticular neurons at hyperpolarizing potentials as well. The point of difference from the specific neurons is the fact that the reticular neurons do not appear to return to a low firing rate with further reductions in membrane potential.

This contributes additional nonlinear dynamics to any modelling approach and the relationship between neuron activity and membrane potential for the thalamic neurons becomes more complicated than for neurons in the cortex.

In our thalamic model we treat the specific neurons analogously to the cortical excitatory neurons. That is, they are considered to have a purely excitatory effect on post-synaptic neurons and the mapping from membrane potential to firing rate is modelled by a standard sigmoid function. The reticular neuron population is treated as having a purely inhibitory effect, however, as a first approximation to modelling the current flows at hyperpolarizing membrane potentials, we map membrane potential to firing rate with a two-to-one 'dipped' sigmoid function. This bimodal function allows both extreme depolarized and extreme hyperpolarized membrane potentials to be mapped to a high firing rate for the reticular populations:

$$Q_s(t) = \frac{Q_s^{\max}}{1 + e^{-c(V_s(t)-\theta_s)/\sigma_s}} \tag{5.16}$$

$$Q_r(t) = Q_r^1(t) + Q_r^2(t), \qquad Q_r^1(t) = \frac{Q_r^{\max}}{1 + e^{-c(V_r(t)-\theta_{r,1})/\sigma_{r,1}}} \tag{5.17}$$

and

$$Q_r^2(t) = Q_r^{\max}\left[1 - \frac{1}{1 + e^{-c(V_r(t)-\theta_{r,2})/\sigma_{r,2}}}\right].$$

The bimodal mapping function for the reticular neuron population is generated by linearly combining a sigmoid function and its horizontally displaced mirror image (see Eq. (5.17) and Fig 5.2). The threshold voltage values, $\theta_{r,1}, \theta_{r,2}$, for this function have been separated and the center of the 'dip' is located at $\frac{\theta_{r,1}+\theta_{r,2}}{2} = -58$ mV.

5.3 Analysis

Having described the general structure of the thalamic model and the addition of the new mapping function for the reticular neurons, we investigate the stationary states of the system by setting the time derivatives of the model equations to zero. As for the cortical model, solving

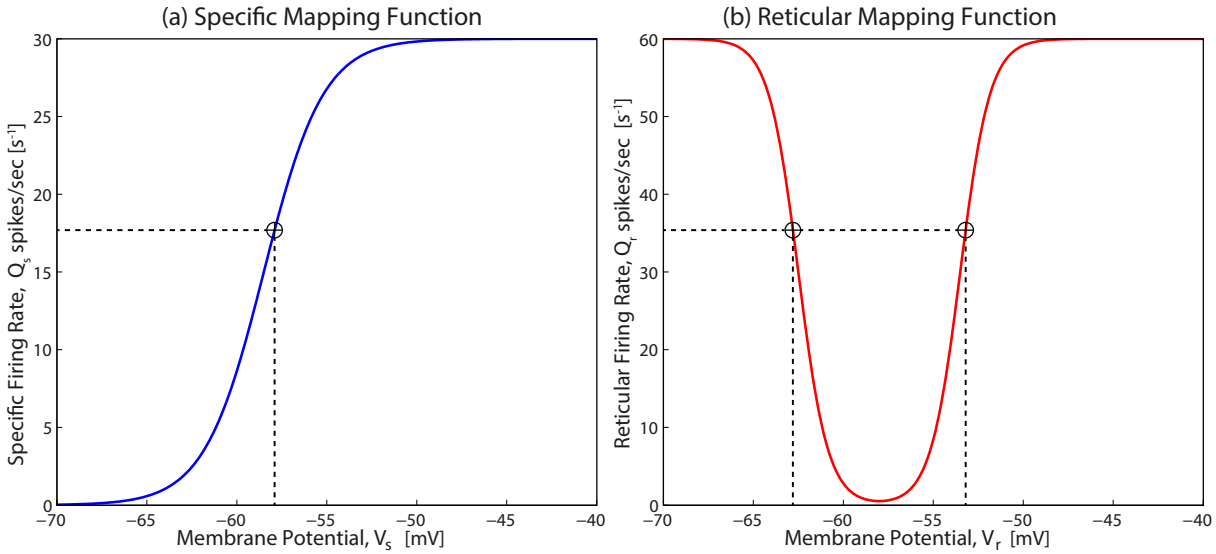

Figure 5.2: Mapping of membrane potential to firing rate for both the mean specific (a) and reticular (b) neurons. The reticular mapping function is a novel description allowing hyperpolarized membrane potentials to be mapped to a high firing rate.

this system of equations proves to be impossible analytically due to the nature of the mapping functions, and instead we use a slightly modified form of the computational method in Ch. 4.

5.3.1 Stationary States for the Thalamic Model

When we investigated the cortical model's equilibrium states we searched over the excitatory firing rate domain, Q_e^{eq}, as all system variables could be calculated unambiguously from a given excitatory firing rate. A state in the thalamic model, however, can not be uniquely described by the analogous specific firing rate, Q_s^{eq} because of the reticular neurons two-to-one mapping of a membrane potential to a firing rate. We instead begin the search for the stationary states by selecting a range of feasible reticular membrane potentials, $V_r^{\text{eq}} = [-70... - 40]$ mV.

Again for notational simplicity (and unless otherwise stated) we will assume that all firing rates and membrane potentials in Sections 5.3.1 – 5.3.2 are at equilibrium, i.e. $Q_e = Q_e^{\text{eq}}$.

Combining the time-independent forms of the input flux equations (5.10–5.13) and the membrane potential equations (5.14–5.15) yields a pair of coupled nonlinear equations for equilibrium firing rates,

$$Q_s = f(V_r, Q_r) = \frac{V_r - V_r^{\text{rest}} - \rho_r \psi_{rr} N_{rr} Q_r}{\rho_s \psi_{sr} N_{sr}} \tag{5.18}$$

$$Q_r = g(V_s, Q_s) = \frac{V_s^{\text{eq}} - V_s^{\text{rest}} - \rho_s \psi_{ss} [N_{ss} Q_s + + \nu_{ns} \phi_n]}{\rho_r \psi_{rs} N_{rs}}. \tag{5.19}$$

The range of reticular membrane potentials, V_r, can be equated to corresponding firing rates, Q_r using Eq. (5.17) (as this is a one-to-one mapping). Inputting both of these ranges into Eq.(5.18) we can then obtain equilibrium specific firing rates, Q_s. We map Q_s back to a membrane potential using an inverted form of the specific mapping function, Eq. (5.16).

$$V_s = -\left(\frac{\sigma_s}{c_s}\right) \ln\left[\frac{Q_s^{\max}}{Q_s} - 1\right] + \theta_s \tag{5.20}$$

Feeding Q_s and V_s into Eq. (5.19) we are able to produce another set of reticular population firing rates Q_r'.

To map this firing rate back to a membrane potential, which will have two possible values (the only unique value is at the bottom of the dip), we use a method similar to that used to find the cortical model stationary states. Taking the Q_r' firing rate we compare it to firing rates produced by inputting a range of membrane potentials, V_r^{search}, into the mapping function (5.17). Computing the difference between the search-range firing rates and the input firing rate that we're trying to invert ($\Delta Q_r = Q_r - Q_r^{\text{search}}$), we are able to generate a plot of V_r vs ΔQ_r whose x-axis intercepts are the membrane potentials that produce the firing rate inputted.

We use the `fzero()` MATLAB function which accepts a window of two points straddling the intercept and performs successive bisections to polish our estimate for each of the two candidate membrane potentials.

We can now compare the inputted reticular membrane potential with the potential output from the mapping function inversion ($\Delta V_r = V_r - V_r'$). We plot $V_{r,\text{in}}$ vs ΔV_r where the intercepts, $\Delta V_r = 0$, are the equilibrium states of the model. Again using `fzero()` to refine the potentials

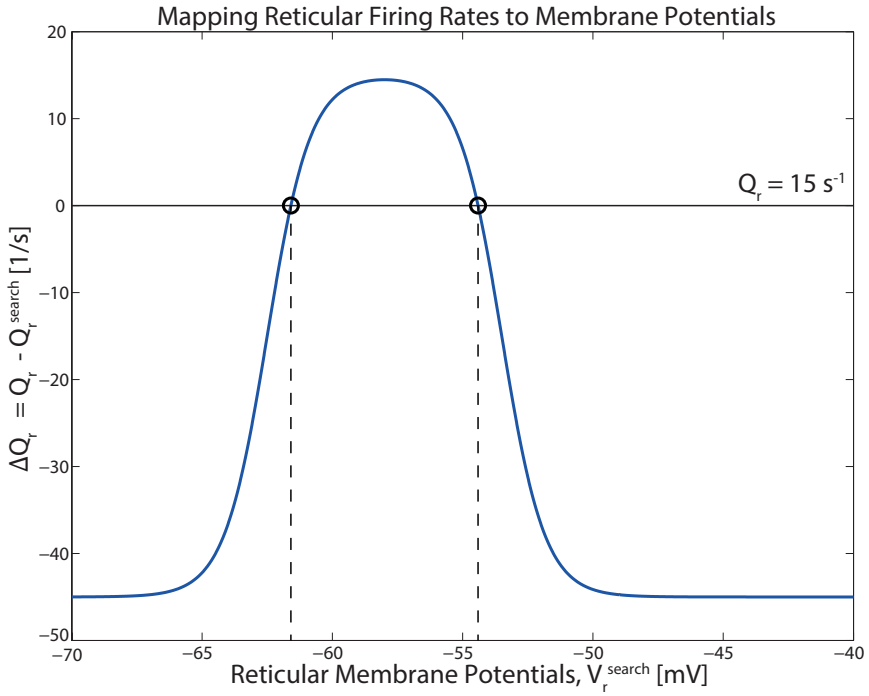

Figure 5.3: Inverting a reticular neuron population firing rate to two candidate membrane potentials.

and combining these into equations (5.16–5.19) we are able to define complete stationary states for the model (see Fig. 5.4).

In the steady state analysis for the cortical model, we plotted Q_e and Q_i vs the anaesthetic parameter λ_i which showed a hysteresis effect. The hysteresis effect is a clinically-observed feature

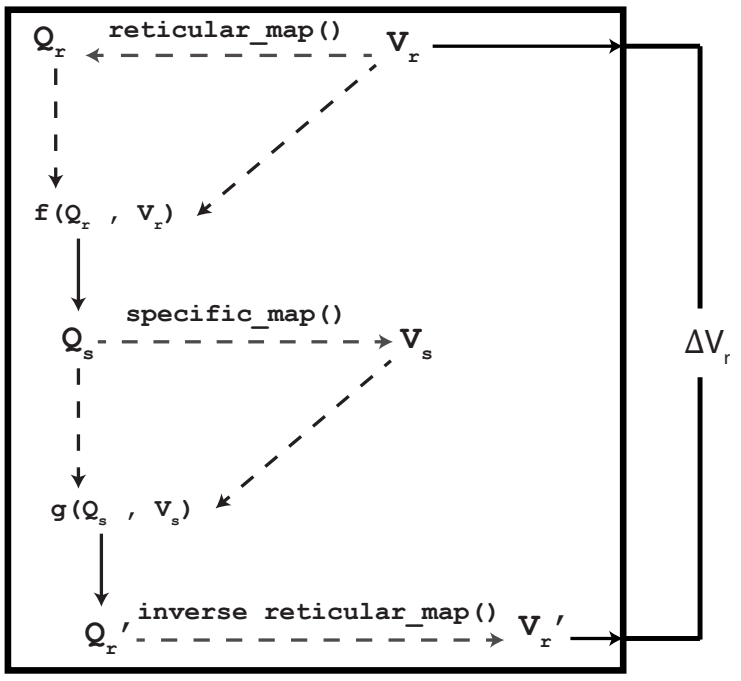

Figure 5.4: Information flow showing the algorithm for finding the steady state solutions for an isolated thalamus.

of anaesthesia and corresponds to different levels of an anaesthetic for *loss of consciousness* and *return of consciousness* although the mechanism producing this effect is not clear. Producing the analogous plots, Q_s and Q_r vs the anaesthetic parameter λ_r, for the thalamic model we expect some form of a hysteresis effect due the similarities in the two model structures.

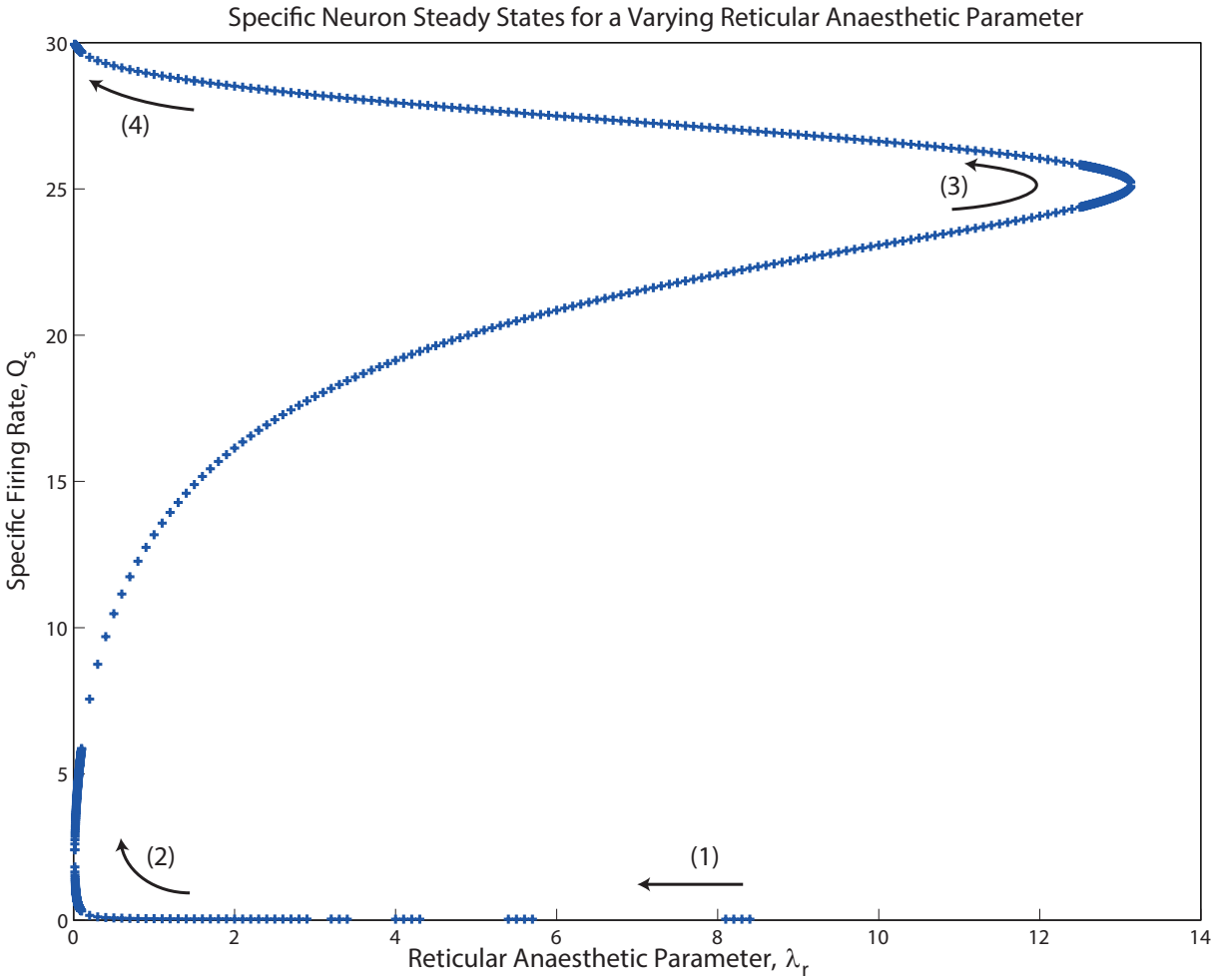

Figure 5.5: Distribution of equilibrium firing rates of the specific neuron population with respect to the λ_r anaesthetic scaling parameter.

The resulting steady state specific firing rate, Q_s, vs λ_r plot is similar to the Q_e steady states for a varying inhibition parameter. The curve does indicate a hysteresis effect, like that of the cortex, however this is over a much broader region of anaesthetic parameter. The point-density increases in Figs 5.5 and 5.6 (near the two turning points) were needed in order to confidently associate adjacent points.

The steady states on the lower branch of Fig 5.5 (upper branch of Fig 5.6) are a unique feature of the thalamic model on comparison with the cortex. Here the two neuron groupings are in opposing states with the specific neurons low firing and the reticular neurons high firing. For

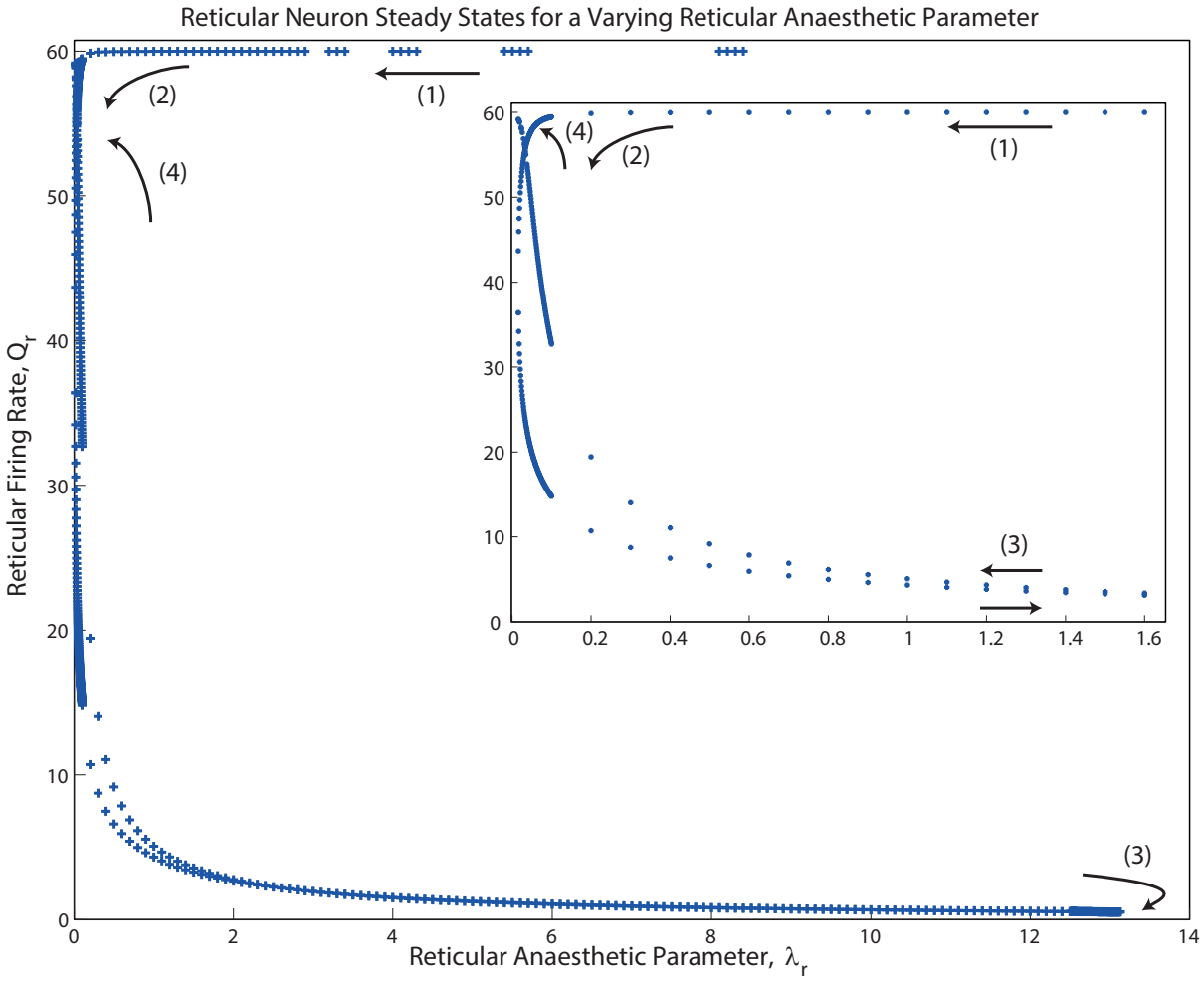

Figure 5.6: Distribution of equilibrium states of the reticular neuron population with respect to the λ_r anaesthetic scaling parameter.

the steady states of the cortical model both the excitatory and inhibitory populations tended to be in similarly high-firing or low-firing states.

The sparse distribution of these points as λ_r is increased is due to the run time of the code that produces both plots. As the steady states described by Q_s tending towards zero correspond to Q_r tending towards $Q_r^{\max}$, the MATLAB code mapping V_r to Q_r becomes strained and the state finding code takes exponentially longer to run (with a sufficient run time my MATLAB code could find these steady states). Run times for finding a root in the cortical model are ~ 0.006 s and for the thalamic model this increases to ~ 6 s.

5.3.2 Stability

In order to calculate the likelihood of the thalamic model occupying one of the predicted steady states in simulation, we need to make a statement about steady state stabilities. We construct

the Jacobian matrix for the thalamic model by expressing each of the its second-order flux equations as two first-order equations after defining some auxiliary variables.

$$\frac{d\Phi_{es}}{dt} = \Pi_{es} \tag{5.21}$$

$$\frac{d\Pi_{es}}{dt} = \gamma_{es}^2 \left[N_{ss}Q_s + \nu_{sn}\phi_n(t) - \Phi_{es}\right] - 2\gamma_{es}\Pi_{es} \tag{5.22}$$

$$\frac{d\Phi_{is}}{dt} = \Pi_{is} \tag{5.23}$$

$$\frac{d\Pi_{is}}{dt} = \gamma_{is}^2 \left[N_{rs}Q_r - \Phi_{is}\right] - 2\gamma_{is}\Pi_{is} \tag{5.24}$$

$$\frac{d\Phi_{er}}{dt} = \Pi_{er} \tag{5.25}$$

$$\frac{d\Pi_{er}}{dt} = \gamma_{er}^2 \left[N_{sr}Q_s - \Phi_{er}\right] - 2\gamma_{er}\Pi_{er} \tag{5.26}$$

$$\frac{d\Phi_{ir}}{dt} = \Pi_{ir} \tag{5.27}$$

$$\frac{d\Pi_{ir}}{dt} = \gamma_{ir}^2 \left[N_{rr}Q_r - \Phi_{ir}\right] - 2\gamma_{ir}\Pi_{ir} \tag{5.28}$$

We define a thalamic state as 10-element vector,

$$\text{state} = \left[V_s \;\; V_r \;\; \Phi_{es} \;\; \Phi_{is} \;\; \Phi_{er} \;\; \Phi_{ir} \;\; \Pi_{es} \;\; \Pi_{is} \;\; \Pi_{er} \;\; \Pi_{ir}\right]^{\mathrm{T}} \tag{5.29}$$

A 10×10 Jacobian matrix can now be formed by partially differentiating each first order DE (Eqs 5.21–5.28) with respect to each of the state variables. MATLAB is able to quickly return the set of ten eigenvalues corresponding to the matrix with the `eig()` function. The dominant eigenvalue (largest positive) characterizes the dynamics of the model at the steady state with which the eigenvalue is associated.

Computing the dominant eigenvalue for each of the predicted steady states from Sec 5.3.1 we are now able to produce more revealing plots of the steady state firing rates vs λ_r.

As for the cortical stationary state plots, the states along the middle branch of Fig 5.7 are consistently unstable and those on the upper and lower branches are stable.

Figure 5.9 shows where the steady state solutions of the thalamus lie on their corresponding mapping function curves. The blue regions represent states that are stable and the red regions those that are unstable. The steady states from the isolated cortical model suggested that the cortex will tend to exist in a mutually excited or mutually inhibited state. Although there were predicted steady states of the cortex that were a mix of firing from both population types these were mostly unstable solutions. The stability of the thalamic roots appear similar to those of the cortex when comparing the excitatory and specific populations. Regions 1 through 3 on the mapping functions, however, explores the most significant difference for the thalamic model compared to the cortical model with a high firing rate mapping to a hyperpolarized membrane potential in the reticular neuron population. For part of region 1 through 2 the thalamus demonstrates this new feature of having stable states of high firing in the reticular neuron population and low firing in the specific population, a ‘winner takes all’ outcome.

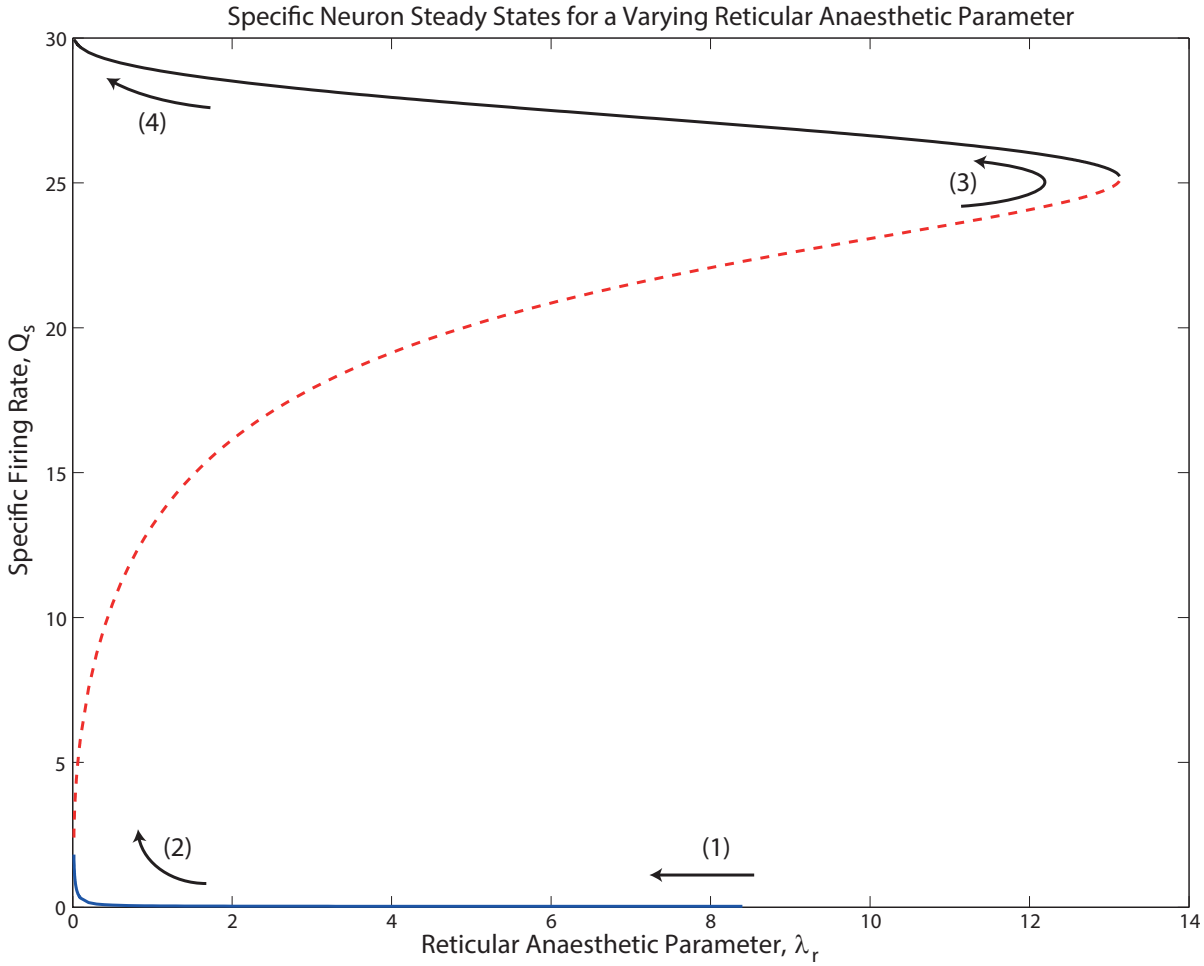

Figure 5.7: Stability of the predicted stationary states for the specific neuron population. A dashed line is predicted to be unstable and a solid line to be stable.

5.4 Simluation

We use an Euler update method to compute the time-evolution of the state parameters of Eq. (5.29). The system is initialized by selecting V_s^0 and V_r^0, setting the time-derivatives of the thalamic model to zero and then solving for the remaining state variables. A range of states is then produced using,

$$\text{state}(i+1) = \text{state}(i) + \frac{d\,\text{state}(i)}{dt} * dt + \text{noise} * \sqrt{dt}. \tag{5.30}$$

We select the number of data points to be simulated and the time step dt then a MATLAB loop implements the Euler update of Eq. (5.30). The predicted steady states from Fig 5.7 are plotted as dashed lines on Figs. 5.11–5.12 and we see good agreement with the simulation final states.

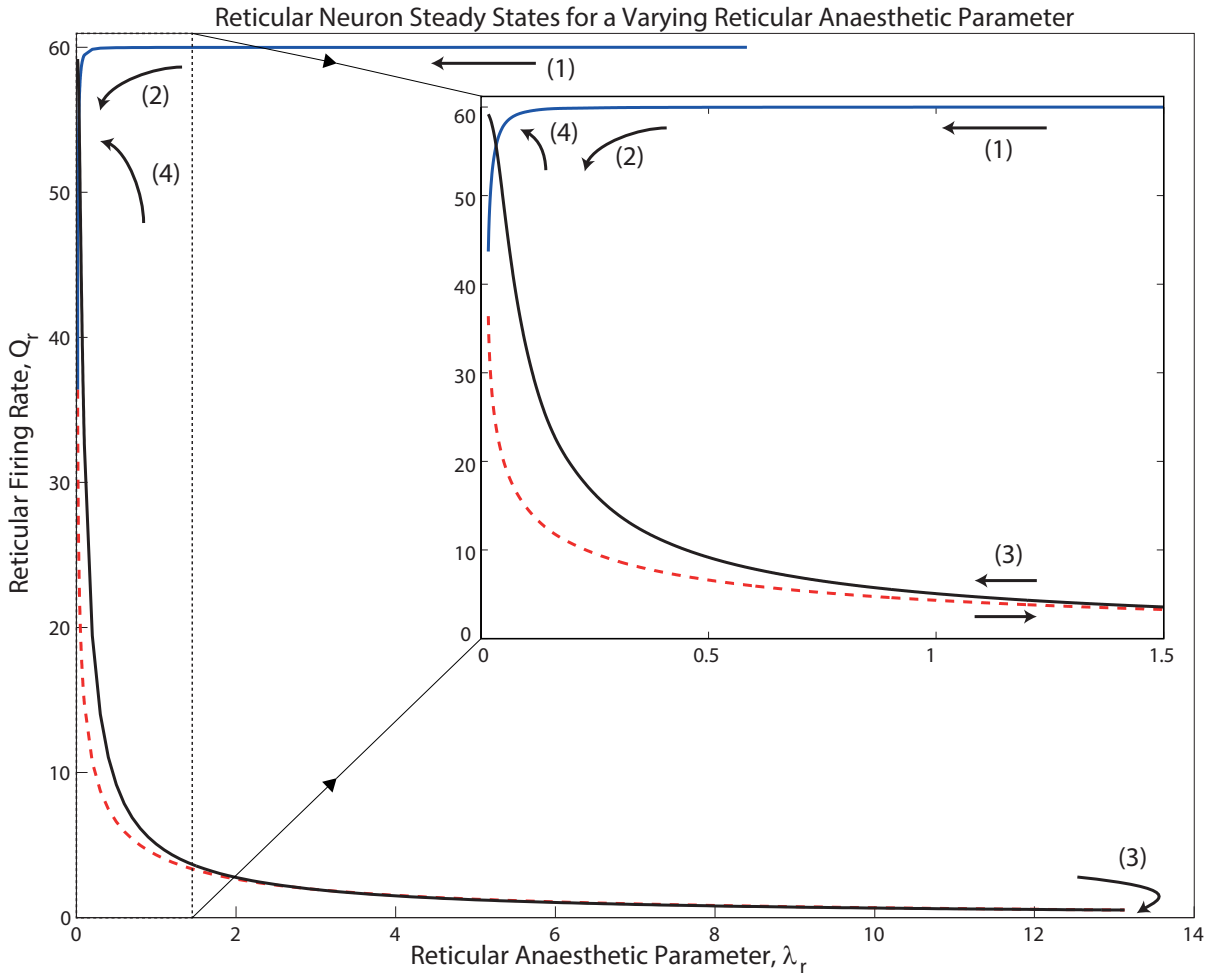

Figure 5.8: Stability of the predicted stationary states for the reticular neuron population. A dashed line is predicted to be unstable and a solid line to be stable.

Starting from the unstable mid-branch for $\lambda_r = 1$, the Q_s activity can either 'fall' to the upper-branch high-firing state (Fig 5.11 (a)) or 'fall' to the lower-branch low-firing state (Fig 5.12

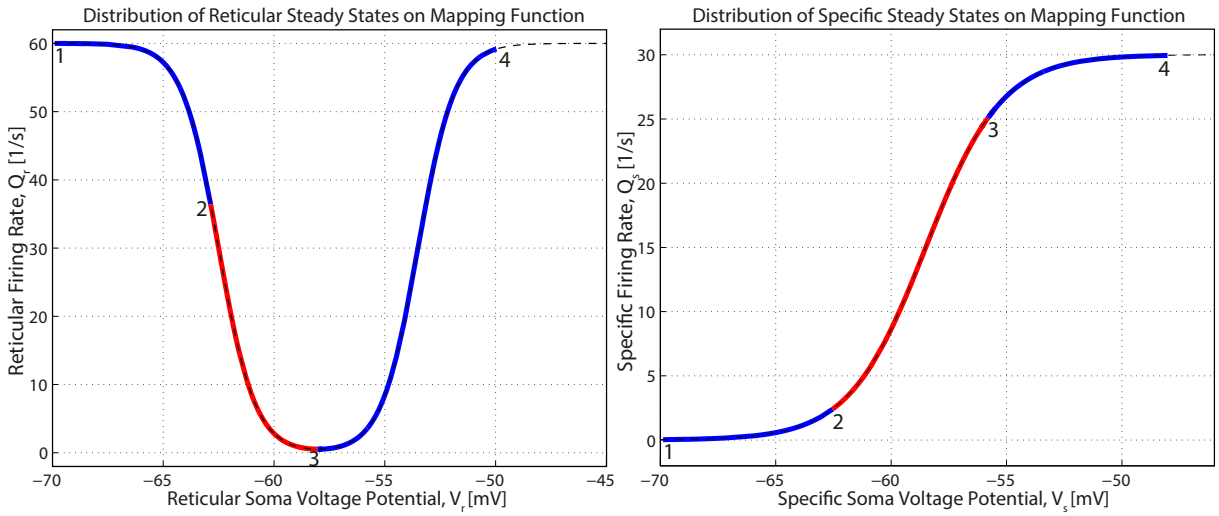

Figure 5.9: Predicted stationary states for the thalamic populations distributed on the firing rate to membrane potential mapping functions. Blue regions are stable states and red regions are unstable states. Each region is numbered to show its correlation to the corresponding region in the opposite graph.

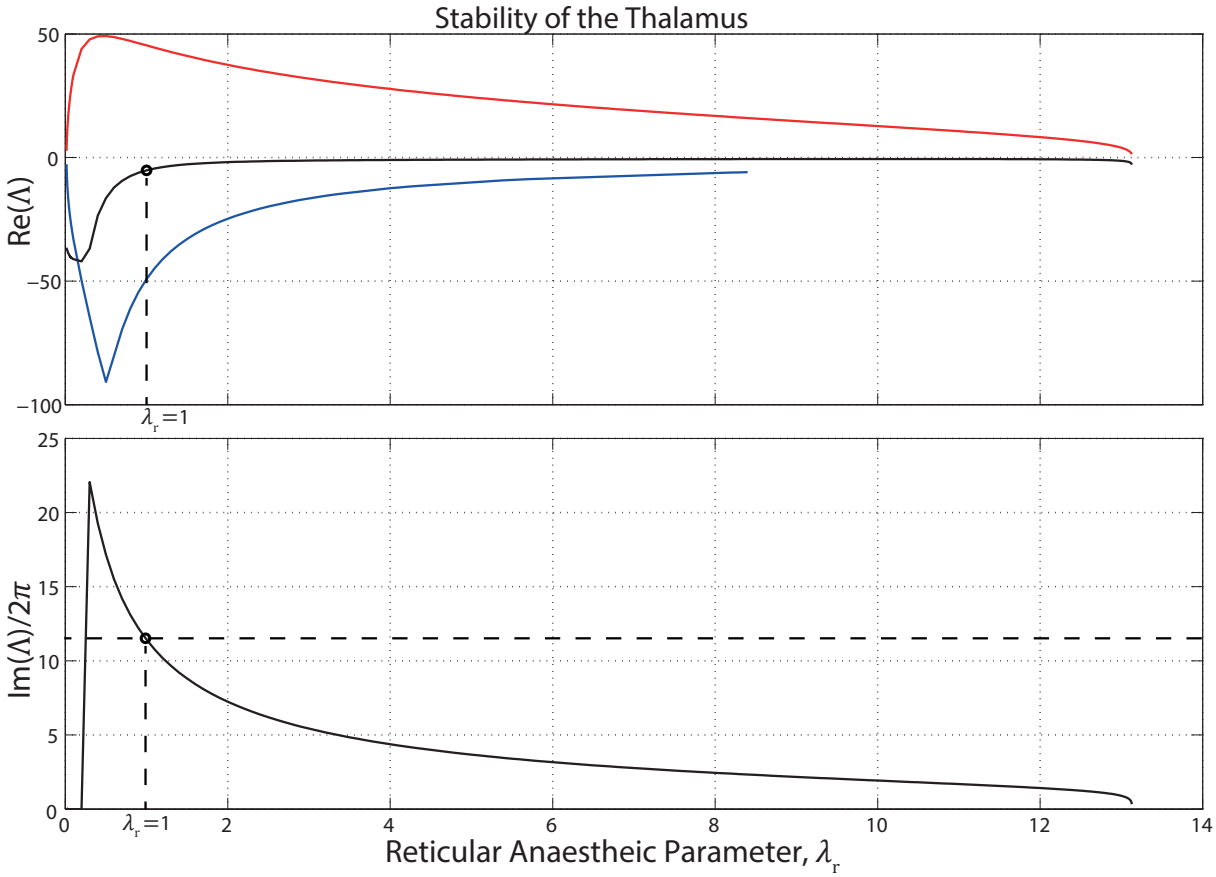

Figure 5.10: Details the nature of the dominant eigenvalues associated with the predicted steady states in Fig. 5.7.

(a)).

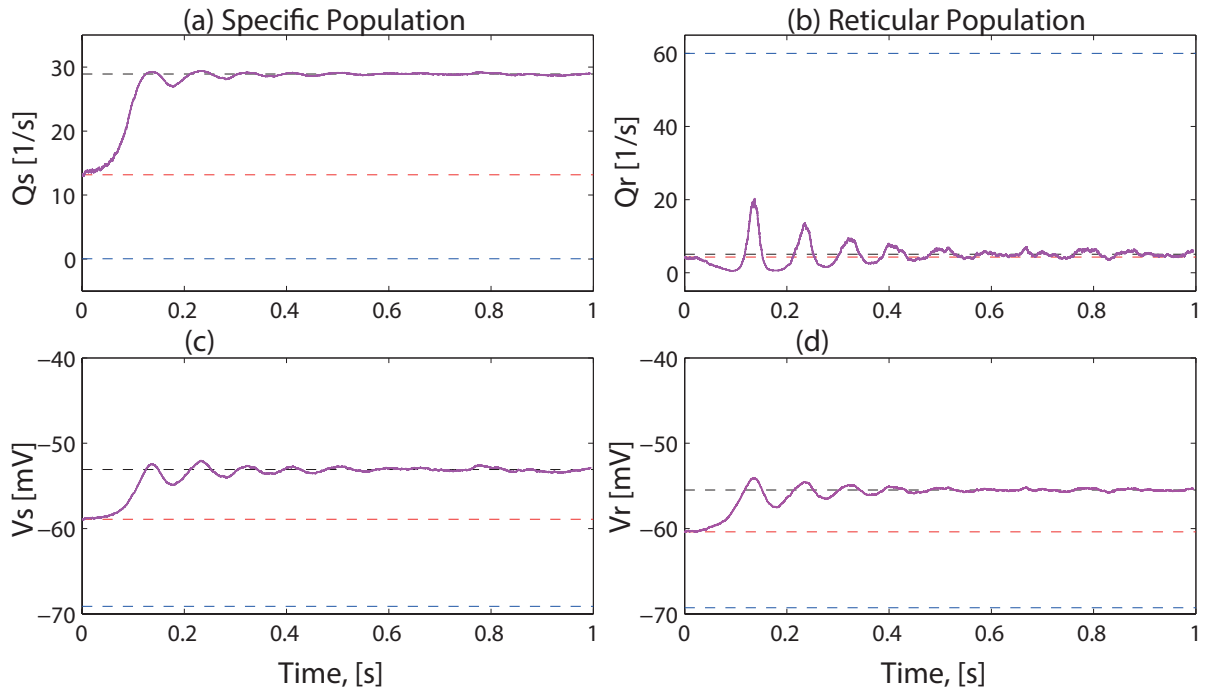

Figure 5.11: $\lambda_r = 1$. Initial state is the unstable middle branch of Fig. 5.7.

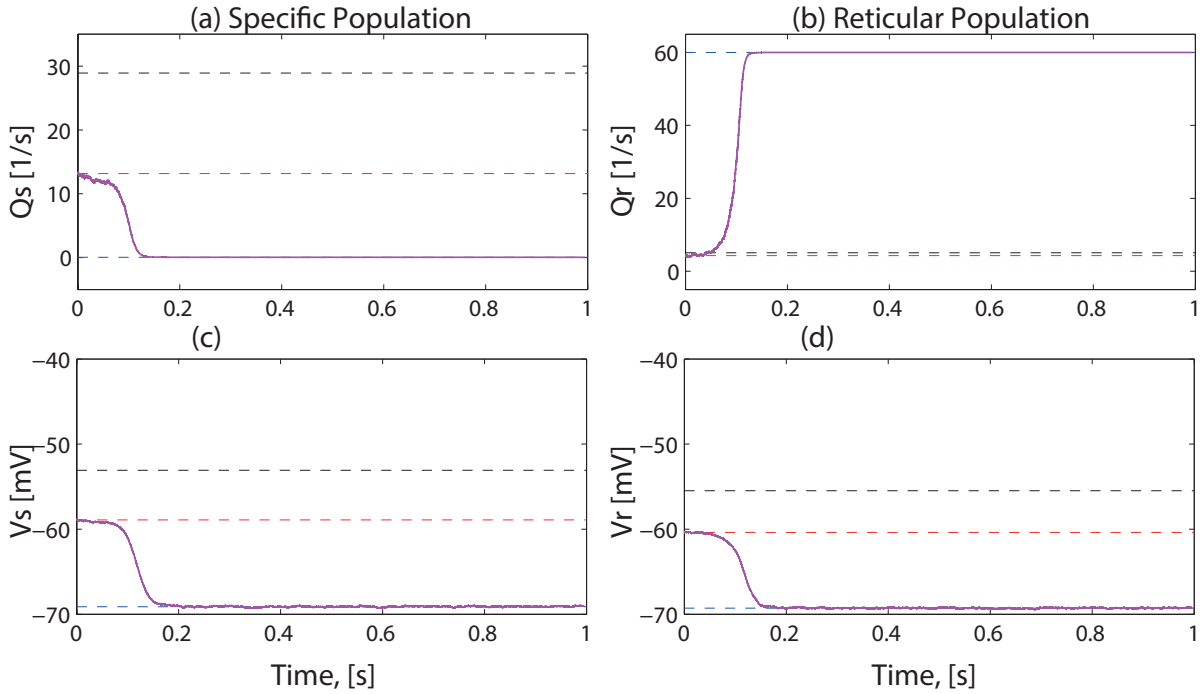

Figure 5.12: Same settings as for Fig 5.11, but a different noise sequence produces a distinctly different final state.

Figure 5.11 shows oscillatory behaviour post transition to the upper state. The frequency of this oscillation is $\approx$ 12 Hz which is consistent with the imaginary component of the corresponding eigenvalue when divided by 2π (see Fig. 5.10).

5.5 Conclusion

The mean-field isolated thalamic model has a lot of similarities with the mean-field isolated cortical model in its mathematical structure. The main differences in the thalamic model are the lack of long-range connection synapses, the bimodal function mapping reticular membrane potential to firing rate, and several small changes in parameter settings (mainly the connection constants). This results in the hysteretic 'S-bend' curve when plotting steady state specific firing rates against anaesthetic scaling parameter λ_r. A hysteresis effect was previously observed in the cortical model analysis but the thalamic result is stretched over a much broader region of scaling parameter λ_r.

The oscillatory behaviour observed in simulation is in agreement with our stability analysis in Sec. 5.3.1 and has a 'spindle-like' frequency ($\approx$ 12 Hz). Note that this thalamic model does not require the definition of an explicit generator for these spindle frequencies and they are instead an inherent property of the model.

It is also important to mention the relatively large range of the anaesthetic scaling considered for the isolated thalamus. λ_r is a scaling parameter that increases the decay time for an inhibitory post-synaptic potential (IPSP). This scaling occurs whilst maintaining the peak potential and subsequently an increase in λ_r will corresponded to an increase in the area under the IPSP function which relates directly to chloride transfer across the cell membrane. A clinically-feasible value for deep propofol anaesthesia would be $\lambda_r \sim 3$.

Chapter 6

Thalamo-Cortical System

6.1 A Mean-field Thalamo-Cortex

In Chapters 4–5 we explored the Waikato mean-field model of the cortex and detailed Prof. Moira Steyn-Ross' proposed structure for a new model of the thalamus based on this mean-field approach. From the outset the intention of this research was to extend the existing cortical model by incorporating a thalamus. To accomplish this we have defined two specific forms of the macrocolumn: the cortical macrocolumn containing populations of excitatory and inhibitory neurons, and the thalamic macrocolumn containing populations of specific (relay) and reticular neurons. Our strategy for the thalamo-cortical system is to combine the isolated cortical (Chap. 4) and thalamic (Chap. 5) model structures by adding two-way coupling terms into the flux equations.

6.2 The Thalamo-Cortical Model

Inhibitory neurons are known to have short axons [3] confining their direct neuron connections to a *short* range. The reticular neurons, which are the inhibiting neurons of the thalamic macrocolumn, are similarly considered *short* range. Therefore the *long* range connections between the thalamus and cortex can then be considered as stemming from only the cortical excitatory and thalamic specific populations. We consider connections from the cortical excitatory neurons to both the specific and reticular populations, and from the thalamic specific neurons back to both the excitatory and inhibitory populations, see Fig. 6.1. Much like the *long* range excitatory connections within the isolated cortex, we model the connecting flux equations between thalamic and cortical populations as four damped wave equations.

Cortex to thalamus:

$$\left[\left(\frac{\partial}{\partial t}+v\Lambda_{ek}\right)^2-v^2\nabla^2\right]\phi^{\mathrm{c}}_{ek}(\mathbf{r},t)=v^2\Lambda^2_{ek}Q_e(\mathbf{r},t),\qquad k=s,r \tag{6.1}$$

Thalamus to cortex:

$$\left[\left(\frac{\partial}{\partial t}+v\Lambda_{sb}\right)^2-v^2\nabla^2\right]\phi^{\mathrm{sc}}_{sb}(\mathbf{r},t)=v^2\Lambda^2_{sb}Q_s(\mathbf{r},t),\qquad b=e,i \tag{6.2}$$

where $\Lambda_{ek}=100\ \mathrm{m}^{-1}$ and $\Lambda_{sb}=400\ \mathrm{m}^{-1}$ are the inverse-length scales for the long-range axonal connections; $v=1.4\ \mathrm{ms}^{-1}$ is the axonial propagation velocity, and $\nabla^2=\partial/\partial x^2+\partial/\partial y^2$ is the Laplacian operator.

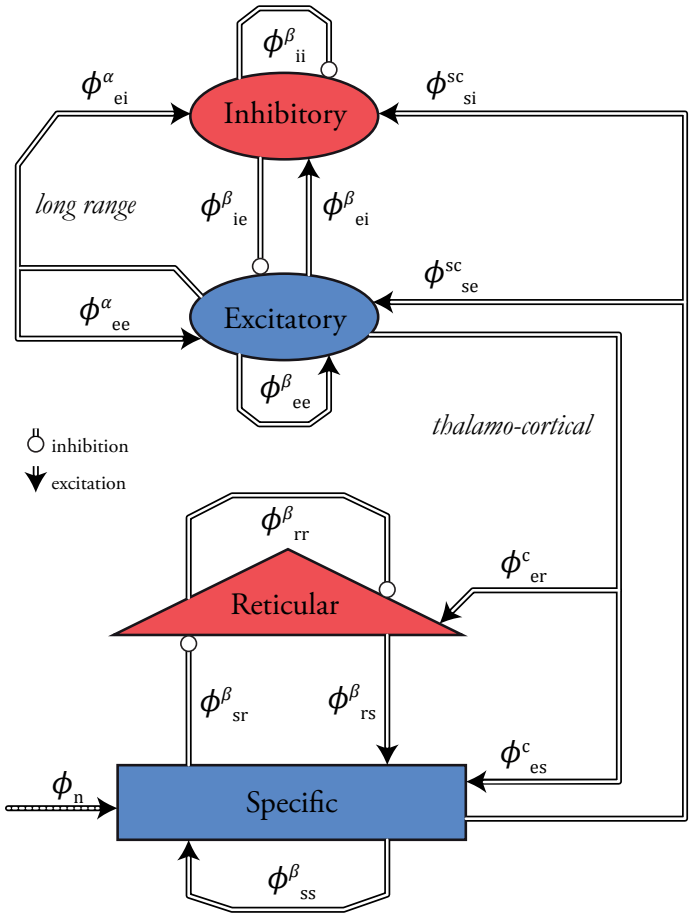

Figure 6.1: Relational diagram of interacting flux terms for the coupled thalamo-cortical model. Subscripts describe the neuron groups interacting, reading left to right, i.e. a $\rightarrow$ b. Superscripts describe connection types; short range [β], long-range [α], cortical [c], and sub-cortical [sc]. The effect of a connection is described by the line termination symbol; *circle* = inhibition, *arrow* = excitation.

Table 6.1: Thalamo-Cortical Model Parameters

Symbol	Description	Value	Unit
Λ_{es},Λ_{er}	inverse-length scales cortex-to-thalamus	$100, 100$	m^{-1}
Λ_{se},Λ_{si}	inverse-length scales thalamusto-cortex	$400, 400$	m^{-1}
v	long-range axonal velocity	1.4	ms^{-1}
$\gamma^0_{eb,ib}$	non-scaled rate-constants $b = e, i$	170, 50	s^{-1}
$\gamma^0_{ek,ik}$	non-scaled rate-constants $k = s, r$	170, 50	s^{-1}
N_{es}, N_{er}	number of cortex-to-thalamus connections	2700, 1100	–
N_{se}, N_{si}	number of thalamus-to-cortex connections	800, 600	–

Ignoring the spatial terms in Eqs. (6.1) and (6.2), the excitatory flux differential equations of the cortical model (previously Eqs. (4.10) and (4.12)) are redefined as,

$$\left(\frac{d}{dt} + \gamma_{ee}\right)^2 \Phi_{ee} = \gamma_{ee}^2 \left[N_{ee}^{\alpha}\phi_{ee}^{\alpha}(t) + N_{ee}^{\beta}\phi_{ee}^{\beta}(t) + N_{se}\phi_{se}^{\mathrm{sc}}(t)\right], \tag{6.3}$$

$$\left(\frac{d}{dt} + \gamma_{ei}\right)^2 \Phi_{ei} = \gamma_{ei}^2 \left[N_{ee}^{\alpha}\phi_{ei}^{\alpha}(t) + N_{ei}^{\beta}\phi_{ei}^{\beta}(t) + N_{si}\phi_{si}^{\mathrm{sc}}(t)\right]. \tag{6.4}$$

where the cortical inhibitory flux equations remain as defined in Chapter 4, Eqs. (4.11) and (4.13).

The updated excitatory flux differential equations of the thalamic model (previously Eqs. (5.10) and (5.12)) are

$$\left(\frac{d}{dt} + \gamma_{es}\right)^2 \Phi_{es} = \gamma_{es}^2 \left[N_{ss}Q_s(t) + N_{es}\phi_{es}^{\mathrm{c}}(t) + \nu_{ns}\phi_n\right], \tag{6.5}$$

$$\left(\frac{d}{dt} + \gamma_{er}\right)^2 \Phi_{er} = \gamma_{er}^2 \left[N_{sr}Q_s(t) + +N_{er}\phi_{er}^{\mathrm{c}}(t)\right]. \tag{6.6}$$

where the thalamic inhibitory flux equations remain as defined in Chapter 5, Eqs. (5.11) and (5.13).

6.3 Analysis

Before the two-way coupling between the thalamic and cortical populations is explored we first investigate how the additional terms in the new flux equations (6.3–6.6) might contribute to any variations from the the previously observed steady states solutions of the isolated models.

In our model we have assumed that the reticular and inhibitory anaesthetic scaling parameters are identical, i.e. $\lambda_i = \lambda_r$.

6.3.1 Steady States: Cortex to Thalamus

Recalling the isolated thalamic model from Ch. 5, we introduce a one-way coupling term entering the thalamic macrocolumn via Eq. (6.1). Here, as for the isolated thalamus, we start the search for the steady states by selecting the anaesthetic scaling parameter.

For the rest of Section 6.3, we will assume state variables to be at equilibrium unless otherwise stated, e.g. $Q_e = Q_e^{\mathrm{eq}}$.

The time and space-independent solution to Eq. (6.1) leads to $\phi_{ek}^{\mathrm{c}} = Q_e$. Because the coupling is one-way for this section, meaning the cortex receives no input from the thalamus, we assume the cortex is occupying one of its isolated equilibrium states.

The equilibrium solutions to Eq. (6.5), (6.6) therefore are

$$\Phi_{es} = N_{ss}Q_s + N_{es}Q_e + \nu_{ns}\phi_n, \tag{6.7}$$

$$\Phi_{er} = N_{sr}Q_s + +N_{er}Q_e. \tag{6.8}$$

The distribution of predicted thalamic steady states is shown in Fig. 6.2. The inputs from the cortex are just the steady states from the isolated cortical model in Ch. 4. The thalamic steady states are now much more diversely distributed over the finer region of λ_r due to the cortical model's sensitivity in this region. The single high-firing state of the cortex for low anaesthetic parameter saturates the thalamic model and we lose the smooth turning point seen on Fig. 5.7.

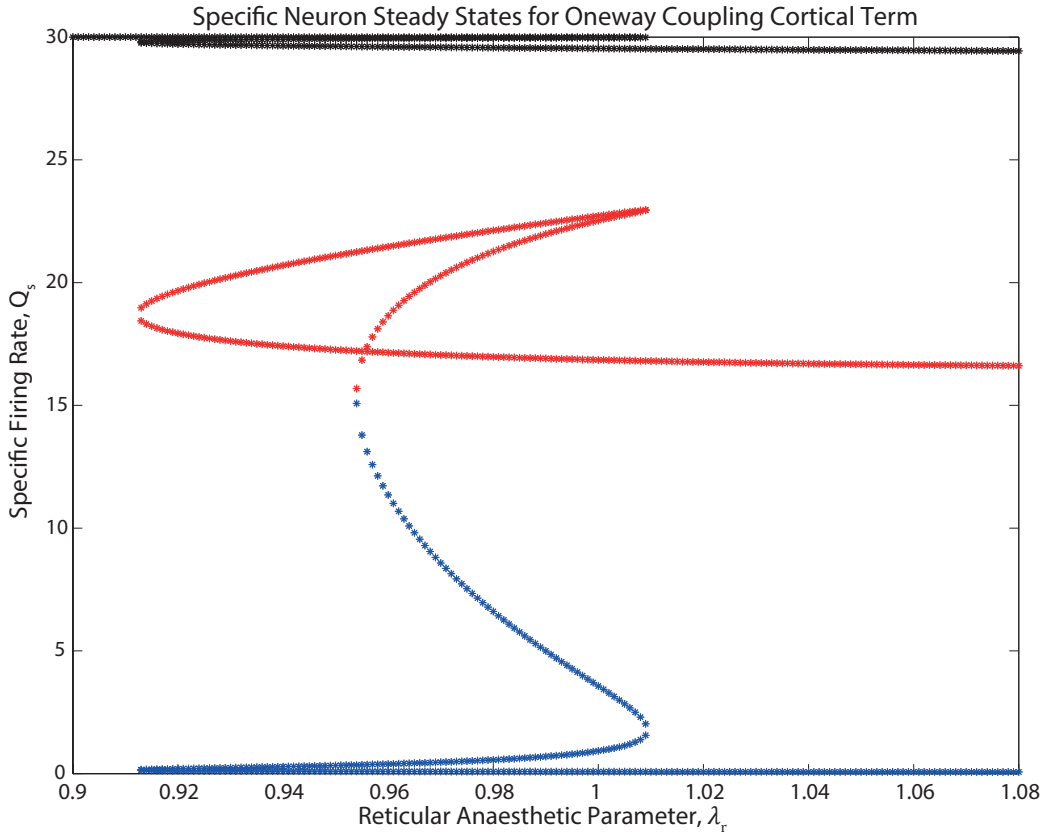

Figure 6.2: Stationary states for the specific neuron population receiving input from the cortex. Red markers indicate unstable steady states. Blue and black markers are both stable states.

The low-firing steady state of the cortex for large anaesthetic parameter has little effect on the thalamic model and the previously produced characteristic 'S-bend' for the isolated thalamus is present.

6.3.2 Steady States: Thalamus to Cortex

Recalling the isolated cortical model from Ch. 4, we introduce a one-way coupling connecting the thalamus to the cortical macrocolomn via Eq. (6.2). The wave equations mapping *long* range excitatory firing rates to input flux have equilibrium solutions $\phi^{\alpha}_{ek} = Qe$. We also take a coarse-graining limit over the short range leading to $\phi^{\beta}_{ek} = Q_e$. Substituting the homogeneous time-independent solutions for the wave equations ($\phi_{sk} = Q_s$) into the flux equations (6.3 – 6.4) leads to,

$$\Phi_{ee} = \left[N^{\alpha}_{ee} + N^{\beta}_{ee}\right] Q_e + N_{se} Q_s, \tag{6.9}$$

$$\Phi_{ei} = \left[N_{ei}^{\alpha} + N_{ei}^{\beta}\right] Q_e + N_{si} Q_s. \tag{6.10}$$

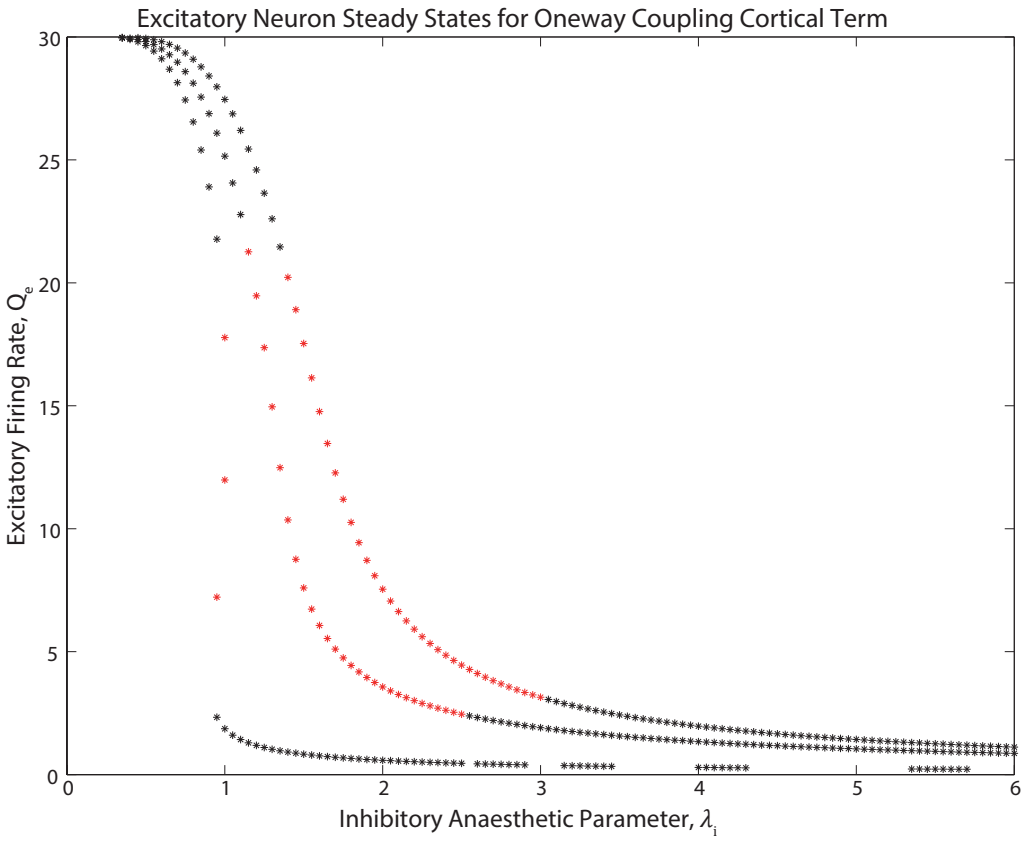

Figure 6.3: Stationary states for the excitatory neuron population receiving steady state input from the thalamus. Red markers indicate unstable steady states. Black markers are stable states.

The upper (large λ_r) turning point of the specific population steady-state curve, Fig. 5.7, has a corresponding turning point on the one-way coupled cortical steady states where the two 'right-most' branches from Fig. 6.3 meet at $\lambda_i \sim 13$.

The addition of the thalamic firing rates has shifted the unstable steady states of the cortex to a higher region of λ_i. The three state region of the isolated cortex has been strectched out for the two high-firing specific states, taking on a sigmoidal shape with a single steady state for each λ_i.

6.3.3 Steady States: Thalamo-Cortical System

Finally we implement the two-way feedback between both the thalamic and the cortical populations. Eqs. (6.1) and (6.2) are incorporated into the root finding code for both systems and a

similar method is used to that of Chapters 4–5.

We begin our search for the steady states of the coupled system by selecting a range of excitatory firing rates, Q_e. Each of these values is passed to the thalamic root-finding MATLAB code which returns the corresponding thalamic steady states. The resulting specific firing rates, Q_s, for which there may be multiple for a given Q_e, are then passed on to the cortical root-finding code which returns another excitatory firing rate, Q'_e. Similar to the method used in Ch. 4 and 5 we take the difference of the input and output excitatory firing rates ($\Delta Q_e = Q_e - Q'_e$) and plot it against the anaesthetic scaling parameter. The x-axis intercepts of this plot correspond to the steady states of the coupled system.

The ΔQ_e discrepancy plot here is considerably more complicated than for the isolated models, as multiple roots of the thalamus may be associated with a single input Q_e. The MATLAB code looks for the thalamic root that allows ΔQ_e to get closest to zero. Changes in the thalamic root used may cause sign changes in the ΔQ_e leading to the detection of false steady states. By tracking which thalamic root is used, the MATLAB code will switch the sign of the ΔQ_e point to handle this case.

Once the root-finding code has found a window of Q_e points that straddles a steady state, the `fzero()` function is again used to polish the root. Each time `fzero()` refines a root of the cortex it performs a full scan for the roots of thalamus. I remove the need to perform another full scan of the thalamus after a cortical root has been polished by storing the V_r value last used by `fzero()` and calculating the steady state of the thalamus from that.

The overall run time of this coupled root-finder is extremely slow compared to the search times for the two isolated models. This is due largely to the number of `fzero()` function calls required. The search density varies during run-time in order to make the code more efficient, however, this makes the time taken to return the steady states of a given anaesthetic scaling parameter also vary significantly.

To compute the stability of the steady states we define a new state vector for both the cortex and the thalamus that takes into account the couping terms. The state vector for the cortex are now contains 18 state variables,

$$\text{cortical\_state} = [V_e \;\; V_i \;\; \Pi_{ee} \;\; \Pi_{ie} \;\; \Pi_{ei} \;\; \Pi_{ii} \;\; \Phi_{ee} \;\; \Phi_{ie} \;\; \Phi_{ei} \;\; \Phi_{ii} \;\; \phi^{\alpha}_{ee} \;\; \kappa_{ee} \;\; \phi^{\alpha}_{ei} \;\; \kappa_{ei} \;\; \chi_{se} \;\; \phi^{sc}_{se} \;\; \chi_{si} \;\; \phi^{sc}_{si}]^{\mathrm{T}} \tag{6.11}$$

where we have expressed the two second-order coupling equations, Eq. (6.2), as four first-order equations by again defining some auxiliary variables,

$$\frac{\partial \phi^{\mathrm{sc}}_{se}}{\partial t} = \chi_{se}, \qquad \frac{\partial \phi^{\mathrm{sc}}_{si}}{\partial t} = \chi_{si}, \tag{6.12}$$

$$\frac{\partial \chi_{se}}{\partial t} = v^2 \Lambda^2_{se} \left[Q_s - \phi^{\mathrm{sc}}_{se}\right] + v^2 \nabla^2 \phi^{\mathrm{sc}}_{se} - 2v\Lambda_{se}\chi_{se}, \tag{6.13}$$

$$\frac{\partial \chi_{si}}{\partial t} = v^2 \Lambda^2_{si} \left[Q_s - \phi^{\mathrm{sc}}_{si}\right] + v^2 \nabla^2 \phi^{\mathrm{sc}}_{si} - 2v\Lambda_{si}\chi_{si}. \tag{6.14}$$

We define the 14 state variables for the thalamus as,

$$\text{thalamic\_state} = [V_s \;\; V_r \;\; \Phi_{es} \;\; \Phi_{is} \;\; \Phi_{er} \;\; \Phi_{ir} \;\; \Pi_{es} \;\; \Pi_{is} \;\; \Pi_{er} \;\; \Pi_{ir} \;\; \kappa_{es} \;\; \phi^{c}_{es} \;\; \kappa_{er} \;\; \phi^{c}_{er}]^{\mathrm{T}}. \tag{6.15}$$

Similarly, we express the coupling terms, Eqs. (6.1), as four first-order equations,

$$\frac{\partial \phi^{\mathrm{c}}_{es}}{\partial t} = \kappa_{es}, \qquad \frac{\partial \phi^{\mathrm{c}}_{er}}{\partial t} = \kappa_{er}, \tag{6.16}$$

$$\frac{\partial \kappa_{es}}{\partial t} = v^2 \Lambda^2_{es} \left[Q_e - \phi^{\mathrm{c}}_{es}\right] + v^2 \nabla^2 \phi^{\mathrm{c}}_{es} - 2v\Lambda_{es}\kappa_{es}, \tag{6.17}$$

$$\frac{\partial \kappa_{er}}{\partial t} = v^2 \Lambda_{er}^2 \left[Q_e - \phi_{er}^{\mathrm{c}} \right] + v^2 \nabla^2 \phi_{er}^{\mathrm{c}} - 2v \Lambda_{er} \kappa_{er}, \tag{6.18}$$

The total run-time to produce the thalamo-cortical steady states shown in Fig. 6.4 was about 2.5 weeks! The falsified points, marked as 'pluses', proved difficult to debug due to the non-linearities of the search algorithm, and in fact I was unable to recover these false roots when I probed the region more finely suggesting the outliers have been an artifact of an inadequate search density.

A hysteretic 'S-bend' curve is observed in Fig. 6.3 (c) is similar to that of the isolated thalamic model in Ch. 5. A notable difference is the firing rates on middle branch which increase slightly with reduction in λ_i before joining the low-firing steady state branch; for the isolated model this was a smooth parabolic-like curve. Also different from both isolated model steady states is the region of instability on the top branch, $1 \leq \lambda_i \leq 5$.

For the isolated cortical model, the distribution of steady states was more sensitive to changes in the anaesthetic scaling parameter than the isolated thalamic model. Large values of λ_i tended to suppress the high firing steady states of the cortex with only low-firing states remaining, this feature appears to still be present in the coupled model. Similarly, the isolated thalamic model tended to exist in a contrasted "winner takes all" state, i.e., high firing in specific populations, low firing in reticular populations and vice versa. These features are also still present.

6.4 Simulation

We again use an Euler update method for the coupled system. The system is initialized by selecting V_e^0, V_i^0, V_s^0 and V_r^0. The remaining state variables are computed by setting the time-derivatives of the coupled model to zero and solving.

$$\text{cortical\_ state}(i+1) = \text{cortical\_state}(i) + \frac{d\ \text{cortical\_state}(i)}{dt} * dt + \text{cort\_noise} * \sqrt{dt}, \tag{6.19}$$

$$\text{thalamic\_ state}(i+1) = \text{thalamic\_state}(i) + \frac{d\,\text{thalamic\_state}(i)}{dt} * dt + \text{thal\_noise} * \sqrt{dt}. \quad (6.20)$$

The first simulations we ran were in a region of λ_i where the high-firing and lower-firing steady state solutions were predicted to be stable. Plot (c) in Fig. 6.6 shows the transition from the initial unstable middle branch to the low firing stable steady state. Another run with these settings, Fig. 6.7, using a different noise sequence, shows the system 'falling' to the high-firing steady state which is also predicted to be stable. The oscillatory dynamics observed here are consistent with the imaginary part of the states eigenvalue, giving a damped oscillation of frequency ~ 3.5 Hz.

Figure 6.8 shows that for $\lambda_i = 4.4$, the high-firing steady state becomes unstable and delta-band oscillations (~ 3 Hz) emerge in thalamo-cortical system as it transitions to the stable low-firing state.

The $\lambda_i = 1.1$ run, shown in Figure 6.9, is interesting as the reticular population in the thalamus exhibits spindle-like oscillation (~ 15.5 Hz). However these oscillation do not carry through, in any significant sense, into the specific population and either cortical population.

6.5 Spindle Frequencies

In an attempt to propagate the spindle frequencies observed in Fig. 6.9, to all thalamo-cortical populations, I modified two parameters within the model structure. It is important to note that I did not define the steady states for this section due to time constraints and no physiological basis is given to the parameter changes made.

In order to carry the spindle frequencies into the specific population, I increase the connection constant scaling flux from the reticular population entering the specific population, i.e. $N_{rs} = 550$ is increased to $N_{rs} = 900$. The flux entering the specific population from the cortex still appeared to dominate, therefore I decrease the connection constant scaling input from the excitatory population, i.e. $N_{es} = 2700$ is decreased to $N_{es} = 1350$. Figure 6.10 shows the simulation for $\lambda_i = 1.1$ with initial conditions near those of the high-firing steady state branch from Fig. 6.4 (c). Values of N_{es} larger than 1350 caused damping of the spindle oscillations and

reducing N_{es} below 1350 caused the oscillations to grow suggesting the steady state associated with the spindle oscillations had become unstable.

6.6 Conclusion

The method we used to solve the steady states for the thalamo-cortical system is slow to implement in a MATLAB environment. To limit the run-time we employed several optimization techniques, including dynamically changing search densities during runtime, which may have resulted in the code occasionally returning false steady states. Of the 297 steady states returned for Fig. 6.4, only 4 were found to disagree with the system behaviour observed during simulation. These spurious states are identifiable on close inspection of Fig. 6.4.

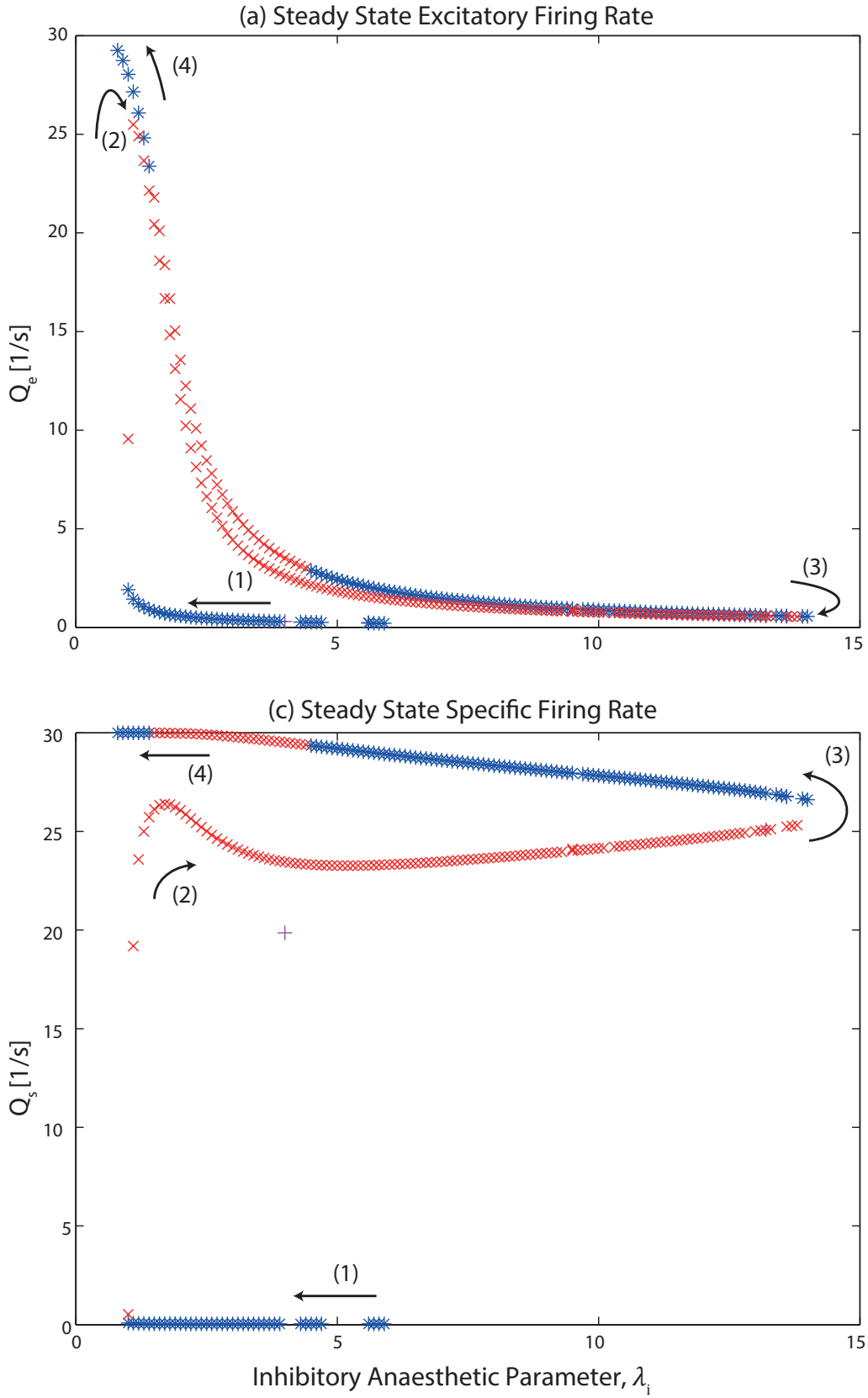

Figure 6.4: Excitatory and specific population steady state firing rates for the complete coupled thalamocortical system. The 'plus' marker shows states returned by the root finding MATLAB code that did not agree with simulations. Blue 'stars' are stable steady states and red 'crosses' are steady states predicted to be unstable.

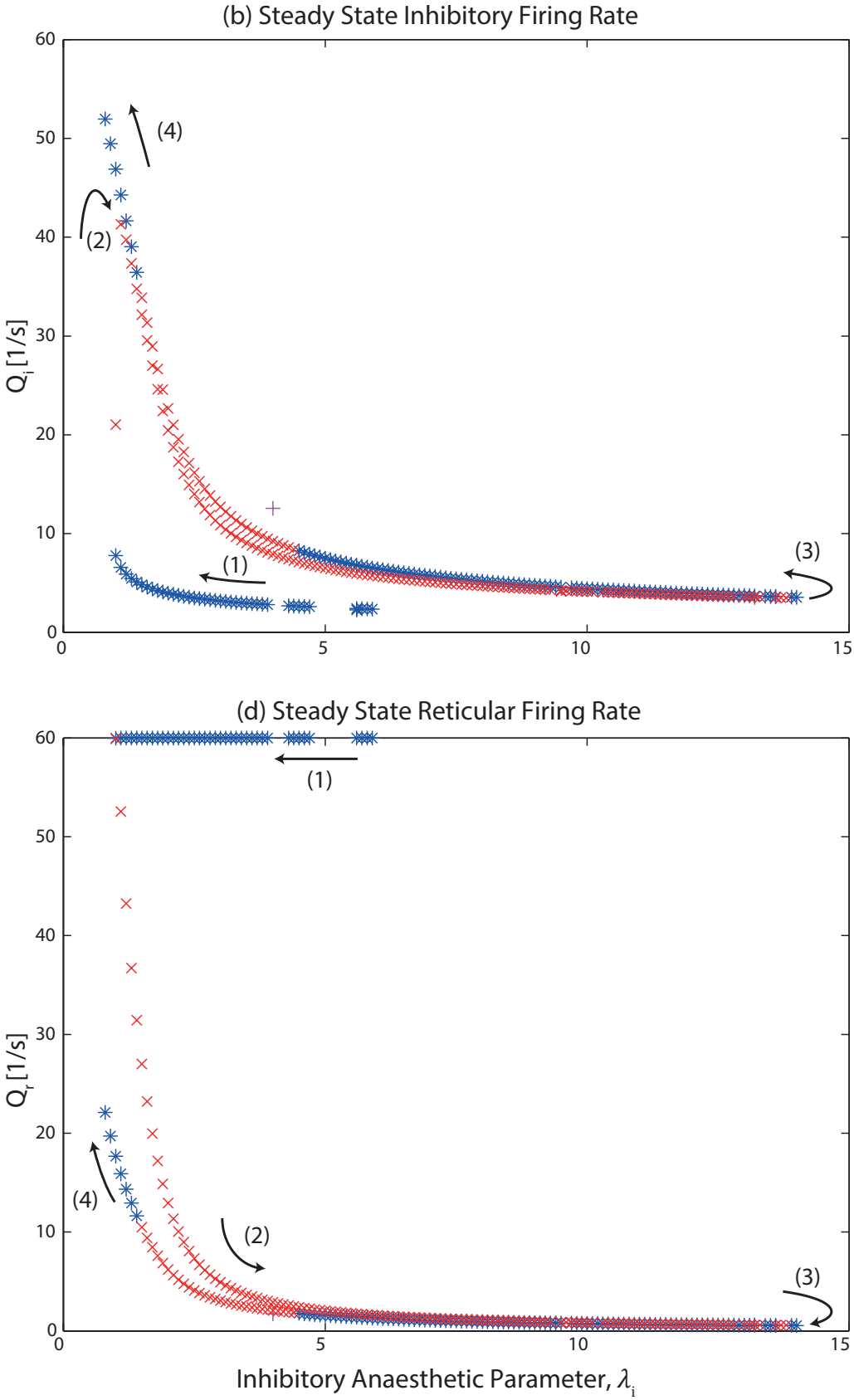

Figure 6.5: Inhibitory and reticular population steady state firing rates for the complete coupled thalamo-cortical system. The 'plus' marker shows states returned by the root finding MATLAB code that did not agree with simulations. Blue 'stars' are stable steady states and red 'crosses' are steady states predicted to be unstable.

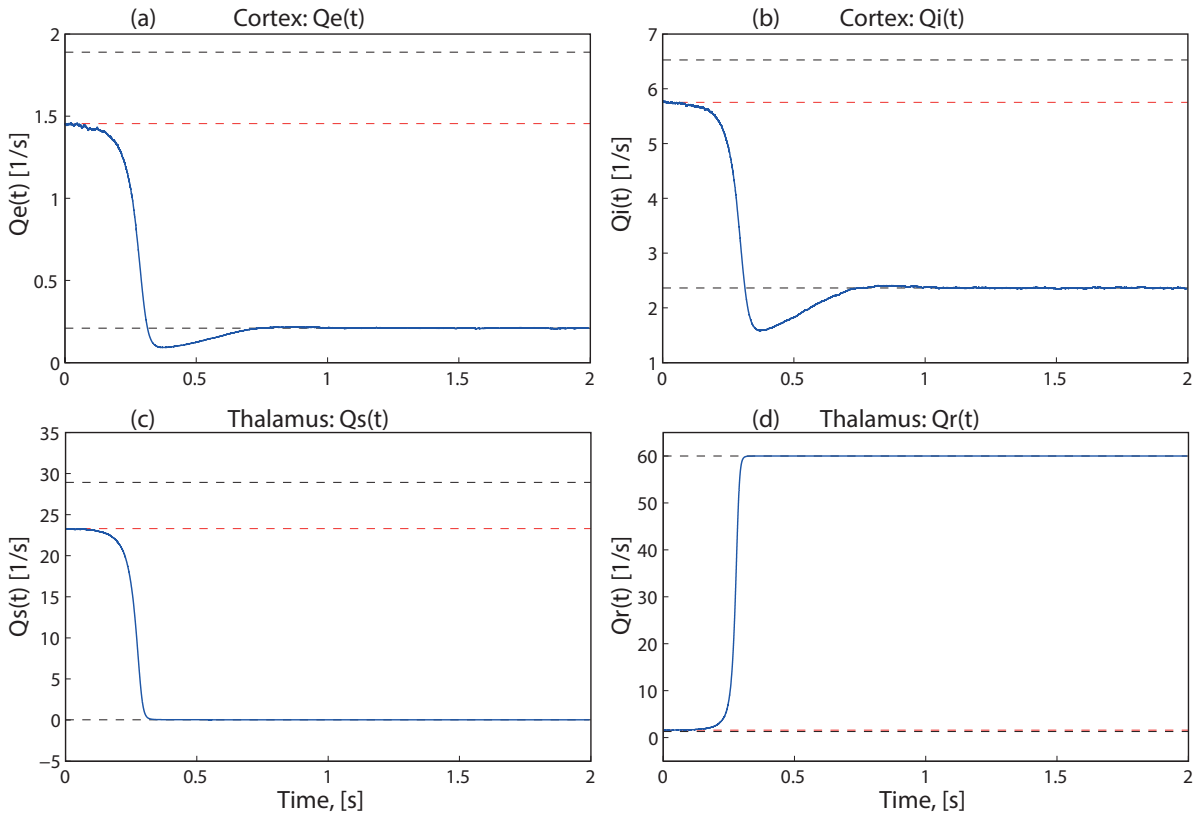

Figure 6.6: Thalamo-cortical simulation for $\lambda_i = 5.9$. Initialized to the unstable middle branch from Fig. 6.4.

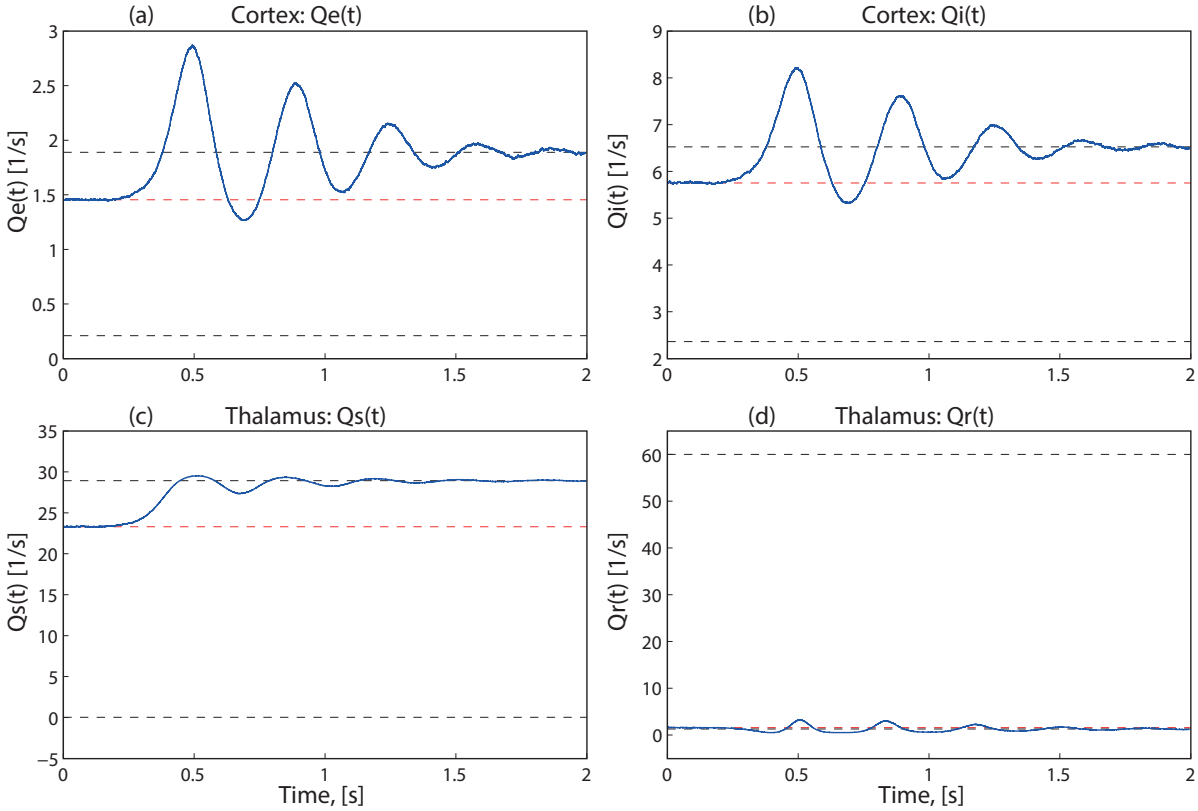

Figure 6.7: Same settings as for Fig. 6.6, but with a different noise sequence producing a distinctly different final state.

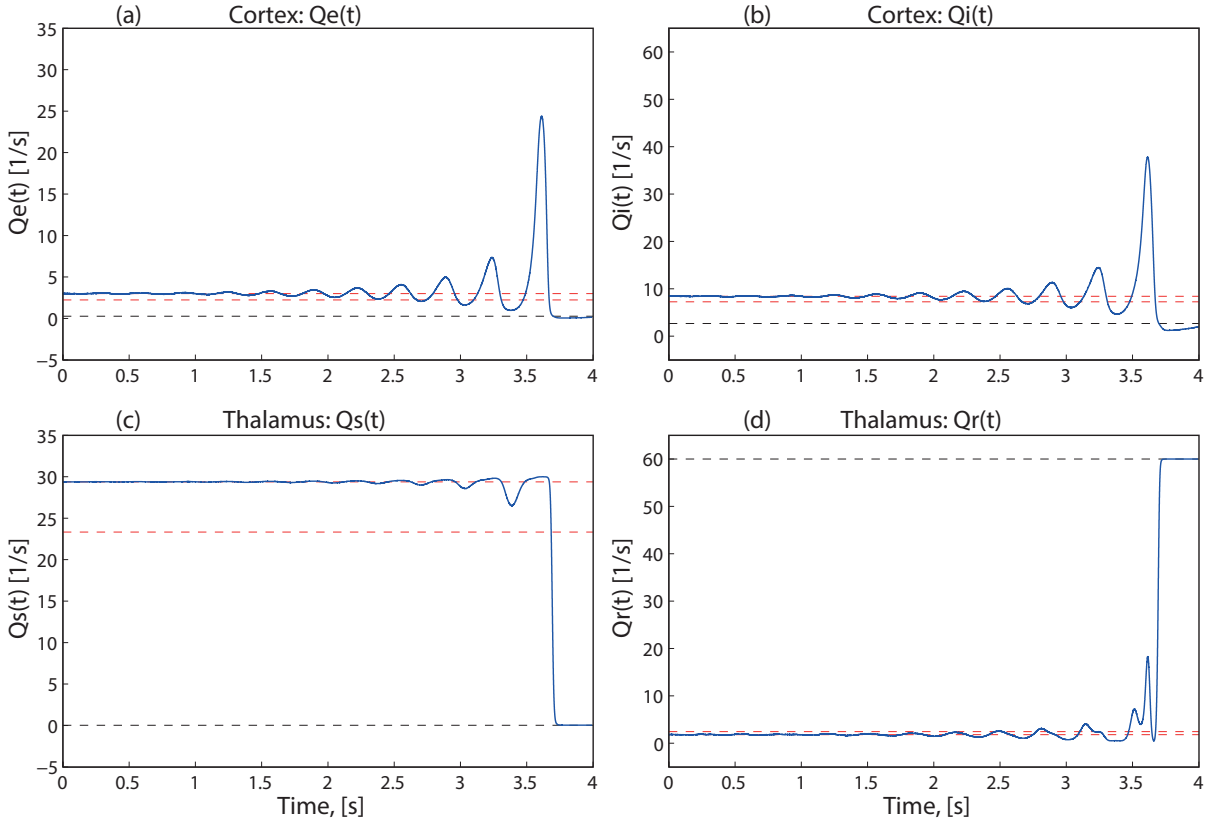

Figure 6.8: Thalamo-cortical simulation for $\lambda_i = 4.4$. System initialized to the high firing steady state which is predicted to be unstable. Note the emergence of delta-band (~ 3 Hz) oscillations in the cortex.

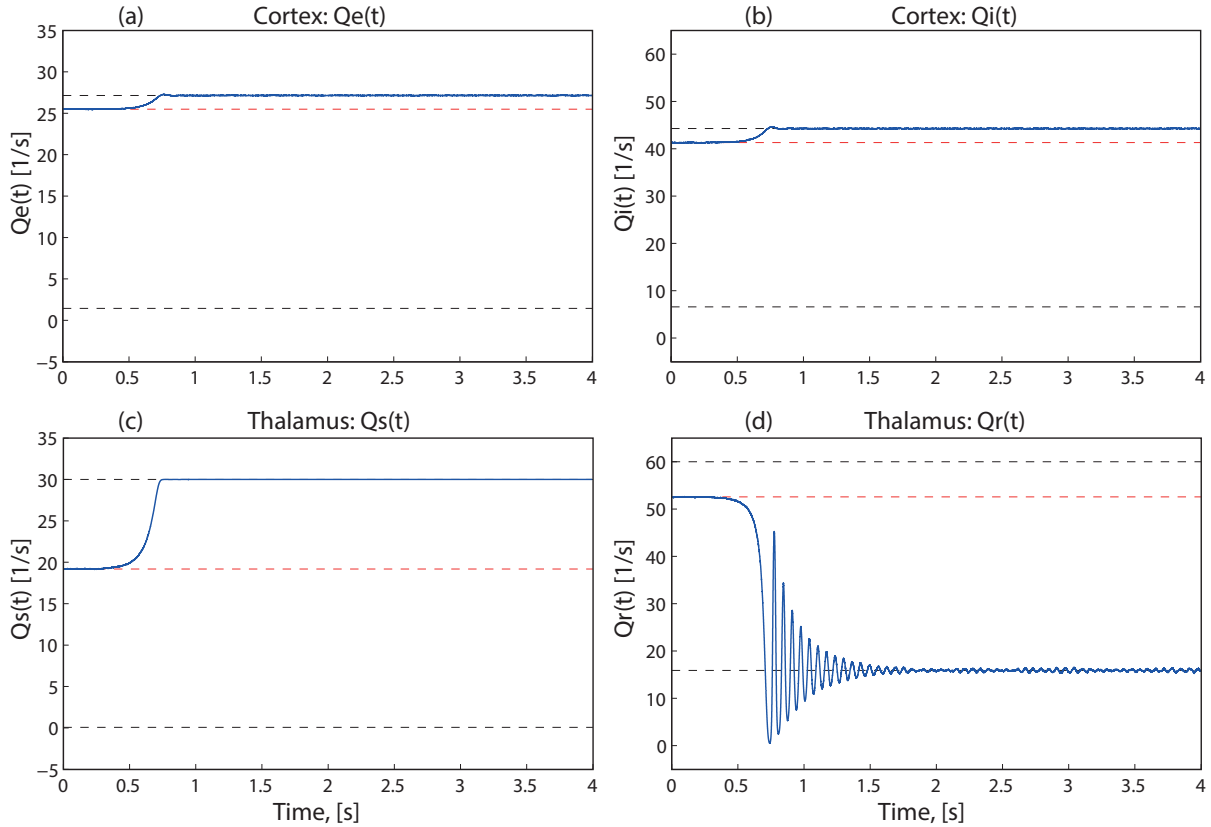

Figure 6.9: Thalamo-cortical simulation for $\lambda_i = 1.1$. Spindle-like oscillations (frequency ~ 15.5 Hz) in the reticular neuron population after transition to the low-firing steady state.

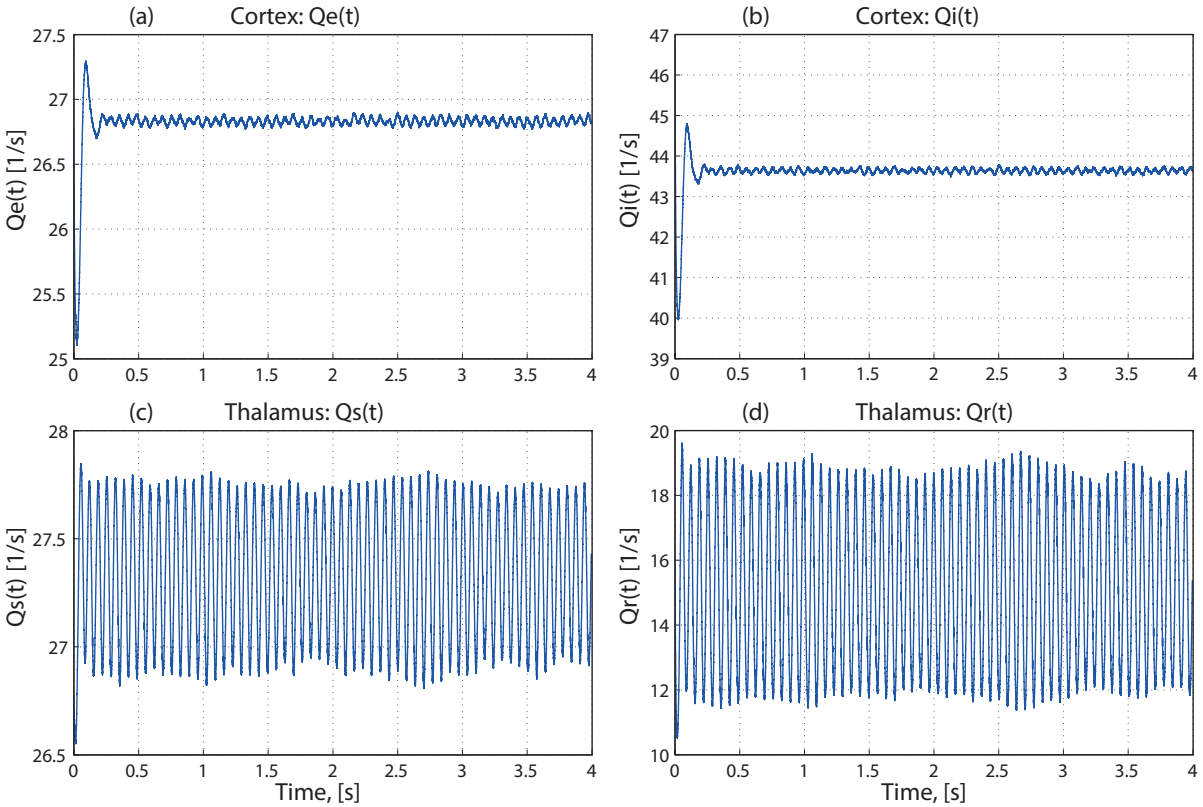

Figure 6.10: Simulation with modified thalamo-cortical parameters for $\lambda_i = 1.1$. Spindle-like oscillations (frequency $\sim$ 15 Hz) in all populations. Connection parameters modified, $N_{rs} = 900$, $N_{es} = 1350$.

Chapter 7

Summary

7.1 Conclusion

Based on the work of Steyn-Ross *et al.* and Liley *et al.* we presented a mean-field model of the cortex. We demonstrated the hysteresis effect present in the distribution of the stationary states of the model. This history dependence is a common feature observed in clinical anaesthetics corresponding to a separation of the anaesthetic levels required to drive a neuron population *unconscious* and then return it to a *conscious* state. We demonstrated the model's tendency to exist in either a high-firing, excited state or a low-firing, inhibited state. We presented the mathematical structure to model the effects of an anaesthetic such as propofol and demonstrated its effects on the cortical stationary states.

A mean-field model of a thalamus, structured similarly to the mean-field cortical model, was defined. We assumed only local excitation within the model, ignoring *long-range* connections within the thalamic macrocolumn. For the reticular neuron population, a novel, bimodal, mapping function was constructed from sigmoids, allowing a hyperpolarized membrane potential to be associated with a high firing rate. A history dependence for the thalamic model was also found to be present, however, over a much larger scale of anesthetic effect. The thalamic model also had a tendency to exist in either a high-firing, excited state or a low-firing, inhibited state.

A coupling of the isolated cortical and thalamic models was presented. By defining four damped wave equations, excitation terms from the thalamus' specific population were connected to both cortical subpopulations, and excitation terms from the cortex were connected to both thalamic subpopulations. We first performed stationary state analysis on the one-way coupling of the two isolated systems. The fully coupled systems stationary states and their stabilities was then investigated. Again a hysteresis effect was present.

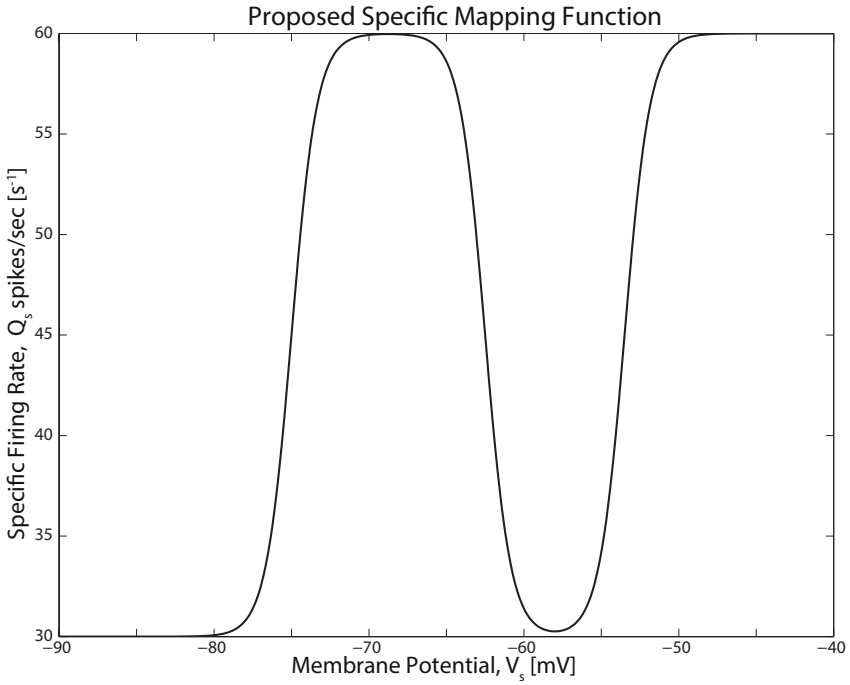

Figure 7.1: More realistic mapping function relating membrane potential to population firing rate.

7.2 Further Work

In this thesis we have investigated a first approximation to modelling the current flows present in the reticular neuron populations of the thalamus for hyperpolarizing membrane potentials. However, it has been shown that the specific population also has unique electrophysical properties. A more accurate extension of this model would incorporate the increase in specific population firing rates observed for hyperpolarized membrane potentials, and further reductions in the membrane potential relating to low-firing. This could be achieved with the definition of a new mapping function of the form,

$$Q_s(t) = Q_s^1(t) + Q_s^2(t) + Q_s^3(t) \tag{7.1}$$

$$Q_s^1(t) = \frac{Q_s^{\max}/2}{1 + e^{c(V_s(t) - \theta_{s,1})/\sigma_{s,1}}} \quad Q_s^2(t) = \frac{Q_s^{\max}/2}{1 + e^{c(V_s(t) - \theta_{s,2})/\sigma_{s,2}}} \quad Q_s^3(t) = \frac{Q_s^{\max}/2}{1 + e^{c(V_s(t) - \theta_{s,3})/\sigma_{s,3}}}$$

Appendix A

Jacobian Matrix Elements

A.1 Coupled Cortical Model: non-zero elements

For the isolated cortical model set the coupling variables, χ_{se}, ϕ^{sc}_{se}, χ_{si} , ϕ^{sc}_{si} to zero and ignore their derivatives f_{15}, f_{16}, f_{17}, f_{18}.

$$\text{state} = [V_e \;\; V_i \;\; \Phi_{ee} \;\; \Phi_{ei} \;\; \Phi_{ie} \;\; \Phi_{ii} \;\; \Pi_{ee} \;\; \Pi_{ei} \;\; \Pi_{ie} \;\; \Pi_{ii} \;\; \phi^{\alpha}_{ee} \;\; \phi^{\alpha}_{ei} \;\; \kappa_{ee} \;\; \kappa_{ei} \;\; \chi_{se} \;\; \phi^{sc}_{se} \;\; \chi_{si} \;\; \phi^{sc}_{si}]^{\mathrm{T}}$$

$$\frac{d(\text{state})}{dt} = [f_1 \;\; f_2 \;\; f_3 \;\; f_4 \;\; f_5 \;\; f_6 \;\; f_7 \;\; f_8 \;\; f_9 \;\; f_{10} \;\; f_{11} \;\; f_{12} \;\; f_{13} \;\; f_{14} \;\; f_{15} \;\; f_{16} \;\; f_{17} \;\; f_{18}]$$

$$\frac{\partial f_1}{\partial V_e} = \frac{1}{\tau_e}\left[- \frac{\rho_e \Phi_{ee}}{V_e^{\text{rev}} - V_e^{\text{rest}}} - \frac{\rho_i \Phi_{ie}}{V_i^{\text{rev}} - V_e^{\text{rest}}} - 1 \right] \tag{A.1}$$

$$\frac{\partial f_1}{\partial \Phi_{ee}} = \frac{\rho_e \psi_{ee}}{\tau_e}, \qquad \frac{\partial f_1}{\partial \Phi_{ie}} = \frac{\rho_e \psi_{ie}}{\tau_e} \tag{A.2}$$

$$\frac{\partial f_2}{\partial V_i} = \frac{1}{\tau_i}\left[- \frac{\rho_e \Phi_{ei}}{V_e^{\text{rev}} - V_i^{\text{rest}}} - \frac{\rho_i \Phi_{ii}}{V_i^{\text{rev}} - V_i^{\text{rest}}} - 1 \right] \tag{A.3}$$

$$\frac{\partial f_2}{\partial \Phi_{ei}} = \frac{\rho_e \psi_{ei}}{\tau_i}, \qquad \frac{\partial f_2}{\partial \Phi_{ii}} = \frac{\rho_i \psi_{ii}}{\tau_i} \tag{A.4}$$

$$\frac{\partial f_3}{\partial \Pi_{ee}} = 1, \qquad \frac{\partial f_4}{\partial \Pi_{ei}} = 1, \qquad \frac{\partial f_5}{\partial \Pi_{ie}} = 1, \qquad \frac{\partial f_6}{\partial \Pi_{ii}} = 1 \tag{A.5}$$

$$\frac{\partial f_7}{\partial V_e} = \gamma_{ee}^2 \left[\frac{N_{ee}^{\beta}\, c\, Q_e^{\max} \exp(-c(V_e - \theta_e)/\sigma_e))}{\sigma_e (1 + \exp(-c(V_e - \theta_e)/\sigma_e)))^2} \right] \tag{A.6}$$

$$\frac{\partial f_7}{\partial \Phi_{ee}} = -\gamma_{ee}^2, \qquad \frac{\partial f_7}{\partial \Pi_{ee}} = -2\gamma_{ee}, \qquad \frac{\partial f_7}{\partial \phi_{ee}^{\alpha}} = \gamma_{ee}^2 N_{ee}^{\alpha}, \qquad \frac{\partial f_7}{\partial \phi_{se}^{\mathrm{sc}}} = -\gamma_{ee}^2 N_{se} \tag{A.7}$$

$$\frac{\partial f_8}{\partial V_e} = \gamma_{ei}^2 \left[\frac{N_{ei}^{\beta}\, c\, Q_e^{\max} \exp(-c(V_e - \theta_e)/\sigma_e))}{\sigma_e (1 + \exp(-c(V_e - \theta_e)/\sigma_e)))^2} \right] \tag{A.8}$$

$$\frac{\partial f_8}{\partial \Phi_{ei}} = -\gamma_{ei}^2, \qquad \frac{\partial f_8}{\partial \Pi_{ei}} = -2\gamma_{ei}, \qquad \frac{\partial f_8}{\partial \phi_{ei}^{\alpha}} = \gamma_{ei}^2 N_{ee}^{\alpha}, \qquad \frac{\partial f_8}{\partial \phi_{si}^{\mathrm{sc}}} = -\gamma_{ei}^2 N_{si} \tag{A.9}$$

$$\frac{\partial f_9}{\partial V_i} = \gamma_{ie}^2 \left[\frac{N_{ie}^{\beta}\, c\, Q_i^{\max} \exp(-c(V_i - \theta_i)/\sigma_i))}{\sigma_i (1 + \exp(-c(V_i - \theta_i)/\sigma_i)))^2} \right] \tag{A.10}$$

$$\frac{\partial f_9}{\partial \Phi_{ie}} = -\gamma_{ie}^2, \qquad \frac{\partial f_9}{\partial \Pi_{ie}} = -2\gamma_{ie} \tag{A.11}$$

$$\frac{\partial f_{10}}{\partial V_i} = \gamma_{ii}^2 \left[\frac{N_{ii}^{\beta}\, c\, Q_i^{\max} \exp(-c(V_i - \theta_i)/\sigma_i))}{\sigma_i (1 + \exp(-c(V_i - \theta_i)/\sigma_i)))^2} \right] \tag{A.12}$$

$$\frac{\partial f_{10}}{\partial \Phi_{ii}} = -\gamma_{ii}^2, \qquad \frac{\partial f_{10}}{\partial \Pi_{ii}} = -2\gamma_{ii} \tag{A.13}$$

$$\frac{\partial f_{11}}{\partial \kappa_{ee}} = 1, \qquad \frac{\partial f_{12}}{\partial \kappa_{ei}} = 1 \tag{A.14}$$

$$\frac{\partial f_{13}}{\partial V_e} = v^2 \Lambda_{ee}^2 \left[\frac{c\, Q_e^{\max} \exp(-c(V_e - \theta_e)/\sigma_e))}{\sigma_e (1 + \exp(-c(V_e - \theta_e)/\sigma_e)))^2} \right] \tag{A.15}$$

$$\frac{\partial f_{13}}{\partial \phi_{ee}^{\alpha}} = -v^2 \Lambda_{ee}^2, \qquad \frac{\partial f_{13}}{\partial \kappa_{ee}} = -2v\Lambda_{ee} \tag{A.16}$$

$$\frac{\partial f_{14}}{\partial V_e} = v^2 \Lambda_{ei}^2 \left[\frac{c\, Q_e^{\max} \exp(-c(V_e - \theta_e)/\sigma_e))}{\sigma_e (1 + \exp(-c(V_e - \theta_e)/\sigma_e)))^2} \right] \tag{A.17}$$

$$\frac{\partial f_{14}}{\partial \phi_{ei}^{\alpha}} = -v^2 \Lambda_{ei}^2, \qquad \frac{\partial f_{14}}{\partial \kappa_{ei}} = -2v\Lambda_{ei} \tag{A.18}$$

$$\frac{\partial f_{15}}{\partial \chi_{se}} = -2v\Lambda_{se}, \qquad \frac{\partial f_{15}}{\partial \phi_{se}^{\mathrm{sc}}} = -v^2 \Lambda_{se}^2, \qquad \frac{\partial f_{16}}{\partial \chi_{se}} = 1 \tag{A.19}$$

$$\frac{\partial f_{17}}{\partial \chi_{si}} = -2v\Lambda_{si}, \qquad \frac{\partial f_{17}}{\partial \phi_{si}^{\mathrm{sc}}} = -v^2 \Lambda_{si}^2, \qquad \frac{\partial f_{18}}{\partial \chi_{si}} = 1 \tag{A.20}$$

A.2 Coupled Thalamic Model: non-zero elements

For the isolated thalamic model set the coupling variables, κ_{es}, ϕ^{c}_{es}, κ_{er}, ϕ^{c}_{er} to zero and ignore their derivatives f_{11}, f_{12}, f_{13}, f_{14}.

$$\begin{aligned}\text{state} &= [V_s \;\; V_r \;\; \Phi_{es} \;\; \Phi_{is} \;\; \Phi_{er} \;\; \Phi_{ir} \;\; \Pi_{es} \;\; \Pi_{is} \;\; \Pi_{er} \;\; \Pi_{ir} \;\; \kappa_{es} \;\; \phi^{\mathrm{c}}_{es} \;\; \kappa_{er} \;\; \phi^{\mathrm{c}}_{er}]^{\mathrm{T}} \\ \frac{d(\text{state})}{dt} &= [f_1 \;\; f_2 \;\; f_3 \;\; f_4 \;\; f_5 \;\; f_6 \;\; f_7 \;\; f_8 \;\; f_9 \;\; f_{10} \;\; f_{11} \;\; f_{12} \;\; f_{13} \;\; f_{14}]\end{aligned}$$

$$\frac{\partial f_1}{\partial V_s} = \frac{1}{\tau_s}\left[- \frac{\rho_s \Phi_{es}}{V_s^{\mathrm{rev}} - V_s^{\mathrm{rest}}} - \frac{\rho_r \Phi_{is}}{V_r^{\mathrm{rev}} - V_s^{\mathrm{rest}}} - 1\right] \tag{A.21}$$

$$\frac{\partial f_1}{\partial \Phi_{es}} = \frac{\rho_s \psi_{ss}}{\tau_s}, \qquad \frac{\partial f_1}{\partial \Phi_{is}} = \frac{\rho_r \psi_{rs}}{\tau_s} \tag{A.22}$$

$$\frac{\partial f_2}{\partial V_r} = \frac{1}{\tau_r}\left[- \frac{\rho_s \Phi_{er}}{V_s^{\mathrm{rev}} - V_r^{\mathrm{rest}}} - \frac{\rho_r \Phi_{ir}}{V_r^{\mathrm{rev}} - V_r^{\mathrm{rest}}} - 1\right] \tag{A.23}$$

$$\frac{\partial f_2}{\partial \Phi_{er}} = \frac{\rho_s \psi_{sr}}{\tau_r}, \qquad \frac{\partial f_2}{\partial \Phi_{ir}} = \frac{\rho_r \psi_{rr}}{\tau_r} \tag{A.24}$$

$$\frac{\partial f_3}{\partial \Pi_{es}} = 1, \qquad \frac{\partial f_4}{\partial \Pi_{is}} = 1, \qquad \frac{\partial f_5}{\partial \Pi_{er}} = 1, \qquad \frac{\partial f_6}{\partial \Pi_{ir}} = 1 \tag{A.25}$$

$$\frac{\partial f_7}{\partial V_s} = \gamma_{es}^2 \left[\frac{N_{ss}^{\beta}\, c\, Q_s^{\max} \exp(-c(V_s - \theta_s)/\sigma_s))}{\sigma_s (1 + \exp(-c(V_s - \theta_s)/\sigma_s)))^2} \right] \tag{A.26}$$

$$\frac{\partial f_7}{\partial \Phi_{es}} = -\gamma_{es}^2, \qquad \frac{\partial f_7}{\partial \Pi_{es}} = -2\gamma_{es}, \qquad \frac{\partial f_7}{\partial \phi_{es}^{\mathrm{c}}} = \gamma_{es}^2 N_{es} \tag{A.27}$$

$$\frac{\partial f_8}{\partial V_r} = \gamma_{is}^2 N_{rs}^{\beta} \left[\frac{c\, Q_r^{\max} \exp(-c(V_r - \theta_{r,1})/\sigma_{r,1}))}{\sigma_{r,1}(1+\exp(-c(V_r-\theta_{r,1})/\sigma_{r,1})))^2} - \frac{c\, Q_r^{\max} \exp(c(V_r - \theta_{r,2})/\sigma_{r,2}))}{\sigma_{r,2}(1+\exp(c(V_r-\theta_{r,2})/\sigma_{r,2})))^2} \right] \tag{A.28}$$

$$\frac{\partial f_8}{\partial \Phi_{is}} = -\gamma_{is}^2, \qquad \frac{\partial f_8}{\partial \Pi_{is}} = -2\gamma_{is} \tag{A.29}$$

$$\frac{\partial f_9}{\partial V_s} = \gamma_{er}^2 \left[\frac{N_{sr}^{\beta}\, c\, Q_s^{\max} \exp(-c(V_s - \theta_s)/\sigma_s))}{\sigma_s(1+\exp(-c(V_s-\theta_s)/\sigma_s)))^2} \right] \tag{A.30}$$

$$\frac{\partial f_9}{\partial \Phi_{er}} = -\gamma_{er}^2, \qquad \frac{\partial f_9}{\partial \Pi_{er}} = -2\gamma_{er}, \qquad \frac{\partial f_9}{\partial \phi_{er}^{\mathrm{c}}} = \gamma_{er}^2 N_{er} \tag{A.31}$$

$$\frac{\partial f_{10}}{\partial V_r} = \gamma_{ir}^2 N_{rr}^{\beta} \left[\frac{c\, Q_r^{\max} \exp(-c(V_r - \theta_{r,1})/\sigma_{r,1}))}{\sigma_{r,1}(1+\exp(-c(V_r-\theta_{r,1})/\sigma_{r,1})))^2} - \frac{c\, Q_r^{\max} \exp(c(V_r - \theta_{r,2})/\sigma_{r,2}))}{\sigma_{r,2}(1+\exp(c(V_r-\theta_{r,2})/\sigma_{r,2})))^2} \right] \tag{A.32}$$

$$\frac{\partial f_{10}}{\partial \Phi_{ir}} = -\gamma_{ir}^2, \qquad \frac{\partial f_{10}}{\partial \Pi_{ir}} = -2\gamma_{ir} \tag{A.33}$$

$$\frac{\partial f_{11}}{\partial \kappa_{es}} = -2v\Lambda_{es}, \qquad \frac{\partial f_{11}}{\partial \phi_{es}^{\mathrm{c}}} = -v^2\Lambda_{es}^2, \qquad \frac{\partial f_{12}}{\partial \kappa_{es}} = 1 \tag{A.34}$$

$$\frac{\partial f_{13}}{\partial \kappa_{er}} = -2v\Lambda_{er}, \qquad \frac{\partial f_{13}}{\partial \phi^{\mathrm{c}}_{er}} = -v^2\Lambda^2_{er}, \qquad \frac{\partial f_{14}}{\partial \kappa_{er}} = 1 \tag{A.35}$$

Appendix B

MATLAB Code

B.1 Isolated Cortex: Steady State Finder

```
function [Qe_root, Qi_root, Ve_root, Vi_root] = SS_rootFinder_cort(...
    lambda_e, lambda_i, del_VeRest, plotGraph, dN)
%function for finding the stationary
%states of the mean-field cortical
%equations

%Based on the code of Alistair Steyn-Ross
%Created by Eli Muller
%   July 2012

set(0, 'defaultaxesfontsize', 12);
format long;

if nargin == 0
        [lambda_e, lambda_i, del_VeRest] = deal(1, 1, 1.5); % 'wake'
%         [lambda_e, lambda_i, del_VeRest] = deal(1, 1.018, 1.5); % 'coma'
    plotGraph = 0;
        dN = 3000;
end

global H
H = init_spat_het_globs;
```

```
N_max = 8*128000;
numRoots = 0;
%%%%%%%%%%%%%%   Searching for roots   %%%%%%%%%%%%%%%%%%%
while((numRoots == 0 || numRoots == 2) && dN <= N_max)

    %Search range of feasible Q_e
    Qe = linspace(0, H.Qe_max, dN)'; % transposed

    %Computes an array of values comparing Qe and a reverse calulated Qe
    delta_Qe = Qe_diff(Qe, lambda_e, lambda_i, del_VeRest);

    %Finds the index of the sign change correspnding to the points
    %straddle the Qe root
    signCh_Qe = delta_Qe(1:end-1).*delta_Qe(2:end);
    signCh_Qe_index = find(signCh_Qe < 0);

    numRoots = length(signCh_Qe_index);
    if(numRoots == 0 || numRoots == 2)
        %Increase search density, expecting 1 or 3 roots
        dN = 2*dN;
    end
end

if(numRoots == 0)
   disp('Failed to find a root --- skipped')
end

%Finds the intervals of Qe which straddle the axis crossing
if numRoots >= 1
   window_Qe = [Qe(signCh_Qe_index) Qe(signCh_Qe_index+1)];

    if any(isnan(window_Qe(:)))
        disp('Error: NaN in bracket');
    end
```

```
end

%Using fzero() to refine Qe root and then reverse calculating Qi, Ve Vi
%roots
Qe_root = NaN*ones(numRoots, 1);
Qi_root = NaN*ones(numRoots, 1);
Ve_root = NaN*ones(numRoots, 1);
Vi_root = NaN*ones(numRoots, 1);
for i = 1: numRoots
        Qe_root(i) = fzero('Qe_diff', window_Qe(i,:), [], [], ...
                           lambda_e, lambda_i, del_VeRest);
        Ve_root(i) = invsig(Qe_root(i), 'e');

        Qi_root(i) = g_Ve(Qe_root(i), Ve_root(i), ...
                           lambda_e, lambda_i, del_VeRest);
        Vi_root(i) = invsig(Qi_root(i), 'i');
end

%Graphing Excitatory Firing rate vs delta V
if plotGraph
    figure(10)

    %Excitatory Firing Rate
    Qe = linspace(0, H.Qe_max, dN)'; % transposed
    Ve = invsig(Qe, 'e');

    Qi_prime = g_Ve(Qe, Ve, lambda_e, lambda_i, del_VeRest);
    Vi_prime = invsig(Qi_prime, 'i');

    Qe_prime = f_Vi(Qi_prime, Vi_prime, lambda_e, lambda_i, del_VeRest);
    Ve_prime = invsig(Qe_prime, 'e');

    plot(Qe, Ve-Ve_prime)
    grid on;
```

```
    title('');
    xlabel('Excitatory Firing Rate, (s^{-1})');
    ylabel('Difference in Excitatory Voltage, {\Delta}V (mV)');
    hold off;
end

end

function delta_Qe = Qe_diff(Qe_in, lambda_e, lambda_i, del_VeRest)
%Computes the difference between sample excitatory firing rate
%and the reverse calculated firing rate
%

%Excitatory ---> Inhibitory
Ve_in = invsig(Qe_in, 'e');
Qi_temp = g_Ve(Qe_in, Ve_in, lambda_e, lambda_i, del_VeRest);

%Inhibitory ---> Excitatory
Vi_temp = invsig(Qi_temp, 'i');
Qe_out = f_Vi(Qi_temp, Vi_temp, lambda_e, lambda_i);

%Calculate the difference
delta_Qe = Qe_out - Qe_in;

end



function Qe_out = f_Vi(Qi_in, Vi_in, lambda_e, lambda_i)
%Uses Qi and Vi to compute Qe
%
%       Qe = f(Vi)

global H
```

```
%subcortical noise constant
sub_cort_drive_ei = H.Nse*0.05;

%Calculate Psi constants for i
psi_Vei = Psi_ab(Vi_in, 'ei');
psi_Vii = Psi_ab(Vi_in, 'ii');

numer = Vi_in - H.Vi_rest - (lambda_i* H.gi * psi_Vii .* ...
    (H.Nii_b .* Qi_in));
denom = lambda_e* H.ge * psi_Vei;



Qe_out = (numer ./ denom - sub_cort_drive_ei) / (H.Nei_ab);
Qe_out = clampQ(Qe_out, 'e');   %Restrain Qe to reasonable range
end

function Qi_out = g_Ve(Qe_in, Ve_in, lambda_e, lambda_i, del_VeRest)
%Uses Qe and Ve to compute Qi
%
%       Qi = g(Ve)

global H

%subcortical noise constant
sub_cort_drive_ee = H.Nse*0.05;

%Calculate Psi values for e
psi_Vie = Psi_ab(Ve_in, 'ie');
psi_Vee = Psi_ab(Ve_in, 'ee');

numer = Ve_in - H.Ve_rest - del_VeRest - lambda_e* H.ge * psi_Vee .*...
    (H.Nee_ab * Qe_in + sub_cort_drive_ee);
denom = lambda_i* H.gi * psi_Vie;
```

```
Qi_out = (numer ./ denom) / H.Nie_b;
Qi_out = clampQ(Qi_out, 'i');   %Restrain Qi to reasonable range
end

function psi_out = Psi_ab(Vb, Index)
%weighting functions
%
%

global H

%Phi Constants

    switch Index
        case 'ee'
            psi_out = (H.Ve_rev - Vb)./(H.Ve_rev-H.Ve_rest);
        case 'ei'
            psi_out = (H.Ve_rev - Vb)./(H.Ve_rev-H.Vi_rest);
        case 'ie'
            psi_out = (H.Vi_rev - Vb)./(H.Vi_rev-H.Ve_rest);
        case 'ii'
            psi_out = (H.Vi_rev - Vb)./(H.Vi_rev-H.Vi_rest);
    end
end

function [Qa] = clampQ(Qa, Type)
%restricts firing rates to a feasible range
%
%
global H
    for i=1:length(Qa)
        if strcmp(Type, 'e')
            if Qa(i) <=0 || Qa(i) >=H.Qe_max
```

```
                Qa(i) = NaN;
            end
        elseif strcmp(Type, 'i')
            if Qa(i) <=0 || Qa(i) >=H.Qi_max
                Qa(i) = NaN;
            end
        end
    end
end

function [V] = invsig(Q, Type)
%function mapping firing rates
%to membrane potentials
%

global H
    Q = clampQ(Q, Type);

    if strcmp(Type, 'e')
        V = ((-H.sigma_e*sqrt(3))/pi)*log((H.Qe_max./Q)-1)+H.theta_e;
    elseif strcmp(Type, 'i')
        V = ((-H.sigma_i*sqrt(3))/pi)*log((H.Qi_max./Q)-1)+H.theta_i;
    end

end

function [Q] = sig(V, Type)
%function mapping membrane potentials
%to firing rates
%
global H

    if strcmp(Type, 'e')
        Q = H.Qe_max./(1+exp(-(pi/(H.sigma_e*sqrt(3))).*(V-H.theta_e)));
```

```
    elseif strcmp(Type, 'i')
        Q = H.Qi_max./(1+exp(-(pi/(H.sigma_i*sqrt(3))).*(V-H.theta_i)));
    end

end
```

B.2 Isolated Thalamus: Steady State Finder

```
function [Qs_root, Qr_root, Vs_root, Vr_root] = SS_rootFinder_thalamus(...
    lambda_s, lambda_r)
%function for finding the isolated thalamic roots
%by searching over a range of reticluar membrane
%potentials

%By Eli Muller
%   July 2012
%   Modified December 2012
%   Modified April 23rd 2013
%   Finalized November 15th 2013

set(0, 'defaultaxesfontsize', 12);
format long;



if nargin == 0
        [lambda_s, lambda_r] = deal(1, 1); % 'wake'
%         [lambda_s, lambda_r] = deal(1, 1.018); % 'coma'
        dN = 20;
    plotGraph = 1;
end

%Initialise Constants
global H
```

```
H = init_spat_het_globs;



%number of roots found
numRoots = 0;

%search density of Vr
dN = 20;

%Specify the number of search range refinements to be performed
N_max = 70;
%store number of refinements
count = 0;

%Search Range for Vr
Vr = [-70: 1/dN: -40]'; % transposed [mV]

%%%%%%%%%%%%%%   Searching for roots   %%%%%%%%%%%%%%%%%%%
while(numRoots < 3 && count < N_max)

    if(count > 0)
        Vr = sub_Vr';
    end

    %Computes an array of values comparing Vr and a reverse calulated Vr
    delta_Vr = Vr_diff(Vr, lambda_s, lambda_r);

    %looks for a sign change in delta_Vr corresponding to a root
    signCh_Vr = delta_Vr(1:end-1).*delta_Vr(2:end);
    signCh_Vr_index = find(signCh_Vr < 0);

    numRoots = length(signCh_Vr_index);

    %Check to see if any NaN boundaries need refining
```

```
    if(isempty(find(isnan(delta_Vr),1)))
        count = N_max;
    %Refine Search
    elseif(numRoots < 3)
        %increase by one for each refinment
        %maximum refinement is loopEnd
        count = count+1;
        sub_Vr = [];

        %Search for adjacent NaN and real terms
        for p=1:length(delta_Vr)-1

            if(isnan(delta_Vr(p)) && ~isnan(delta_Vr(p+1)) ||...
                    ~isnan(delta_Vr(p)) && isnan(delta_Vr(p+1)))

                sub_int =  Vr(p)+abs((Vr(p)-Vr(p+1)))/2;

                sub_Vr = [sub_Vr Vr(p) sub_int];

            else
                sub_Vr = [sub_Vr Vr(p)];
            end

        end
        %Redefine new Vr interval
        sub_Vr = [sub_Vr Vr(end)];
    end
end

if(numRoots == 0)
   disp('Failed to find a root --- skipped')
end

%%% Finds the intervals of Vr which straddle the Vr root
```

```
if numRoots >= 1

   window_Vr = [Vr(signCh_Vr_index) Vr(signCh_Vr_index+1)];

    if any(isnan(window_Vr(:)))
        disp('Error: NaN in bracket');
    end
end

%Using fzero() to refine Vr_root and then reverse calculating Qr, Qs, Vs
%roots
Qs_root = NaN*ones(numRoots, 1);
Qr_root = NaN*ones(numRoots, 1);
Vs_root = NaN*ones(numRoots, 1);
Vr_root = NaN*ones(numRoots, 1);
for i=1: numRoots
    Vr_root(i) = fzero('Vr_diff', window_Vr(i,:), [], [], ...
                                lambda_s, lambda_r);

    Qr_root(i) = reticular_sigmoid(Vr_root(i), 'norm');

    Qs_root(i) = f_Vr(Qr_root(i), Vr_root(i), ...
                                lambda_s, lambda_r);
    Vs_root(i) = invsig(Qs_root(i));

end

toc
end



function delta_Vr = Vr_diff(Vr_in, lambda_s, lambda_r)
%Computes the difference between sample reticular soma potentials
%and the reverse calculated potentials
```

```
%
global H

Qr_in = reticular_sigmoid(Vr_in,'norm');

%Reticulate ---> Specific
Qs_temp = f_Vr(Qr_in, Vr_in, lambda_s, lambda_r);

%Specific ---> Reticular
Vs_temp = invsig(Qs_temp);
Qr_out = g_Vs(Qs_temp, Vs_temp, lambda_s, lambda_r);

%Dual Valued
Vr_out = reticular_sigmoid(Qr_out,'inv');

%The middle of the dipped reticular mapping function
sig_mid = (H.theta_r1+H.theta_r2)/2;

%Selects the delta that is from the same side of the sigmoid as input
%voltage
for i=1:length(Vr_in)
    if(Vr_in(i) <= sig_mid)
        delta_Vr(i,1) = Vr_out(i,1) - Vr_in(i);
    else
        delta_Vr(i,1) =Vr_in(i) -  Vr_out(i,2);
    end
end

end



function Qs_out = f_Vr(Qr_in, Vr_in, lambda_s, lambda_r)
%Uses Qr Vr to compute Qs
%
```

```
%       Qs = f(Vr)

global H

%Calculate Psi values for r
psi_Vsr = Psi_ab(Vr_in, 'sr');
psi_Vrr = Psi_ab(Vr_in, 'rr');

numer = Vr_in - H.Vi_rest - (lambda_r* H.gi * psi_Vrr * H.Nrr .* Qr_in);
denom = lambda_s* H.ge * psi_Vsr;



Qs_out = (numer ./ denom)/H.Nsr;
Qs_out = clampQ(Qs_out, 's');   %Restrain Qs to reasonable range
end

function Qr_out = g_Vs(Qs_in, Vs_in, lambda_s, lambda_r)
%Uses Qs Vs and phi_es to compute Qr
%
%       Qr = g(Vs)

global H

%Calculate Psi values for s
psi_Vrs = Psi_ab(Vs_in, 'rs');
psi_Vss = Psi_ab(Vs_in, 'ss');

%sub_thalamic input stimulus
ext_stim = H.nu_ns*H.phi_n;

numer = Vs_in - H.Vs_rest - lambda_s* H.ge * psi_Vss .* ...
    (H.Nss * Qs_in + ext_stim);
denom = lambda_r* H.gi * psi_Vrs;
```

```
Qr_out = (numer ./ denom)/H.Nrs;
Qr_out = clampQ(Qr_out, 'r');   %Restrain Qr to reasonable range
end

function psi_out = Psi_ab(Vb, Index)
%Reversal Potential function
%for the thalamic neurons
%[dimensionless]
%

global H


    switch Index
        case 'ss'
            psi_out = (H.Vs_rev - Vb)./(H.Vs_rev-H.Vs_rest);
        case 'sr'
            psi_out = (H.Vs_rev - Vb)./(H.Vs_rev-H.Vr_rest);
        case 'rs'
            psi_out = (H.Vr_rev - Vb)./(H.Vr_rev-H.Vs_rest);
        case 'rr'
            psi_out = (H.Vr_rev - Vb)./(H.Vr_rev-H.Vr_rest);
    end
end

function [Qa] = clampQ(Qa, Type)
%Clamping function for constraining firing rates
%to within feasible range
%

global H

    for i=1:length(Qa)
```

```
        if strcmp(Type, 's')
            if Qa(i) <=0 || Qa(i) >=H.Qs_max
                Qa(i) = NaN;
            end
        elseif strcmp(Type, 'r')
            if Qa(i) <=0 || Qa(i) >=H.Qr_max
                Qa(i) = NaN;
            end
        end
    end
end

function [Vs] = invsig(Qs)
    %function mapping firing rates to
    %membrane potentials

    global H

    Qs = clampQ(Qs, 's');

    Vs = ((-H.sigma_e*sqrt(3))/pi)*log((H.Qs_max./Qs)-1)+H.theta_e;

end

function [Qs] = sig(Vs)
    %function mapping membrane potentials
    %to firing rates

    global H


     Qs = H.Qs_max./(1+exp(-(pi/(H.sigma_e*sqrt(3))).*(Vs-H.theta_e)));
end
```

B.3 Thalamo-Cortcial System: Steady State Finder

Modified form of the root finder from Section B.1.

```
function [Qe_root, Qi_root, Ve_root, Vi_root, Qs_root, Qr_root, Vs_root,...
    Vr_root] = SS_rootFinder_cort_coupled(lambda_e, lambda_i,...
    del_VeRest, sc, plotGraph, dN)
%computes the steady states
%of a coupled thalamo-cortical system
%

%Created by Eli Muller
%   November 2012

set(0, 'defaultaxesfontsize', 12);
format long;

global Vr
Vr = [];

if nargin == 0
        [lambda_e, lambda_i, del_VeRest, sc] = deal(1, 5.6, 1.5, 0.2);
%         [lambda_e, lambda_i, del_VeRest, sc] = deal(1, 1.018, 1.5, 0.2);
    plotGraph = 0;
        dN = 300;
    lambda_s = lambda_e;
    lambda_r = lambda_i;
end

global H
H = init_spat_het_globs;

N_max = 1200;
numRoots = 0;
```

```
%%%%%%%%%%%%%%   Searching for roots   %%%%%%%%%%%%%%%%%%
while(numRoots <= 2 && dN <= N_max)

    Qe = linspace(0, H.Qe_max, dN)'; % transposed

    %Computes an array of values comparing Qe and a reverse calulated Qe
    delta_Qe = Qe_diff(Qe, lambda_e, lambda_i, del_VeRest, sc);

    %sign change straddle root
    signCh_Qe = delta_Qe(1:end-1).*delta_Qe(2:end);
    signCh_Qe_index = find(signCh_Qe < 0);

    numRoots = length(signCh_Qe_index);
    if(numRoots <= 2)
        %Increase search density, expecting 1 or 3 roots
        display('Increasing dN')
        dN = 2*dN;
    end
end

if(numRoots == 0)
   disp('Failed to find a root --- skipped')
end

%Finds the intervals of Qe which straddle the axis crossing
if numRoots >= 1
   window_Qe = [Qe(signCh_Qe_index) Qe(signCh_Qe_index+1)];

    if any(isnan(window_Qe(:)))
        disp('Error: NaN in bracket');
    end
end
```

```
%Using fzero() to refine Qe root and then reverse calculating Qi, Ve Vi
%roots
Qe_root = NaN*ones(numRoots, 1);
Qi_root = NaN*ones(numRoots, 1);
Ve_root = NaN*ones(numRoots, 1);
Vi_root = NaN*ones(numRoots, 1);
Qs_root = NaN*ones(numRoots, 1);
Qr_root = NaN*ones(numRoots, 1);
Vs_root = NaN*ones(numRoots, 1);
Vr_root = NaN*ones(numRoots, 1);
for i = 1: numRoots
        Qe_root(i) = fzero('Qe_diff', window_Qe(i,:), [], [], ...
                                lambda_e, lambda_i, del_VeRest, sc);

    [Qs_prime, Qr_prime, Vs_prime, Vr_prime] = SS_rootFinder_thalamus(...
        Qe_root(i), lambda_e, lambda_i);

    %find correct thalamic root that is associated with the cortical root
    [Y I] = min(abs(Vr_prime - Vr));

    Vr_root(i) = Vr_prime(I);
    Vs_root(i) = Vs_prime(I);
    Qs_root(i) = Qs_prime(I);
    Qr_root(i) = Qr_prime(I);

        Ve_root(i) = invsig(Qe_root(i), 'e');

        Qi_root(i) = g_Ve(Qe_root(i), Ve_root(i), ...
                                Qs_root(i), lambda_e, lambda_i,...
                                del_VeRest, sc);
        Vi_root(i) = invsig(Qi_root(i), 'i');
end

end
```

```
function delta_Qe = Qe_diff(Qe_in, lambda_e, lambda_i, del_VeRest, sc)
%Computes the difference between sample excitatory firing rates
%and the reverse calculated firing rates
%
global Vr
    mark = 0;
    swit = 1;
    debug = [];

    %Loops through all Qe search values
    for i=1:length(Qe_in)

        %Foreach Qe find the corresponding thalamic roots, maybe multiple
        [Qs_root, Qr_root, Vs_root, Vr_root] = SS_rootFinder_thalamus(...
            Qe_in(i), lambda_e, lambda_i);

        delta_temp = [];
        Vr_temp = [];

        %Using each thalamic root Qs input to calculate difference in Q_in
        %and Q_out
        for p=1:length(Qs_root)

            %Excitatory ---> Inhibitory
            Ve_in = invsig(Qe_in(i), 'e');
            Qi_temp = g_Ve(Qe_in(i), Ve_in, Qs_root(p), lambda_e,...
                lambda_i, del_VeRest, sc);

            %Inhibitory ---> Excitatory
            Vi_temp = invsig(Qi_temp, 'i');
            Qe_out = f_Vi(Qi_temp, Vi_temp, Qs_root(p), lambda_e,...
                lambda_i, del_VeRest, sc);
```

```
        %Store the delta value for this combination of Qs and Qe_in
        delta_temp = [delta_temp; Qe_out - Qe_in(i)];

        %Store the Vr_root for computing
        %thalamic state that produced this delta value
        Vr_temp = [Vr_temp; Vr_root(p)];
    end



    %Find the delta value for this Q_in that is closest to zero.
    %As there are multiple thalamic roots which one allows delta Qe to
    %get closest to zero
    [Y I] = min(abs(delta_temp));

    %set mark to initial index denoting the which
    %thalamic root was used
    if(mark == 0)
        mark = I;
    %if the index has changed so has the thalamic root used
    elseif(mark ~= I)
        %check to see if the change in root index has caused a sign
        %change in delta Qe indicating a false root
        if((delta_Qe(i-1) < 0 && delta_temp(I) > 0) ||...
                (delta_Qe(i-1) > 0 && delta_temp(I) < 0))
            %change switch to hide false root
            swit = -1;
        else
            %if the index change didnt change the sign then do nothing
            swit = 1;
        end
        mark = I;
    end
    if(isempty(delta_temp))
        delta_Qe(i) = NaN;
```

```
        else
            delta_Qe(i) = swit*delta_temp(I);
        end
        debug = [debug; swit];
        %Store the last thalamic state used to get a delta Qe
        %Used after fzero has refined the Qe root so that thalamic state
        %can be computed
        Vr = Vr_temp(I);
    end

end

function Qe_out = f_Vi(Qi_in, Vi_in, Qs, lambda_e, lambda_i,...
    del_VeRest, sc)
%Uses Qi and Vi to compute Qe
%
%       Qe = f(Vi)

global H

sub_cort_drive_i = H.Nsi.*Qs;
%Removed: sc*H.phi_ei_sc

%Calculate Psi constants for i
psi_Vei = Psi_ab(Vi_in, 'ei');
psi_Vii = Psi_ab(Vi_in, 'ii');

numer = Vi_in - H.Vi_rest - (lambda_i* H.gi * psi_Vii *...
    H.Nii_b .* Qi_in);
denom = lambda_e* H.ge * psi_Vei;



Qe_out = (numer ./ denom - sub_cort_drive_i) / (H.Nei_ab);
Qe_out = clampQ(Qe_out, 'e');   %Restrain Qe to reasonable range
```

```
end

function Qi_out = g_Ve(Qe_in, Ve_in, Qs, lambda_e, lambda_i,...
    del_VeRest, sc)
%Uses Qe and Ve to compute Qi
%
%       Qi = g(Ve)

global H

sub_cort_drive_e = H.Nse.*Qs;
%Removed:  sc*H.phi_ee_sc

%Calculate Psi values for e
psi_Vie = Psi_ab(Ve_in, 'ie');
psi_Vee = Psi_ab(Ve_in, 'ee');

numer = Ve_in - H.Ve_rest - del_VeRest - lambda_e* H.ge * psi_Vee .*...
    (H.Nee_ab * Qe_in + sub_cort_drive_e);
denom = lambda_i* H.gi * psi_Vie;



Qi_out = (numer ./ denom) / H.Nie_b;
Qi_out = clampQ(Qi_out, 'i');   %Restrain Qi to reasonable range
end

function psi_out = Psi_ab(Vb, Index)
%reversal potential functions
%
%
global H



    switch Index
```

```
        case 'ee'
            psi_out = (H.Ve_rev - Vb)./(H.Ve_rev-H.Ve_rest);
        case 'ei'
            psi_out = (H.Ve_rev - Vb)./(H.Ve_rev-H.Vi_rest);
        case 'ie'
            psi_out = (H.Vi_rev - Vb)./(H.Vi_rev-H.Ve_rest);
        case 'ii'
            psi_out = (H.Vi_rev - Vb)./(H.Vi_rev-H.Vi_rest);
    end
end

function [Qa] = clampQ(Qa, Type)
%restraining firing rates to a
%feasible range

global H
    for i=1:length(Qa)
        if strcmp(Type, 'e')
            if Qa(i) <=0 || Qa(i) >=H.Qe_max
                Qa(i) = NaN;
            end
        elseif strcmp(Type, 'i')
            if Qa(i) <=0 || Qa(i) >=H.Qi_max
                Qa(i) = NaN;
            end
        end
    end
end

function [V] = invsig(Q, Type)
%function mapping firing rates to
%membrane potentials

global H
```

```
    Q = clampQ(Q, Type);

    if strcmp(Type, 'e')
        V = ((-H.sigma_e*sqrt(3))/pi)*log((H.Qe_max./Q)-1)+H.theta_e;
    elseif strcmp(Type, 'i')
        V = ((-H.sigma_i*sqrt(3))/pi)*log((H.Qi_max./Q)-1)+H.theta_i;
    end

end

function [Q] = sig(V, Type)
%function mapping membrane potentials
%to firing rates


global H

    if strcmp(Type, 'e')
        Q = H.Qe_max./(1+exp(-(pi/(H.sigma_e*sqrt(3))).*(V-H.theta_e)));
    elseif strcmp(Type, 'i')
        Q = H.Qi_max./(1+exp(-(pi/(H.sigma_i*sqrt(3))).*(V-H.theta_i)));
    end

end
```

B.4 Isolated Thalamus: Euler Simulation

Code used to implement an euler update of thalamic state variables with noise.

```
function isolated_thalamus_euler_sim()
%Simluation of an Isolated Thalamus
%using an Euler update function
%
```

```
%By Eli Muller 2013
%Modified June 2013
%Modified July 2013
%Modified August 2013
%Modified October 2013



clear all;
format long;
set(0,'DefaultAxesFontSize',14)
set(gcf,'Position',[100 50 1200 600])

%------------------------------  Steady states
[FileName,PathName] = uigetfile('*.mat','Select the MATLAB code file');

load(strcat('data\',FileName));

lambda_r = 10;

t = find(top_state(:,6) == lambda_r);
top = top_state(t,:);

m = find(mid_state(:,6) == lambda_r);
mid = mid_state(m,:);

b = find(bot_state(:,6) == lambda_r);
bot = bot_state(b,:);

eq_state = top;

eig = SS_Stability_Thalamus([eq_state(2), eq_state(3), eq_state(4),...
    eq_state(5), 0],1,eq_state(6))
```

```
%-----------------------------------------------------------------

global H
H = init_spat_het_globs;

nPts = 300000;
dt = 0.00001;

t = [0:nPts]*dt;

%Assigning Memory
thal_state = NaN(nPts,12);
cort_state = NaN(nPts,12);

t_range = nPts*dt;

%Initial Soma Potentials
V_int = [eq_state(4), eq_state(5)];

[Vs_0, Vr_0] = deal(V_int(1), V_int(2));

Qs_0 = sig(Vs_0);
Qr_0 = reticular_sigmoid(Vr_0,'norm');



%Parameter Setting
Qe_0 = 0;
%[lambda_s lambda_r Qe]
params = [1 lambda_r, Qe_0];

%%% Initial Cortical State
cort_state_0 = [];

cort_driv_s = H.Nes*Qe_0;
```

```
cort_driv_r = H.Ner*Qe_0;

%Thalamic Intialization
phi_es_0 = H.Nss*Qs_0+H.nu_ns*H.phi_n + cort_driv_s;
phi_is_0 = H.Nrs*Qr_0;
phi_er_0 = H.Nsr*Qs_0 + cort_driv_r;
phi_ir_0 = H.Nrr*Qr_0;

pi_es_0 = 0;
pi_er_0 = 0;
pi_is_0 = 0;
pi_ir_0 = 0;

%%% Initial Thalamic State
thal_state_0...
    = [Qs_0, Qr_0, Vs_0, Vr_0, pi_es_0, phi_es_0, pi_is_0,...
    phi_is_0, pi_er_0, phi_er_0, pi_ir_0, phi_ir_0];

%%%%%%  Updating function
thal_state(1,:) = thal_state_0;
tic
for i=1:nPts-1

    %Soma Potential Noise
    noise = [0,0,randn(1,1),randn(1,1),0,0,0,0,0,0,0,0,0]./(dt^0.5);

    %%Thalamus Update
    thal_state(i+1,:) = thal_state(i,:) + d_thal_state(...
        t(i),thal_state(i,:),'',params).*dt + noise.*dt;
    thal_state(i+1,1) = sig(thal_state(i+1,3));
    thal_state(i+1,2) = reticular_sigmoid(thal_state(i+1,4),'norm');

     if(mod(i,500) == 0)
```

```
        Realtime_Sim_Plotter(t(1:i+1), thal_state([1:i+1],:),...
            t_range, top,mid,bot);
    end
end
toc



end

function [Qs] = sig(Vs)
global H
%Assume Specific Neurons are all excitatory

    Qs = H.Qs_max./(1+exp(-(pi/(H.sigma_e*sqrt(3))).*(Vs-H.theta_e)));
end

function Realtime_Sim_Plotter(t, state, t_range, top,mid,bot)
%
%
%

%By Eli Mller 2013
clf
t = t';



subplot(221)
    hold on;
    plot([0 t_range], [top(2) top(2)], '--k')
    plot([0 t_range], [mid(2) mid(2)], '--r')
    %plot([0 t_range], [bot(2) bot(2)], '-b')
    plot(t, state(:,1),'-m')
    plot(t(end), state(end,1),'ok')
    xlabel('Time, [s]')
```

```
    ylabel('Qs [1/s]')
    title('Specific Firing Rates')
    axis([0 t_range -5 35])
    box on;
    hold off;

subplot(222)
    hold on;
    plot([0 t_range], [top(3) top(3)], '--k')
    plot([0 t_range], [mid(3) mid(3)], '--r')
    %plot([0 t_range], [bot(3) bot(3)], '-b')
    plot(t, state(:,2),'-m')
    plot(t(end), state(end,2),'ok')
    xlabel('Time, [s]')
    ylabel('Qr [1/s]')
    title('Reticular Firing Rates')
    axis([0 t_range -5 65])
    box on;
    hold off;

subplot(223)
    hold on;
    plot([0 t_range], [top(4) top(4)], '--k')
    plot([0 t_range], [mid(4) mid(4)], '--r')
    %plot([0 t_range], [bot(4) bot(4)], '-b')
    plot(t, state(:,3),'-m')
    plot(t(end), state(end,3),'ok')
    xlabel('Time, [s]')
    ylabel('Vs [1/s]')
    title('Specific Membrane Potentials')
    axis([0 t_range -70 -40])
    box on;
    hold off;
```

```
subplot(224)
    hold on;
    plot([0 t_range], [top(5) top(5)], '--k')
    plot([0 t_range], [mid(5) mid(5)], '--r')
    %plot([0 t_range], [bot(5) bot(5)], '-b')
    plot(t, state(:,4),'-m')
    plot(t(end), state(end,4),'ok')
    xlabel('Time, [s]')
    ylabel('Vr [1/s]')
    title('Reticular Membrane Potentials')
    axis([0 t_range -70 -40])
    box on;
    hold off;

    drawnow
end
```

References

[1] Ashby, W.R.: Principles of the self-organizing system. Principles of Self-organization pp. 255–278 (1962)

[2] Beurle, R.L.: Properties of a mass of cells capable of regenerating pulses. Transactions of the Royal Society (London) **240**, 55–94 (1956)

[3] Braitenberg, V., Schüz, A.: Anatomy of a Cortex: Statistics and Geometry. Springer-Verlag, Berlin (1991)

[4] Brown, E.N., Lydic, R., Schiff, N.D.: General anesthesia, sleep, and coma. New England Journal of Medicine **363**(27), 2638–2650 (2010), URL `http://www.nejm.org/doi/full/10.1056/NEJMra0808281`

[5] Coulter, D.A., Huguenard, J.R., Prince, D.A.: Calcium currents in rat thalamocortical relay neurones: kinetic properties of the transient, low-threshold current. The Journal of physiology **414**(1), 587–604 (1989)

[6] Destexhe, A., Sejnowski, T.J.: Sleep and sleep states: thalamic regulation. Encyclopedia of Neuroscience pp. 973–976 (2009)

[7] Griffith, J.S.: On the stability of brain-like structures. Biophysical Journal **3**, 299–308 (1963)

[8] Hutt, A.: Sleep and Anesthesia: Neural correlates in theory and experiment, vol. 15. Springer (2011)

[9] Leamey, C.A., Sur, M.: The thalamus: A new proposal **34** (2002)

[10] Liley, D.T.J., Cadusch, P.J., Dafilis, M.P.: A spatially continuous mean field theory of electro-cortical activity. Network: Computation in Neural Systems (2002), in press

[11] Liley, D.T.J., Cadusch, P.J., Wright, J.J.: A continuum theory of electro-cortical activity. California Institute of Technology, Santa Barabara, CA (1998)

[12] Liley, D.T.J., Cadusch, P.J., Wright, J.J.: A continuum theory of electro-cortical activity. Neurocomputing **26–27**, 795–800 (1999)

[13] McCormick, D.A., Pape, H.C.: Properties of a hyperpolarization-activated cation current and its role in rhythmic oscillation in thalamic relay neurones. The Journal of Physiology **431**(1), 291–318 (1990)

[14] Mountcastle, V.B.: Modality and topographic properties of single neurons of cats somatic sensory cortex. J. neurophysiol **20**(4), 408–434 (1957)

[15] Nunez, P.L.: Neocortical dynamics and human EEG rhythms. Oxford University Press, USA (1995)

[16] Robinson, P.A., Rennie, C.J., Wright, J.J.: Propagation and stability of waves of electrical activity in the cerebral cortex. Physical Review E **56**, 826–840 (1997)

[17] Robinson, P.A., Rennie, C.J., Wright, J.J., Bourke, P.D.: Steady states and global dynamics of electrical activity in the cerebral cortex. Physical Review E **58**, 3557–3571 (1998)

[18] Robinson, P., Rennie, C., Rowe, D., O'Connor, S.: Estimation of multiscale neurophysiologic parameters by electroencephalographic means. Human Brain Mapping **23**(1), 53–72 (2004)

[19] Soltesz, I., Lightowler, S., Leresche, N., Jassik-Gerschenfeld, D., Pollard, C., Crunelli, V.: Two inward currents and the transformation of low-frequency oscillations of rat and cat thalamocortical cells. The Journal of physiology **441**(1), 175–197 (1991)

[20] Steyn-Ross, D.M.L., Steyn-Ross, D.A., Sleigh, J.W., Liley, D.T.J.: Theoretical electroencephalogram stationary spectrum for a white-noise-driven cortex: Evidence for a general anesthetic-induced phase transition. Physical Review E **60**, 7299–7311 (1999)

[21] Steyn-Ross, M.L., Steyn-Ross, D.A., Sleigh, J.W.: Interacting turing-hopf instabilities drive symmetry-breaking transitions in a mean-field model of the cortex: A mechanism for the slow oscillation. Phys. Rev. X **3**, 021005 (2013), doi:10.1103/PhysRevX.3.021005, URL `http://link.aps.org/doi/10.1103/PhysRevX.3.021005`

[22] Steyn-Ross, M.L., Steyn-Ross, D.A., Sleigh, J.W.: Modelling general anaesthesia as a first-order phase transition in the cortex. Progress in biophysics and molecular biology **85**(2), 369–385 (2004)

[23] Toth, T., Hughes, S., Crunelli, V.: Analysis and biophysical interpretation of bistable behaviour in thalamocortical neurons. Neuroscience **87**(2), 519–523 (1998)

[24] Valencia, M., Artieda, J., Bolam, J.P., Mena-Segovia, J.: Dynamic interaction of spindles and gamma activity during cortical slow oscillations and its modulation by subcortical afferents. PloS one **8**(7), e67540 (2013)

[25] Williams, S.R., Toth, T.I., Turner, J.P., Hughes, S.W., Crunelli, V.: The windowcomponent of the low threshold ca2+ current produces input signal amplification and bistability in cat and rat thalamocortical neurones. The Journal of physiology **505**(3), 689–705 (1997)

[26] Wilson, H.R., Cowan, J.D.: Excitatory and inhibitory interactions in localized populations of model neurons. Biophysical Journal **12**, 1–24 (1972)

[27] Wilson, H.R., Cowan, J.D.: A mathematical theory of the functional dynamics of cortical and thalamic nervous tissue. Kybernetik **13**, 55–80 (1973)

[28] Zhu, J., Uhlrich, D., Lytton, W.: Properties of a hyperpolarization-activated cation current in interneurons in the rat lateral geniculate nucleus. Neuroscience **92**(2), 445–457 (1999)